LEVEL II

(6)

ARPA Order 3291-32
Program Code OD60
Name of Contractor: University of Colorado
Effective Date of Contract: 1 October 1979
Contract Expiration Date: 30 September 1980
Amount of Contract: $80,000
Contract Number: F49620-80-C-0018 new
Principle Investigator: C. B. Archambeau (303)-492-8028
Program Manager: William J. Best (202)-767-5011
Title of Work: Deterministic Methods of Seismic Source Identification

Semi-Annual Technical Report No. 1

1 October 1979- 30 March 1980

Sponsored by
Advanced Research Projects Agency (DOD)
ARPA Order No. 3291-32
Monitored by AFOSR Under Contract No. F49620-80-C-0018

UNCLASSIFIED
SECURITY CLASSIFICATION OF THIS PAGE (When Data Entered)

REPORT DOCUMENTATION PAGE

READ INSTRUCTIONS BEFORE COMPLETING FORM

1. REPORT NUMBER: AFOSR-TR-80-0630
2. GOVT ACCESSION NO.: AD-A088 723
3. RECIPIENT'S CATALOG NUMBER:

4. TITLE (and Subtitle): DETERMINISTIC METHODS OF SEISMIC SOURCE IDENTIFICATION.
5. TYPE OF REPORT & PERIOD COVERED: INTERIM
6. PERFORMING ORG. REPORT NUMBER:

7. AUTHOR(s): C. B. Archambeau
8. CONTRACT OR GRANT NUMBER(s): F49620-80-C-0018, ARPA Order-3297

9. PERFORMING ORGANIZATION NAME AND ADDRESS: University of Colorado, Boulder, CO 80302
10. PROGRAM ELEMENT, PROJECT, TASK AREA & WORK UNIT NUMBERS: AO 3291-3? 0D60

11. CONTROLLING OFFICE NAME AND ADDRESS: DARPA, 1400 Wilson Blvd, Arlington, VA 22209
12. REPORT DATE: Oct 79
13. NUMBER OF PAGES: 112

14. MONITORING AGENCY NAME & ADDRESS (if different from Controlling Office): AFOSR/NP, Bolling AFB, Washington, DC 20332
15. SECURITY CLASS. (of this report): unclassified
15a. DECLASSIFICATION/DOWNGRADING SCHEDULE:

Semi-annual technical rept. no. 1, 1 Oct 79-30 Mar 80

16. DISTRIBUTION STATEMENT (of this Report)

Approved for public release; distribution unlimited.

17. DISTRIBUTION STATEMENT (of the abstract entered in Block 20, if different from Report)

18. SUPPLEMENTARY NOTES

19. KEY WORDS (Continue on reverse side if necessary and identify by block number)

20. ABSTRACT (Continue on reverse side if necessary and identify by block number)

In order to interpret seismic event discrimination in terms of the physical properties of the source and to be able to establish new discrimination techniques we have generalized seismic source models based on relaxation source theory to include the effects of non-homogeneous initial pre-stress. In particular we have considered the effects of strongly concentrated prestress

DD FORM 1 JAN 73 1473 EDITION OF 1 NOV 65 IS OBSOLETE

UNCLASSIFIED 088400

in the vicinity of the shatter zone produced by an explosion.

The important result from the work so far completed are: (1) the spectra of P and S waves radiated due to stress relaxation effects can be strongly peaked, with the nature of the peaking being azimuthally dependent in general and quite strongly dependent on the size and location of the initial stress concentration; (2) the corners or peak frequencies of the P and S wave radiation are different from one another (S lower) and are both shifted to higher frequencies when the stress concentration is close to the shatter zone. In addition, the corner or peak frequency value is related to the size of the stress concentration rather than to the size of the shatter zone; (3) the pattern of first motions from the tectonic release, when the prestress is inhomogenious, is not pure quadrupole with higher order multiples also involved. The ordinary quadrupolar pattern predicted from a homogeneous prestress can be strongly distorted when the prestress is concentrated and can be highly non-quadrupole in form.

TABLE OF CONTENTS

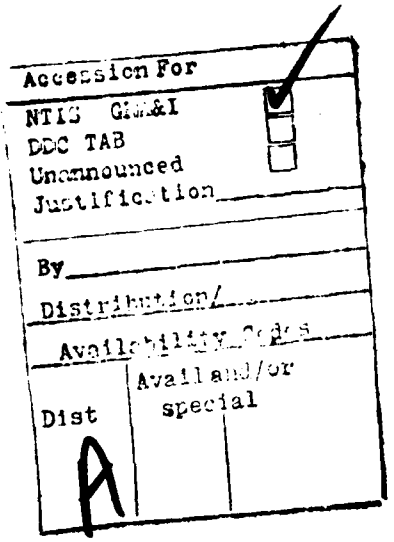

Research on Deterministic Methods of Seismic Source Identification

Report No. 1 - Summary

In order to interpret seismic event discrimination in terms of the physical properties of the source and to be able to establish new discrimination techniques we have generalized seismic source models based on relaxation source theory to include the effects of non-homogeneous initial prestress. In particular we have considered the effects of strongly concentrated prestress in the vicinity of the shatter zone produced by an explosion.

The important result from the work so far completed are: (1) the spectra of P and S waves radiated due to stress relaxation effects can be strongly peaked, with the nature of the peaking being azimuthally dependent in general and quite strongly dependent on the size and location of the initial stress concentration; (2) the corners or peak frequencies of the P and S wave radiation are different from one another (S lower) and are both shifted to higher frequencies when the stress concentration is close to the shatter zone. In addition, the corner or peak frequency value is related to the size of the stress concentration rather than to the size of the shatter zone; (3) the pattern of first motions from the tectonic release, when the prestress is inhomogeneous, is not pure quadrupole with higher order multiples also involved. The ordinary quadrupolar pattern predicted from a homogeneous prestress can be strongly distorted when the prestress is concentrated and can be highly non-quadrupole in form.

Considering both the explosion generated direct compressional wave field and the field produced by such tectonic effects together, the consequences for discrimination and explosion yield determination are:

(1) Short period perturbations in the wave train can be expected to be very complex due to dependence on stress concentration effects. However, the perturbations should be small to moderate for the first cycle of the P wave motion, while being significantly larger for the later part of the P wave train. Body wave magnitude measured from the first P wave cycle should, therefore, be minimally perturbed by stress relaxation effects.

(2) Long period surface wave radiation can be strongly perturbed by tectonic release effects within the whole measureable low frequency band (i.e.g, from approximately 5 sec to 60 sec in period). The perturbations in the observed Rayleigh wave forms can be such as to add to, or subtract from, the explosive generated Rayleigh wave depending on the orientation and magnitude of the prestress in the vicinity of the explosion. The magnitude of this effect can be very (unacceptably) large. In those cases where Love waves are significant, so that tectonic release is involved, then yield estimation using M_s can only be made after correction of the Rayleigh wave measurement using the observed Love wave to deduce the size and configuration of the tectonic source.

Predictions of the radiated seismic wave field from both explosion and earthquake models in the regional and teleseismic distance ranges, for layered, anelastic earth models, have been used to predict entire synthetic

seismograms for purposes of comparisons with observations. Both full wave asymptotic and locked mode approximation methods are being used. Examples of synthetics and comparisons to observations in the regional distance range suggest that most of the seismogram can be understood using current source and medium models. Some specific applications of this capability have been directed toward providing an understanding of the large amplitude Pg signals in the regional distance range, and for studies of regional anleastic characteristics of the earth. The results of these two applications have been to show that: Pg is comprised of a large number of high modes, which can also be viewed as a large number of multiple reflections from the "granitic-basaltic" layer interface in the middle crust; and that the anelastic dissipation function, or Q, is frequency dependent with the anelastic Q increasing with increasing frequency, and that the low velocity zone absorption is srongly variable regionally (and also within particular regions) with the low velocity zone Q dominating the adsorption along teleseismic paths.

I. Introduction

The objectives of the research being conducted are to: (1) Develop methods of seismogram synthesis using mode superposition and related methods, (2) Finalize the theory for source inversion by modal decomposition, (3) Determine the anelastic characteristics of the medium using known source characteristics, (4) Interpret seismic event discrimination in terms of the physical properties of the source, (5) Establish seismic event discrimination methods from formal inversion techniques, and (6) Establish regional discrimination techniques based upon physical properties of the source.

In this report we describe research results relating to seismogram synthesis (item (1) above) and the interpretation of seismic event discrimination in terms of the physical properties of the source (item (4) above).

II. Seismic Source Modeling

In order to interpret seismic event discrimination in terms of the physical properties of the source and to be able to establish new discrimination techniques we have generalized seismic source models based on relaxation source theory to include the effects of non-homogeneous initial prestress (Stevens, 1980). In particular, we have considered the effects of strongly concentrated prestress in the vicinity of the shatter zone produced by an explosion. This work shows in detail how the effects of tectonic release can perturb the normal seismic radiation from an explosion. The results of this work are included in the Appendix A.

The important results from the work so far completed are (1) The spectra of P and S waves radiated due to stress relaxation effects can be strongly peaked, with the nature of the peaking being azimuthally dependent in general and quite strongly dependent on the size and location of the initial stress concentration, (2) The corners or peak frequencies of the P and S wave radiation are different from one another (S lower) and are both shifted to higher frequencies when the stress concentration is close to the shatter zone. In addition, the corner or peak frequency value is related to the size of the stress concentration rather than to the size of the shatter zone, (3) the pattern of first motions from the tectonic release, when the prestress is inhomogeneous, is not pure quadrupole, with higher order multipoles also involved. The ordinary quadrupolar pattern predicted from a homogeneous prestress can be strongly distorted when the prestress is concentrated and can be highly non-quadrupole in form.

When the prestress has an average (homogeneous) component value (near 100 bars or so) and a nonhomogeneous component corresponding to local stress concentrations in the vicinity of explosion produced shatter zone (with stress levels near several hundred bars) then, for this "expected prestress environment", one can predict the following consequences for discrimination and explosive yield estimation:

1. Short period perturbations in the wave train can be expected to be very complex due to dependence on stress concentration effects. However, the perturbations should be small to moderate for the first cycle of the P wave motion, while being significantly larger

for the later part of the P wave train. Body wave magnitude measured from the first P wave cycle should, therefore, be minimally perturbed by stress relaxation effects. Further, corrections to the first cycle of the P wave for tectonic affects could conceivably be made for purposes of yield estimation.

2. Long period surface wave radiation is strongly perturbed by tectonic release effects within the whole measureable low frequency band (i.e., from approximately 5 sec. to 60 sec. in period). The perturbations in the observed Rayleigh wave forms can be such as to add to, or subtract from, the explosive generated Rayleigh wave depending on the orientation and magnitude of the prestress in the vicinity of the explosion. The magnitude of this effect can be very (unacceptably) large. In those cases where Love waves are significant, so that tectonic release is involved, then yield estimation using M_s can only be made after correction of the Rayleigh wave measurement using the observed Love wave to deduce the size and configuration of the tectonic source. Such a correction would be much more reliable, when spherical shatter zone induced tectonic release is involved, than it would be if actual earthquake triggering is involved.

III. Wave Propagation Theory: Synthetic Seismograms

In the course of our development of methods of synthesizing seismograms in the regional and teleseismic distance ranges we have considered two theoretical approaches; in particular mode superposition using a "locked mode" approximation method (Harvey, 1980) and the full wave

asymptotic method (e.g. Cormier, 1980). Results from the full wave theory are described in this report. The Appendix B provides a detailed discussion.

The importance of the full wave theory is that it is applicable at all distance ranges, incorporates sphericity, can be applied to media models with velocity gradients, is a frequency domain theory and as one consequence can incorporate frequency dependent anelastic absorption and scattering, and finally, it is accurate and quite fast computationally.

In our work so far, the theory has been fully developed and coded for the near and regional distance ranges from a seismic source. It is now possible to compute complete seismograms produced by rather complex source models in complex earth models. Programs for this purpose have been used to predict the radiation from explosion and earthquake models in the near and teleseismic distance ranges. Examples of these computations in the near regional distance range are shown in the Appendix B, along with the full theoretical development of the method.

One application of this capability has been to study the anelastic properties of the upper mantle with attention to frequency dependence of the absorption (Lundquist, 1980). In the work to continue we will use this theoretical modeling capability to further study anelasticity, but also to study both earthquakes and explosions in both the regional and teleseismic distance ranges to infer source properties and to define discrimination methods.

References

Stevens, J. (1980) Seismic Radiation from the Sudden Creation of a Spherical Cavity in an Arbitrarily Prestressed Elastic Medium, in press, Geophys. J. Roy. Astr. Soc.

Harvey, D. (1980) Seismogram Synthesis Using Normal Mode Superposition: The Locked Mode Approximation Method, submitted to Geophys. J. Roy. Astrn. Soc.

Cormier, V. (1980) The Synthesis of Complete Seismograms in an Earth Model Specified by Radially Inhomogeneous Layers, submitted to Geophys. J. Roy Astr. Soc.

Lundquist, G. (1980) Constraints on the Absorption Band Model of Q, in press, Jour. Geophys. Res.

Appendix A

Seismic Radiation from the Sudden Creation of a Spherical Cavity in an Arbitrarily Prestressed Elastic Medium

Jeffry L. Stevens

Seismic Radiation from the Sudden Creation of a Spherical Cavity in an Arbitrarily Prestressed Elastic Medium

Summary. We solve the general problem of seismic radiation from the sudden creation of a spherical cavity in an arbitrarily prestressed elastic medium. This problem has direct application to tectonic release due to the creation of a shatter zone by large underground explosions. In addition, however, the problem has essential features in common with the more general earthquake source. Specifically, it can provide an understanding of how an inhomogeneous prestress can affect radiated seismic energy from a tectonic source. The problem is solved through the use of a Green's tensor integral equation in which all quantities are expressed in terms of vector spherical harmonics. We obtain an exact solution and an approximate solution to this problem. The approximate solution may be useful for the study of other failure geometries. The results agree with previous solutions for the case of pure shear. The case of localized inhomogeneous prestress is examined in detail. The primary result of the inhomogeneous prestress is the addition of considerable energy at frequencies above the usual corner frequency. This causes an increase in the corner frequency, a change in the slope of the spectrum near the corner frequency and in some case a strong, low frequency, far field spectral peak. Peaked spectra always exist, however, near the usual quadrupole nodes. Further, the angular distribution of radiation in general will not be pure quadrupole in nature. As an example of a strongly inhomogeneous prestress case, stress concentrations near the source due to a point dislocation and a point center of compression are considered. The radiated waveforms

and spectra then vary greatly with angle, with the spectra peaked strongly at all azimuths in some cases. For these cases the angular distribution of first motions is still relatively simple, but can be deceptive if used to determine a focal mechanism. Because of the canonical relation of this problem to the more general earthquake failure problem, it is to be expected that similar stress concentration effects will occur for earthquakes. Thus, similar changes in corner frequency due to stress concentration effects could lead to errors in earthquake source dimension estimates and the related existence of spectral peaks could lead to errors in seismic moment measurements.

1. Introduction

An earthquake can be considered to result from the creation of an external boundary in a prestressed elastic medium. Similarly, at least some of the anomalous radiation from an explosion can be considered to result from the creation of a shatter zone in a prestressed medium. Here we consider the problem of the sudden creation of a stress free surface in an arbitrarily prestressed medium since this problem contains many of the essential characteristics of the earthquake and explosion induced tectonic release problems. In particular it shows clearly and simply what effects inhomogeneous prestress will have on the observed radiation field We will show that this problem may be treated as an initial value problem or, equivalently, as a stress pulse problem.

We solve this problem exactly for the case of a spherical cavity using vector spherical harmonics in the elastic Green's tensor integral equation in the frequency domain. The result is a relatively simple solution for the radiation field involving nothing more than the inverse of a number of two by two matrices and an inverse Fourier transform. The solution is valid for any arbitrary homogeneous or inhomogeneous prestress and is valid in the near field or far field. Previous solutions to spherical source problems have all been obtained for uniform stress fields. Hirasawa and Sato (1963) found an exact solution for the sudden creation of a spherical cavity in a pure shear stress field. Randall (1964a) used a spherical inclusion in which the material inside suddenly underwent a phase change to become the same as the external material to model deep earthquakes. He applied this to a uniform compressive (1964b) and a uniform shear (1966) prestress. Archambeau (1968) used

a growing, propagating, transparent spherical cavity in a uniform shear field as a model for earthquakes. Minster(1973) refined this model. Burridge and Alterman (1972) found an exact solution for a uniformly growing spherical cavity in a pure shear field. Burridge (1975) used this solution as a test for Archambeau's (1968, 1972) transparent source approximation. Koyama et al. (1973) found an exact solution for the sudden creation of a fluid filled cavity in a pure shear field. Minster and Suteau (1977) examined the relationship between a growing spherical source and a growing circular dislocation with the same growth history.

The case of inhomogeneous prestress is particularly interesting since almost all previous source models have used the boundary condition of homogeneous shear or its equivalent. Actual stress fields in the earth are likely to be highly inhomogeneous. Archambeau (1968, 1972) attempted to allow for a localized prestress by solving the static initial value problem for a homogeneous shear field, but then limiting the effective source region to be within a radius R_s for his dynamic calculations. Snoke (1976) showed that there were problems with this approximation. Bache and Barker (1978) attempted to determine stress variations in the earth during the 1971 San Fernando earthquake by using a solution for a transparent growing sphere in a ~~shear~~ pure shear field, but allowing the magnitude of the stress field to vary during growth. We find, in an exact calculation, that the main effect of the inhomogeneous prestress is appearance of considerable seismic energy at frequencies greater than the usual quadrupole corner frequency. A slightly inhomogeneous prestress results in a nearly quadrupole distribution of radiation, but with anomalous radiation in and near the nodes.

A stress concentration close to the source results in a dramatic increase in corner frequency and the appearance of pronounced spectral peaks at all points of observations. The waveforms produced by a concentrated prestress are substantially different from those produced by a uniform prestress. The angular distribution of first motions, however, may or may not appear to have a quadrupole distribution.

This paper is the first attempt to explicitly calculate the effect of an inhomogeneous prestress on the spectra and waveforms of a dynamic seismic source. The spherical cavity problem can be solved exactly and is the canonical problem which can be used to determine some of the features of failure in other geometries. The results should be important to observational seismologists since the corner frequency is often used to estimate the size of a seismic source and the results of this study indicate large variations in the corner frequency as a function of local prestress inhomogeneity, location, and magnitude. In some cases, for example, increase in the apparent corner frequency occurs and this can cause a gross underestimation of source dimensions. Further, the complexity of the spectrum that can be produced can make the corner difficult to define observationally and peaking of the spectrum can lead to uncertain or erroneous measurements of moment. On the other hand, the theory given here should prove useful for the study of spatial variations of stress in the earth.

We are simplifying the seismic source problem in this paper through the use of instantaneous creation of the failure surface and through the neglect of any consideration of the material inside the cavity. In this way we can examine the effect of an inhomogeneous

stress field on seismic radiation independently of the complexities of finite rupture velocity and certain boundary effects. The formidable general problem of failure in a prestressed medium in which the growth rate is determined by the prestress and the problem is coupled at the boundary to the material inside the cavity has been discussed in detail by Archambeau and Minster (1978).

2. Basic Relations

The problem of the radiation released when a cavity forms in a prestressed medium is conveniently expressed in terms of a Green's tensor integral equation. Consider first the cavity of arbitrary shape shown in figure 1. We assume that the medium is prestressed and that the cavity forms at time $t = 0$. The medium is then displaced from equilibrium initially and relaxes to a new equilibrium state. The displacement field satisfies the elastic equations:

$$\underset{\approx}{L}\cdot\underset{\sim}{u}(\underset{\sim}{x},t) - \rho \frac{\partial^2}{\partial t^2} \underset{\sim}{u}(\underset{\sim}{x},t) = 0 \tag{2.1}$$

$$\text{where } \underset{\approx}{L}\cdot\underset{\sim}{u}(\underset{\sim}{x},t) \equiv \frac{\partial}{\partial x_j} C_{ijk\ell} \frac{\partial}{\partial x_k} u_\ell \tag{2.2}$$

is the elastic operator. $C_{ijk\ell}$ is the constitutive tensor for the medium external to the cavity.

The Green's tensor satisfies the equation:

$$\underset{\approx}{L}\cdot\underset{\approx}{G}(\underset{\sim}{x}, \underset{\sim}{x}_o, t, t_o) - \rho \frac{\partial^2}{\partial t^2} \underset{\approx}{G}(\underset{\sim}{x}, \underset{\sim}{x}_o, t, t_o) = - \underset{\approx}{I}\, \delta(\underset{\sim}{x}-\underset{\sim}{x}_o)\, \delta(t-t_o) \tag{2.3}$$

We will solve this problem in the frequency domain with the aid of vector harmonics. We define the Fourier transform and its inverse:

$$\underset{\sim}{u}(\omega) = \int_{-\infty}^{\infty} \underset{\sim}{u}(t)\, e^{-i\omega t}\, dt \qquad \underset{\sim}{u}(t) = \frac{1}{2\pi} \int_{-\infty}^{\infty} \underset{\sim}{u}(\omega)\, e^{i\omega t}\, d\omega \tag{2.4}$$

The transformed displacement field satisfies

$$\underset{\approx}{L}\cdot\underset{\sim}{u}(\underset{\sim}{x},\omega) + \rho\omega^2\,\underset{\sim}{u}(\underset{\sim}{x},\omega) = 0 \tag{2.5}$$

The transformed Green's tensor satisfies:

$$\underset{\approx}{L}\cdot\underset{\approx}{G}(\underset{\sim}{x},\underset{\sim}{x}_o,\omega) + \rho\omega^2\underset{\approx}{G}(\underset{\sim}{x},\ \underset{\sim}{x}_o,\omega) = -\ \underset{\approx}{I}\ \delta(\underset{\sim}{x}-\underset{\sim}{x}_o) \tag{2.6}$$

It will prove simpler to use vector notation rather than indicial notation throughout this paper, and we define the stress operators:

$$\underset{\approx}{T}(\underset{\sim}{u}) \equiv C_{ijk\ell}\,\frac{\partial}{\partial x_k}\,u_\ell \equiv \tau_{ij} \tag{2.7}$$

$$\underset{\approx}{T}(\underset{\approx}{G}) \equiv C_{ijk\ell}\,\frac{\partial}{\partial x_k}\,G_{\ell m} \tag{2.8}$$

The Green's tensor integral equation for the general case of growing phase boundaries has been derived by Archambeau and Minster (1978). For the case of the instantaneous creation of a boundary it reduces to:

$$\begin{aligned}\underset{\sim}{u}(\underset{\sim}{x},t) = &\int_0^t dt_o \int_\Sigma [\underset{\approx}{G}\cdot\underset{\approx}{T}(\underset{\sim}{u}) - \underset{\sim}{u}\cdot\underset{\approx}{T}(\underset{\approx}{G})]\cdot\hat{n}\,dA_o \\ &- \int_V \rho\left(\underset{\sim}{u}\cdot\frac{\partial \underset{\approx}{G}}{\partial t_o}\right)_{t_o=0} dV_o\end{aligned} \tag{2.9}$$

The last term contains the effect of the initial conditions. The surface integral contains the response of the surface. The first term in this integral will vanish for a stress free surface.

The frequency domain integral equation is:

$$\underset{\sim}{u}(\underset{\sim}{x},\omega) = -\int_{\Sigma} [\underset{\sim}{u}\cdot\underset{\approx}{T}(\underset{\approx}{G}) - \underset{\approx}{G}\cdot\underset{\approx}{T}(\underset{\sim}{u})]\cdot\hat{n}\, dA_o + i\omega\int_{V} \rho\underset{\sim}{u}^*\cdot\underset{\approx}{G}\, dV_o \tag{2.10}$$

where $\underset{\sim}{u}^* = \underset{\sim}{u}(t=0)$, the initial displacement from equilibrium. Again the term containing $\underset{\approx}{T}(\underset{\sim}{u})$ vanishes for a stress free surface.

The initial value term in equations (2.9) and (2.10) can be quite difficult to evaluate. The problem can be made much simpler by defining the "stress pulse equivalent" to the initial value problem. We use the fact that since $\underset{\sim}{u}^*$ is the difference between two static equilibrium fields (the prestressed state without the cavity and the final equilibrium state)

$$\underset{\approx}{L}\cdot\underset{\sim}{u}^* = 0 \tag{2.11}$$

Multiplying this equation by $\underset{\approx}{G}$ and multiplying equation (2.6) by $\underset{\sim}{u}^*$, subtracting and integrating overall space external to the cavity and substituting in equation (2.10) we find that for a stress free cavity of arbitrary shape:

$$\underset{\sim}{u}' = -\int_{\Sigma} \underset{\sim}{u}'\cdot\underset{\approx}{T}(\underset{\approx}{G})\cdot\hat{n}\, dA_o \quad - \frac{1}{i\omega}\int_{\Sigma} \underset{\approx}{G}\cdot\underset{\approx}{T}(\underset{\sim}{u}^*)\cdot\hat{n}\, dA_o \tag{2.12}$$

where $\underset{\sim}{u}'$ is the relative displacement field

$$\underset{\sim}{u}'(\underset{\sim}{x},\omega) = \underset{\sim}{u}(\underset{\sim}{x},\omega) - \underset{\sim}{u}^*(\underset{\sim}{x})/i\omega$$

$\underset{\approx}{T}(\underset{\sim}{u}^*) \cdot \hat{n}$ is the traction drop on the cavity surface between the initial and final state. Since the final tractions are zero for the stress free cavity, $\underset{\approx}{T}(\underset{\sim}{u}^*) \cdot \hat{n}$ is just the initial tractions on the surface due to the existing prestress. Comparing equation(2.12) with equation (2.10), we see that the initial value problem is equivalent to a stress pulse equal in magnitude to minus the initial tractions applied to the cavity surface at time $t = 0$. While the relaxation problem is perhaps more naturally expressed as an initial value problem, the solution is much easier when expressed as a stress pulse equivalent.

The infinite space Green's tensor in the frequency domain is given by Ben-Menahem & Singh (1968) in terms of vector spherical harmonics:

$$\underset{\sim}{\underset{\sim}{G}}(\underset{\sim}{x},\underset{\sim}{x}_o) = -\frac{ik_\beta}{4\pi\mu}\sum_{\ell=1,1,0}^{\infty}\frac{2\ell+1}{\ell(\ell+1)}\sum_{m=-\ell}^{\ell}\frac{(\ell-m)!}{(\ell+m)!}\left[\overset{*\varepsilon}{\underset{\sim}{M}}_{\ell m}(r_o)\,\underset{\sim}{M}^{-\varepsilon}_{\ell m}(r)\right.$$

$$\left. + \overset{*\varepsilon}{\underset{\sim}{N}}_{\ell m}(r_o)\,\underset{\sim}{N}^{-\varepsilon}_{\ell m}(r) + \ell(\ell+1)\left(\frac{\beta}{\alpha}\right)^3 \overset{*\varepsilon}{\underset{\sim}{L}}_{\ell m}(r_o)\,\underset{\sim}{L}^{-\varepsilon}_{\ell m}(r)\right] \qquad (2.13)$$

where $\varepsilon = \text{sgn}\,(r-r_o)$ and $r = |\underset{\sim}{x}|$.

$$\underset{\sim}{M}^{\pm} = \underset{\sim}{\nabla} \times (\hat{e}_r\,\psi^{\pm}_\beta)\,;\quad \underset{\sim}{N}^{\pm} = \frac{1}{k_\beta}(\underset{\sim}{\nabla}\times\underset{\sim}{\nabla}\times\hat{e}_r\psi^{\pm}_\beta)\,;\quad L^{\pm} = \frac{1}{k_\alpha}\psi^{\pm}_\alpha$$

$$k_\alpha = \frac{\omega}{\alpha} \quad ; \quad k_\beta = \frac{\omega}{\beta}$$

Here α,β are the P, S velocities of the medium

$$\psi^{\pm}_\alpha = Y_{\ell m}(\theta,\phi)\left\{\begin{matrix} j_\ell(k_\alpha r) \\ h^{(2)}_\ell(k_\alpha r)\end{matrix}\right\}$$

While $\psi^{\pm}_\beta$ is similarly expressed using k_β .

The operation * refers to complex conjugation of the angular part of the function, while the Hankel function remains unchanged. Explicit forms for $\underset{\sim}{M}$, $\underset{\sim}{N}$ and $\underset{\sim}{L}$ are given later (see equation (3.9) - (3.13)).

3. Solution for Arbitrary Prestress

By expanding all relevant quantities in terms of vector spherical harmonics and using the convenient orthogonality properties of these functions, we can find an exact solution for the radiation field for the sudden creation of a spherical cavity in an arbitrarily prestressed medium. We need to solve the equation:

$$\underset{\sim}{u} = \int_{\Sigma} \underset{\sim}{u} \cdot \underset{\approx}{T}(\underset{\approx}{G}) \cdot \hat{n} \, dA + \underset{\sim}{u}^{I} \tag{3.1}$$

Here $\hat{n}$ is the outward normal $\hat{e}_r$ at the spherical surface.
$\underset{\sim}{u}^{I}$ may be either the initial value term:

$$\underset{\sim}{u}^{I} = + i\omega\rho \int_{V} \underset{\sim}{u}^{*} \cdot \underset{\approx}{G} \, dV \tag{3.2}$$

where V is the volume external to the sphere, or the stress pulse term:

$$\underset{\sim}{u}^{I} = \frac{1}{i\omega} \int_{\Sigma} \underset{\approx}{G} \cdot \underset{\approx}{T}(\underset{\sim}{u}^{*}) \cdot \hat{n} \, dA \tag{3.3}$$

The stress pulse term is easier to evaluate. We will now solve equations (3.1) and (3.3) for a general stress field.

Any vector function can be expanded in the following way:

$$\underset{\sim}{u}(r,\theta,\phi) = \sum_{\ell=0}^{\infty} \sum_{m=-\ell}^{\ell} \left\{ a_{\ell m}^{(1)}(r) \, \underset{\sim}{P}_{\ell m}(\theta,\phi) + a_{\ell m}^{(2)}(r) \, \underset{\sim}{B}_{\ell m}(\theta,\phi) + a_{\ell m}^{(3)}(r) \, \underset{\sim}{C}_{\ell m}(\theta,\phi) \right\} \tag{3.4}$$

$\underset{\sim}{P}_{\ell m}$, $\underset{\sim}{B}_{\ell m}$, $\underset{\sim}{C}_{\ell m}$ are vectors defined by (see Morse and Feshbach (1953) or Ben-Menahem and Singh (1968)):

$$\underset{\sim}{P}_{\ell m} = \hat{e}_r \, Y_{\ell m}(\theta,\phi)$$

$$\sqrt{\ell(\ell+1)}\,\underset{\sim}{B}_{\ell m} = \left[\hat{e}_\theta \frac{\partial}{\partial\theta} + \hat{e}_\phi \frac{1}{\sin\theta}\frac{\partial}{\partial\phi}\right] Y_{\ell m}(\theta,\phi) \tag{3.5}$$

$$\sqrt{\ell(\ell+1)}\,\underset{\sim}{C}_{\ell m} = \left[\hat{e}_\theta \frac{1}{\sin\theta}\frac{\partial}{\partial\phi} - \hat{e}_\phi \frac{\partial}{\partial\theta}\right] Y_{\ell m}(\theta,\phi)$$

$$Y_{\ell m}(\theta,\phi) = P_{\ell m}(\cos\theta)\, e^{im\phi}$$

where $P_{\ell m}(x)$ is the associated Legendre function. These vectors have the following orthogonality relations:

$$\int \overline{\underset{\sim}{P}}_{\ell m} \cdot \underset{\sim}{B}_{\ell' m'}\, d\Omega = \int \overline{\underset{\sim}{P}}_{\ell m} \cdot \underset{\sim}{C}_{\ell' m'} d\Omega = \int \overline{\underset{\sim}{B}}_{\ell m} \cdot \underset{\sim}{C}_{\ell' m'} d\Omega = 0$$

and (3.6)

$$\int \overline{\underset{\sim}{P}}_{\ell m} \cdot \underset{\sim}{P}_{\ell' m'} d\Omega = \int \overline{\underset{\sim}{B}}_{\ell m} \cdot \underset{\sim}{B}_{\ell' m'} d\Omega = \int \overline{\underset{\sim}{C}}_{\ell m} \underset{\sim}{C}_{\ell' m'} d\Omega = \delta_{\ell\ell'}\delta_{mm'}\Omega_{\ell m}$$

$$\Omega_{\ell m} = \frac{4\pi}{2\ell+1}\frac{(\ell+m)!}{(\ell-m)!}$$

Either by inspection or by using the orthogonality relations we can expand $\underset{\sim}{u}^I$ in the form:

$$\underset{\sim}{u}^{I}(\omega,r,\theta,\phi) = \sum_{\ell=0}^{\infty} \sum_{m=-\ell}^{\ell} \Big\{ d^1_{\ell m}(r,\omega)\, \underset{\sim}{P}_{\ell m}(\theta,\phi) + d^2_{\ell m}(r,\omega)\, \underset{\sim}{B}_{\ell m}(\theta,\phi) + d^3_{\ell m}(r,\omega)\, \underset{\sim}{C}_{\ell m}(\theta,\phi) \Big\} \tag{3.7}$$

We can also expand the unknown displacement field $\underset{\sim}{u}$ in the form

$$\underset{\sim}{u}(\omega,r,\theta,\phi) = \sum_{\ell=0}^{\infty} \sum_{m=-\ell}^{\ell} \Big\{ b^1_{\ell m}(r,\omega)\, \underset{\sim}{P}_{\ell m}(\theta,\phi) + b^2_{\ell m}(r,\omega)\, \underset{\sim}{B}_{\ell m}(\theta,\phi) + b^3_{\ell m}(r,\omega)\, \underset{\sim}{C}_{\ell m}(\theta,\phi) \Big\} \tag{3.8}$$

The Green's tensor for this problem is given by equation (2.13). In terms of the vectors $\underset{\sim}{P}$, $\underset{\sim}{B}$, $\underset{\sim}{C}$ we can write (Ben-Menahem and Singh (1968))

$$\begin{aligned} \underset{\sim}{M}^{\pm}_{\ell m} &= g^{\pm}_1(y)\, \underset{\sim}{C}_{\ell m} \\ \underset{\sim}{N}^{\pm}_{\ell m} &= g^{\pm}_2(y)\, \underset{\sim}{P}_{\ell m} + g^{\pm}_3(y)\, \underset{\sim}{B}_{\ell m} \\ \underset{\sim}{L}^{\pm}_{\ell m} &= g^{\pm}_4(x)\, \underset{\sim}{P}_{\ell m} + g^{\pm}_5(x)\, \underset{\sim}{B}_{\ell m} \end{aligned} \tag{3.9}$$

where $y = k_\beta r$, $x = k_\alpha r$. The vector $\underset{\sim}{M}$ represents toroidal waves. The vectors $\underset{\sim}{L}$ and $\underset{\sim}{N}$ represent P and S spheroidal waves respectively.

We also need the associated tractions

$$\begin{aligned} \underset{\approx}{T}(\underset{\sim}{M}^{\pm}_{\ell m})\cdot\hat{n} &= \mu h^{\pm}_1(y)\, \underset{\sim}{C}_{\ell m} \\ \underset{\approx}{T}(\underset{\sim}{N}^{\pm}_{\ell m})\cdot\hat{n} &= \mu\Big(h^{\pm}_2(y)\, \underset{\sim}{P}_{\ell m} + h^{\pm}_3(y)\, \underset{\sim}{B}_{\ell m} \Big) \\ \ell(\ell+1)\left(\frac{\beta}{\alpha}\right)^3 \underset{\approx}{T}(\underset{\sim}{L}^{\pm}_{\ell m})\cdot\hat{n} &= \mu\Big(h^{\pm}_4(x)\, \underset{\sim}{P}_{\ell m} + h^{\pm}_5(x)\, \underset{\sim}{B}_{\ell m} \Big) \end{aligned} \tag{3.10}$$

where

$$g_\ell^{1\pm}(y) = \sqrt{\ell(\ell+1)}\, f_\ell^{\pm}(y)$$

$$g_\ell^{2\pm}(y) = \ell(\ell+1)\, \frac{f_\ell^{\pm}(y)}{y}$$

$$g_\ell^{3\pm}(y) = \sqrt{\ell(\ell+1)} \left(f_\ell^{\pm\prime}(y) + \frac{f_\ell^{\pm}(y)}{y} \right)$$

$$g_\ell^{4\pm}(x) = f_\ell^{\mp\prime}(x)$$

$$g_\ell^{5\pm}(x) = \sqrt{\ell(\ell+1)}\, \frac{f_\ell^{\mp}(x)}{x}$$

$$h_\ell^{1\pm}(y) = k_\beta \sqrt{\ell(\ell+1)}\, y\, F_{\ell 1}^{\pm}(y)$$

$$h_\ell^{2\pm}(y) = 2k_\beta\, \ell(\ell+1)\, F_{\ell 1}^{\pm}(y)$$

$$h_\ell^{3\pm}(y) = k_\beta \sqrt{\ell(\ell+1)}\, F_{\ell 3}^{\pm}(y) \qquad (3.11)$$

$$h_\ell^{4\pm}(x) = 2k_\alpha\, F_{\ell 4}^{\pm}(x)\, \ell(\ell+1) \left(\frac{\beta}{\alpha} \right)^3$$

$$h_\ell^{5\pm}(x) = 2k_\alpha \sqrt{\ell(\ell+1)}\, F_{\ell 1}^{\mp}(x)\, \ell(\ell+1) \left(\frac{\beta}{\alpha} \right)^3$$

$$F_{\ell 1}^{\pm}(z) = \frac{1}{(2\ell-1)(2\ell+1)(2\ell+3)} \left[(\ell-1)(2\ell+3) f_{\ell-2}^{\pm}(z) - (2\ell+1)\, f_\ell^{\pm}(z) - (\ell+2)(2\ell-1)\, f_{\ell+2}^{\pm}(z) \right]$$

$$F_{\ell 3}^{\pm}(z) = \frac{1}{(2\ell-1)(2\ell+1)(2\ell+3)} \left[2(\ell^2-1)(2\ell+3) f_{\ell-2}^{\mp}(z) - 3(2\ell+1) f_\ell^{\pm}(z) \right.$$

$$\left. + 2\ell(\ell+2)(2\ell-1)\, f_{\ell+2}^{\pm}(z) \right]$$

$$F^{\pm}_{\ell 4}(z) = \frac{1}{(2\ell-1)(2\ell+1)(2\ell+3)}\Big[\ell(\ell-1)(2\ell+3)\ f^{\pm}_{\ell-2}(z) + (\ell+1)(\ell+2)(2\ell-1)\ f^{\pm}_{\ell+2}(z)$$

$$- (2\ell+1)\left\{2\ell^2 + 2\ell - 1 + \frac{\alpha^2-2\beta^2}{2\beta^2}(2\ell-1)(2\ell+3)\right\} f^{\pm}_{\ell}(z)\Big]$$

where $f^{\pm}_{\ell}$ are spherical Bessel (+) and outgoing Hankel (-) functions. (There is a misprint in Ben-Menahem and Singh's definition of $F_{\ell 3}$ which is corrected here.)

The surface integral in equation (3.1) can now be evaluated. Because of the orthogonality relations (3.6) the surface integrals give either $R^2\Omega_{\ell m}$ or zero. The integral equation has now been reduced to a set of algebraic equations. In fact, the individual terms in the eigenfunction expansion are almost completely uncoupled. The remaining equations for each value of ℓ are:

$$b^1_{\ell m}(r) = \frac{-ik_\beta R^2}{\ell(\ell+1)}\Big(g^{2-}_{\ell}(r)\ b^1_{\ell m}(R)\ h^{2+}_{\ell}(R) + g^{4-}_{\ell}(r)\ b^1_{\ell m}(R)\ h^{4+}_{\ell}(R)$$

$$+ g^{2-}_{\ell}(r)\ b^2_{\ell m}(R)\ h^{3+}_{\ell}(R) + g^{4-}_{\ell}(r)\ b^2_{\ell m}(R)\ h^{5+}_{\ell}(R)\Big) + d^1_{\ell m}(r)$$

(3.12)

$$b^2_{\ell m}(r) = \frac{-ik_\beta R^2}{\ell(\ell+1)}\Big(g^{3-}_{\ell}(r)\ b^1_{\ell m}(R)\ h^{2+}_{\ell}(R) + g^{5-}_{\ell}(r)\ b^1_{\ell m}(R)\ h^{4+}_{\ell}(R)$$

$$+ g^{3-}_{\ell}(r)\ b^2_{\ell m}(R)\ h^{3+}_{\ell}(R) + g^{5-}_{\ell}(r)\ b^2_{\ell m}(R)\ h^{5+}_{\ell}(R)\Big)$$

$$+ d^2_{\ell m}(r)$$

$$b^3_{\ell m}(r) = \frac{-ik_\beta R^2}{\ell(\ell+1)}\Big(g^{1-}_{\ell}(r)\ b^3_{\ell m}(R)\ h^{1+}_{\ell}(R)\Big) + d^3_{\ell m}(r)$$

(The arguments of the g and h functions are understood to be multiplied by k_α or k_β as defined in equation (3.11)).

We can now evaluate these equations at $r = R$ (the cavity radius) and have the solution to the problem.

The coefficients of $\underset{\sim}{C}_{\ell m}$ are uncoupled from the others, so we have immediately letting $\frac{-ik_\beta R^2}{\ell(\ell+1)} = Q_\ell$

$$b^3_{\ell m}(R) = \frac{d^3_{\ell m}(R)}{1 - Q_\ell \; g^{1-}_\ell(R) \; h^{1+}_\ell(R)} \tag{3.13}$$

and at any point r

$$b^3_{\ell m}(r) = d^3_{\ell m}(r) + g^{1-}_\ell(r)\left(\frac{Q_\ell h^{1+}_\ell(R) \; d^3_{\ell m}(R)}{1 - Q_\ell \; g^{1-}_\ell(R) \; h^{1+}_\ell(R)}\right) \tag{3.14}$$

The coefficients $b^1_{\ell m}$ and $b^2_{\ell m}$ are coupled for $\ell \neq 0$. The solution for these is

$$\begin{pmatrix} b^1_{\ell m}(R) \\ b^2_{\ell m}(R) \end{pmatrix} = Q_\ell \begin{pmatrix} A_{11} & A_{12} \\ A_{21} & A_{22} \end{pmatrix} \begin{pmatrix} b^1_{\ell m}(R) \\ b^2_{\ell m}(R) \end{pmatrix} + \begin{pmatrix} d^1_{\ell m}(R) \\ d^2_{\ell m}(R) \end{pmatrix} \tag{3.15}$$

where
$$\begin{aligned} A_{11} &= g^{2-}_\ell(R)\, h^{2+}_\ell(R) + g^{4-}_\ell(R)\, h^{4+}_\ell(R) \\ A_{12} &= g^{2-}_\ell(R)\, h^{3+}_\ell(R) + g^{4-}_\ell(R)\, h^{5+}_\ell(R) \\ A_{21} &= g^{3-}_\ell(R)\, h^{2+}_\ell(R) + g^{5-}_\ell(R)\, h^{4+}_\ell(R) \\ A_{22} &= g^{3-}_\ell(R)\, h^{3+}_\ell(R) + g^{5-}_\ell(R)\, h^{5+}_\ell(R) \end{aligned} \tag{3.16}$$

and

$$\begin{pmatrix} b^1_{\ell m}(R) \\ b^2_{\ell m}(R) \end{pmatrix} = \left(\underset{\sim}{I} - Q_\ell \underset{\sim}{A} \right)^{-1} \begin{pmatrix} d^1_{\ell m}(R) \\ d^2_{\ell m}(R) \end{pmatrix} \tag{3.17}$$

This requires the inversion of only a 2 x 2 matrix. Substitution into equation (3.12) gives the exact solution to this problem.

The case $\ell=0$ must be treated separately since $\underset{\sim}{B}_{oo} = \underset{\sim}{C}_{oo} = 0$. Setting $b^2_{oc} = 0$ we can immediately solve for b^1_{oo}.

$$b_{oo}^{1}(R) = \frac{d_{oo}^{1}(R)}{1-Q_o\, g_o^{4-}(R)\, h_o^{4}(R)} \tag{3.18}$$

$$b_{oo}^{1}(r) = d_{oo}^{1}(r) + \frac{Q_o g_o^{4-}(r)\, h_o^{4+}(R)\, d_{oo}^{1}(R)}{1 - Q_o\, g_o^{4}(R)\, h_o^{4+}(R)} \tag{3.19}$$

The factors of $\ell(\ell+1)$ in Q_o and h_o^4 cancel.

Inspection of the solution (equation 3.12) shows that the displacement field consists only of outgoing spherical waves. If desired, the solution can be written:

$$\underset{\sim}{u}(\underset{\sim}{x},\omega) = \sum_{\ell=0}^{\infty} \sum_{m=-\ell}^{\ell} \alpha_{\ell m}(\omega)\, \underset{\sim}{M}^{-}_{\ell m} + \beta_{\ell m}(\omega)\, \underset{\sim}{N}^{-}_{\ell m} + \gamma_{\ell m}(\omega)\, \underset{\sim}{L}^{-}_{\ell m}$$

where the coefficients $\alpha_{\ell m}$, $\beta_{\ell m}$, $\gamma_{\ell m}$ are determined by comparison with equation (3.12). The first term is a toroidal wave, the second a spheroidal shear wave and the third a spheroidal compressional wave.

4. Pure Shear

The case of the creation of a spherical failure surface in a pure shear field has been used as an element in a model for earthquakes by Archambeau (1968) and Randall (1966). Archambeau (1972) used this as a model to predict anomalous stress wave radiation from explosions. Randall's solution is equivalent to the stress pulse solution which is used here as the initial value term. This problem was solved exactly by Hirasawa and Sato (1963). Their results are reproduced in Koyama et al. (1973). Koyama et al. solved the problem of the creation of a fluid filled cavity in a pure shear field. They report little difference in the waveforms for the two cases.

It is possible to do this problem in two ways. An expression for $\underset{\sim}{u}^*$ is given by Landau and Lifschitz (1970, p. 24). After some effort it can be shown that this can be written in terms of vector spherical harmonics with only the coefficients of $\underset{\sim}{B}_{2m}$ and $\underset{\sim}{P}_{2m}$ non-zero. The initial value integral (equation 3.2) can then be performed. This leads to a very messy expression. It is much easier to use the stress pulse solution and evaluate equation (3.3). $\underset{\approx}{T}(\underset{\sim}{u}^*)\cdot\hat{n}$ is easily found. The initial normal tractions are simply those of a pure shear stress field resolved onto a spherical surface. The final normal tractions are zero. So $\underset{\approx}{T}(\underset{\sim}{u}^*)\cdot\hat{\underset{\sim}{n}} = \sigma_{ij}n_j$ with $\sigma_{11} + \sigma_{22} + \sigma_{33} = 0$ for the most general pure shear field. We need to write these in terms of vector spherical harmonics. After some algebra it can be shown that the most general pure shear field can be written:

$$\underset{\approx}{T}(\underset{\sim}{u^*})\cdot\hat{n} = \sum_{m=-2}^{2} A_{2m}\left(\underset{\sim}{P}_{2m} + \frac{\sqrt{6}}{2}\underset{\sim}{B}_{2m}\right) \tag{4.1}$$

where A_{2m} are coefficients determined by the choice of cartesian stress tensor.

In terms of the cartesian components of the shear stress:

$$\begin{aligned}
A_{22} &= \frac{1}{12}(\sigma_{11} - \sigma_{22}) + \frac{1}{6i}\sigma_{12} \\
A_{21} &= \frac{1}{3}\sigma_{13} + \frac{1}{3i}\sigma_{23} \\
A_{20} &= \sigma_{33} \\
A_{2-1} &= -2\sigma_{13} + \frac{2}{i}\sigma_{23} \\
A_{2-2} &= 2(\sigma_{11} - \sigma_{22}) - \frac{4}{i}\sigma_{12}
\end{aligned} \tag{4.2}$$

Now we can evaluate equation (3.3)

$$\underset{\sim}{u}^I = \frac{1}{i\omega}\int_{\Sigma} \underset{\approx}{G}\cdot\underset{\approx}{T}(\underset{\sim}{u}^*)\cdot\hat{n}\, dA$$

The non-vanishing part of G is

$$\underset{\approx}{G}(\underset{\sim}{x},\underset{\sim}{x}_o) = \frac{-ik_\beta}{4\pi\mu}\frac{5}{6}\sum_{m=-2}^{2}\frac{(2-m)!}{(2+m)!}\left(\underset{\sim}{N}^{*+}_{2m}(\underset{\sim}{x}_o)\,\underset{\sim}{N}^{-}_{2m}(\underset{\sim}{x}) + 6\left(\frac{\beta}{\alpha}\right)^3 \underset{\sim}{L}^{*+}_{2m}(\underset{\sim}{x}_o)\,\underset{\sim}{L}^{-}_{2m}(\underset{\sim}{x})\right) \tag{4.3}$$

Evaluating the surface integral we find

$$u^I = \sum_{m=-2}^{2} \left[d^1_{2m} \underset{\sim}{P}_{2m} + d^2_{2m} \underset{\sim}{B}_{2m} \right] \tag{4.4}$$

where, using the notation of equation (3.11)

$$d^1_{2m} = -\frac{R^2}{6\mu\beta} A_{2m} \left[\left(g_2^{2+}(y_o) + \frac{\sqrt{6}}{2} g_2^{3+}(y_o) \right) g_2^{2-}(y) \right.$$
$$\left. + 6 \left(\frac{\beta}{\alpha} \right)^3 \left(g_2^{4+}(x_o) + \frac{\sqrt{6}}{2} g_2^{5+}(x_o) \right) g_2^{4-}(x) \right]$$

$$d^2_{2m} = -\frac{R^2}{6\mu\beta} A_{2m} \left[\left(g_2^{2+}(y_o) + \frac{\sqrt{6}}{2} g_2^{3+}(y_o) \right) g_2^{3-}(y) \right. \tag{4.5}$$
$$\left. + 6 \left(\frac{\beta}{\alpha} \right)^3 \left(g_2^{4+}(x_o) + \frac{\sqrt{6}}{2} g_2^{5+}(x_o) \right) g_2^{5-}(x) \right]$$

$$x_o = k_\alpha R \qquad x = k_\alpha r \qquad y_o = k_\beta R \qquad y = k_\beta r$$

These coefficients can be substituted into equation (3.17) to obtain the exact solution to this problem. In the far-field approximation g_2^- and g_5^- vanish. The solution then corresponds to a radial P wave and a transverse S wave as it should. The far field P and S spectra for the initial value/stress pulse (eq. 4.4) solution and the exact solution are shown in figure 2. The initial value spectrum contains a large number of dips not present in the exact solution. Burridge (1975) pointed out that these dips result from the stress discontinuity at the end of the pulse. This is a

consequence of the fact that without the inclusion of the surface term (eq. 3.1) there are in effect no boundaries in the medium. All disturbances are then propagated at the corresponding velocity of the medium. The resulting pulses will have a duration equal to the travel time across the cavity. The farfield P and S waveforms are shown in figure 3 for both the initial value and exact solutions. The solution agrees exactly with the solution of Hirasawa and Sato (1963). Their spectra and waveforms are reproduced in Koyama et al. (1973) and match figures 2 and 3.

5. Radiation from Non-Uniform Stress Fields

We want to consider the radiation from a stress free sphere spontaneously created in an arbitrarily prestressed elastic medium. This should be a good model for predicting the tectonic release from explosions. It should also be a good model for the study of spontaneous failure in an inhomogeneous stress field. Minster and Suteau (1977) have examined the question of failure geometry in some detail. The main differences between the planar source and the spherical source is that for the planar source the amplitude is reduced by a factor of 3 and the waveform is smeared out over a longer period of time due to interference of spherical waves leaving different parts of the surface at different times. This smearing effect can also be seen in the numerical results of Madariaga (1976). While we do not expect exact agreement between the radiation produced by an earthquake and radiation produced by a spherical cavity, the cavity can provide information on general features such as the angular distribution and approximate waveforms. Since the spherical cavity problem is exactly solvable, it provides a useful tool for the investigation of the general problem of failure in an inhomogeneous stress field.

The first question to be answered is the nature of different kinds of prestress which are physically acceptable. Any region of the earth, especially seismically active regions will contain many dislocations. These dislocations will act like some complicated distribution of (equivalent) static body forces in the medium. The initial field satisfies $\underset{\approx}{L} \cdot \underset{\sim}{u}^i = \underset{\sim}{f}$ and the final field satisfies $\underset{\approx}{L} \cdot \underset{\sim}{u}^f = \underset{\sim}{f}$, so the difference field satisfies $\underset{\approx}{L} \cdot \underset{\sim}{u}^* = 0$, the static elastic equation

with no body forces acting. This difference field must be finite at infinity. Since we are interested in the region outside $r = R$, the solution representation need not be finite at $r = 0$. The most general static displacement field satisfying these conditions can be expressed in terms of the following eigenvectors (Ben-Menahem and Singh, 1968):

$$\begin{aligned}
\underset{\sim}{N}^{-}_{\ell m} &= r^{-\ell-2}\left[\sqrt{\ell(\ell+1)}\,\underset{\sim}{B}_{\ell m} - (\ell+1)\,\underset{\sim}{P}_{\ell m}\right] \\
\underset{\sim}{F}^{-}_{\ell m} &= r^{-\ell}\,\frac{1}{\gamma}\left[(\gamma-\ell)\,\sqrt{\ell(\ell+1)}\,\underset{\sim}{B}_{\ell m} + (\gamma+\ell-1)\,\ell\,\underset{\sim}{P}_{\ell m}\right] \\
\underset{\sim}{M}^{-}_{\ell m} &= r^{-\ell-1}\,\sqrt{\ell(\ell+1)}\,\underset{\sim}{C}_{\ell m}
\end{aligned} \tag{5.1}$$

where

$$\gamma = 4(1-\sigma) = \frac{2\alpha^2}{\alpha^2 - \beta^2}$$

The displacement field is then

$$\underset{\sim}{u}^{*}(r) = \sum_{\ell m} a_{\ell m}\,\underset{\sim}{N}^{-}_{\ell m} + c_{\ell m}\,\underset{\sim}{F}^{-}_{\ell m} + f_{\ell m}\,\underset{\sim}{M}^{-}_{\ell m} \tag{5.2}$$

We are now in a position to compute the radiation field. The easiest way to do this is, again, to use the stress pulse solution

$$\underset{\sim}{u} = \int_{\Sigma} \underset{\sim}{u} \cdot \underset{\approx}{\underset{\sim}{T}}(\underset{\approx}{\underset{\sim}{G}}) \cdot \hat{n}\,dA + \underset{\sim}{u}^{I} \tag{5.3}$$

where

$$\underset{\sim}{u}^I = \frac{1}{i\omega} \int_\Sigma \underset{\approx}{G} \cdot \underset{\approx}{T}(\underset{\sim}{u}^*) \cdot \hat{n} dA \tag{5.4}$$

We need to compute $\underset{\approx}{T}(\underset{\sim}{u}^*) \cdot \hat{e}_r$ for $\underset{\sim}{u}^*$ given in equation 5.2. The stress field is given in spherical coordinates by:

$$\tau_{rr} = \lambda\varepsilon + 2\mu \frac{\partial u_r}{\partial r}$$

$$\tau_{\theta r} = \mu[\frac{\partial u_\theta}{\partial r} + \frac{1}{r}(\frac{\partial u_r}{\partial \theta} - u_\theta)]$$

$$\tau_{\phi r} = \mu[\frac{\partial u_\phi}{\partial r} + \frac{1}{r\sin\theta}(\frac{\partial u_r}{\partial \phi} - \sin\theta\, u_\phi)] \tag{5.5}$$

where

$$\varepsilon = \frac{\partial u_r}{\partial r} + \frac{1}{r}(\frac{\partial u_\theta}{\partial \theta} + 2u_r) + \frac{1}{r\sin\theta}\frac{\partial u_\phi}{\partial \phi} + \frac{\cot\theta}{r} u_\theta$$

We consider any function of the form:

$$\underset{\sim}{u}(r,\theta,\phi) = \sum_{\ell,m}\left[f_{1\ell m}(r)\, \underset{\sim}{P}_{\ell m}(\theta,\phi) + f_{2\ell m}(r)\, \underset{\sim}{B}_{\ell m}(\theta,\phi) + f_{3\ell m}(r)\, \underset{\sim}{C}_{\ell m}(\theta,\phi)\right] \tag{5.6}$$

Using the expressions for $\underset{\sim}{P}$, $\underset{\sim}{B}$ and $\underset{\sim}{C}$ (equations 3.5) and the equation for $Y_{\ell m}(\theta,\phi)$:

$$\left[\frac{\partial^2}{\partial\theta^2} + \cot\theta \frac{\partial}{\partial\theta} + \frac{1}{\sin^2\theta}\frac{\partial^2}{\partial\phi^2} + \ell(\ell+1)\right] Y_{\ell m}(\theta,\phi) = 0 \tag{5.7}$$

we have after some algebra:

$$\underset{\sim}{T}(\underset{\sim}{u}) \cdot \hat{e}_r = \sum_{\ell m} [\lambda(\frac{\partial f_{1\ell m}}{\partial r} + \frac{2f_{1\ell m}}{r} - \sqrt{\ell(\ell+1)}\ \frac{f_{2\ell m}}{r}) + 2\mu \frac{\partial f_{1\ell m}}{\partial r}] \underset{\sim}{P}_{\ell m}(\theta,\phi)$$

$$+ \mu(\frac{\partial f_{2\ell m}}{\partial r} + \sqrt{\ell(\ell+1)}\ \frac{f_{1\ell m}}{r} - \frac{f_{2\ell m}}{r})\ \underset{\sim}{B}_{\ell m}(\theta,\phi)$$

$$+ \mu(\frac{\partial f_{3\ell m}}{\partial r} - \frac{f_{3\ell m}}{r})\ \underset{\sim}{C}_{\ell m}(\theta,\phi) \qquad (5.8)$$

comparing with expression (5.2) we find

$$\underset{\approx}{T}(\underset{\sim}{u}^*) \cdot \hat{e}_r = \sum_{\ell m} \underset{\sim}{P}_{\ell m}(\theta,\phi) \left\{ a_{\ell m}\, r^{-\ell-3}\, [2\mu(\ell+1)\ (\ell+2)] \right.$$

$$\left. + \frac{c_{\ell m}}{\gamma}\, r^{-\ell-1}\, [(\gamma+\ell-1)\ (\lambda\ell-2\ell^2\ (\lambda+\mu)) + \lambda\ell(\ell+1)(2\ell-1)] \right\}$$

$$+ \sqrt{\ell(\ell+1)}\ \underset{\sim}{B}_{\ell m}(\theta,\phi)\ \left\{ a_{\ell m}\, r^{-\ell-3}\, 2\mu(-(\ell+2)) \right.$$

$$\left. + \frac{c_{\ell m}}{\gamma}\, r^{-\ell-1}\, \mu(2\ell^2-\gamma) \right\}$$

$$+ \sqrt{\ell(\ell+1)}\ \underset{\sim}{C}_{\ell m}(\theta,\phi) \left\{ f_{\ell m}\, r^{-\ell-2}\, \mu(-(\ell+2)) \right\} \qquad (5.9)$$

Comparing this with results from the last section, we find that pure shear corresponds to

$$a_{2m} = \frac{6}{5} R^2\, k_{2m}$$

$$c_{2m} = \gamma\, k_{2m} \qquad (5.10)$$

where k_{2m} are constants depending on the stress magnitude and orientation.

Using the Green's tensor (eq. 2.13) for $r > r_o$ with $r_o = R$, and using the notation of equations (3.11), we can now evaluate equation (5.4) for the most general initial stress field, we have:

$$\underset{\sim}{u}^I = \frac{-R^2}{\beta\mu} \sum_{\ell=0}^{\infty} \frac{1}{\ell(\ell+1)} \sum_{m=-\ell}^{\ell} \tag{5.11}$$

$$f_{\ell m}\, g_\ell^{1-}(k_\beta r)\left[s_{\ell 1}(R)\; g_\ell^{1+}(k_\beta R)\right] \underset{\sim}{C}_{\ell m}(\theta,\phi)$$

$$+ a_{\ell m}\, g_\ell^{2-}(k_\beta r)\left[s_{\ell 2}(R)\; g_\ell^{2+}(k_\beta R) + s_{\ell 4}(R)\; g_\ell^{3+}(k_\beta R)\right] \underset{\sim}{P}_{\ell m}(\theta,\phi)$$

$$+ c_{\ell m}\, g_\ell^{2-}(k_\beta r)\left[s_{\ell 3}(R)\; g_\ell^{2+}(k_\beta R) + s_{\ell 5}(R)\; g_\ell^{3+}(k_\beta R)\right] \underset{\sim}{P}_{\ell m}(\theta,\phi)$$

$$+ a_{\ell m}\, g_\ell^{3-}(k_\beta r)\left[s_{\ell 2}(R)\; g_\ell^{2+}(k_\beta R) + s_{\ell 4}(R)\; g_\ell^{3+}(k_\beta R)\right] \underset{\sim}{B}_{\ell m}(\theta,\phi)$$

$$+ c_{\ell m}\, g_\ell^{3-}(k_\beta r)\left[s_{\ell 3}(R)\; g_\ell^{2+}(k_\beta R) + s_{\ell 5}(R)\; g_\ell^{3+}(k_\beta R)\right] \underset{\sim}{B}_{\ell m}(\theta,\phi)$$

$$+ a_{\ell m}\, g_\ell^{4-}(k_\alpha r)\; \ell(\ell+1)\left(\frac{\beta}{\alpha}\right)^3\left[s_{\ell 2}(R)\; g_\ell^{4+}(k_\alpha R) + s_{\ell 4}(R)\; g_\ell^{5+}(k_\beta R)\right] \underset{\sim}{P}_{\ell m}(\theta,\phi)$$

$$+ c_{\ell m}\, g_\ell^{4-}(k_\alpha r)\; \ell(\ell+1)\left(\frac{\beta}{\alpha}\right)^3\left[s_{\ell 3}(R)\; g_\ell^{4+}(k_\alpha R) + s_{\ell 5}(R)\; g_\ell^{5+}(k_\beta R)\right] \underset{\sim}{P}_{\ell m}(\theta,\phi)$$

$$+ a_{\ell m}\, g_\ell^{5-}(k_\alpha r)\; \ell(\ell+1)\left(\frac{\beta}{\alpha}\right)^3\left[s_{\ell 2}(R)\; g_\ell^{4+}(k_\alpha R) + s_{\ell 4}(R)\; g_\ell^{5+}(k_\beta R)\right] \underset{\sim}{B}_{\ell m}(\theta,\phi)$$

$$+ c_{\ell m}\, g_\ell^{5-}(k_\alpha r)\; \ell(\ell+1)\left(\frac{\beta}{\alpha}\right)^3\left[s_{\ell 3}(R)\; g_\ell^{4+}(k_\alpha R) + s_{\ell 5}(R)\; g_\ell^{5+}(k_\beta R)\right] \underset{\sim}{B}_{\ell m}(\theta,\phi)$$

where the static s functions are given by:

$$
\begin{aligned}
s_{\ell 1} &= \frac{-\mu(\ell+2)}{R^{\ell}}\sqrt{\ell(\ell+1)} \\
s_{\ell 2} &= \frac{2\mu(\ell+1)(\ell+2)}{R^{\ell+1}} \\
s_{\ell 3} &= \frac{(\gamma+\ell-1)(\lambda\ell-2\ell^2(\lambda+\mu)) + \lambda\ell(\ell+1)(2\ell-1)}{\gamma\, R^{\ell-1}} \\
s_{\ell 4} &= -\frac{2\mu(\ell+2)\sqrt{\ell(\ell+1)}}{R^{\ell+1}} \\
s_{\ell 5} &= \frac{\mu(2\ell^2-\gamma)\sqrt{\ell(\ell+1)}}{\gamma\, R^{\ell-1}}
\end{aligned}
\tag{5.12}
$$

This is the initial value field corresponding to a stress pulse applied at r = R at time t=0 in an infinite medium. The first term in this expression corresponds to a toroidal shear wave. The next four terms corresponds to a spheroidal shear wave and the last four terms correspond to a compressional wave. In the farfield $g_{\ell}^{2-} = g_{\ell}^{5-} = 0$. Then the remaining terms correspond to a pure radial P-wave and a pure transverse S wave. The coefficients of $\underset{\sim}{P}$, $\underset{\sim}{B}$ and $\underset{\sim}{C}$ correspond to $d^1_{\ell m}$, $d^2_{\ell m}$ and $d^3_{\ell m}$ in equations (3.14) and (3.17). Thus, (5.11) determines the complete solution for the radiation field due to creation of a spherical cavity with the most general prestress.

The coefficients $a_{\ell m}$, $c_{\ell m}$, and $f_{\ell m}$ are independent until a specific prestress is defined. These coefficients depend on the static field only and are independent of frequency. There will therefore be three independent waves - a toroidal wave and two spheroidal waves for each value of ℓ. The spectra for $\ell = 2$ are shown in figure 4. The two spheroidal waves corresponding to coefficients $a_{\ell m}$, $c_{\ell m}$ are labeled P1, SV1, and P2, SV2, respectively. The

toroidal mode is labeled SH. It is interesting to note that the $\ell = 2$ modes consist partially of peaked spectra and partly of spectra which are flat in the low frequency limit. The linear combination of these (eq. 5.10) that corresponds to pure shear has a flat spectrum.

The $\ell = 2$ waveforms are shown in Figure 5. These look much different than the waveforms for pure shear, but in fact the linear combination of these given in equation (5.10) is the pure shear pulse.

The waveforms for higher ℓ values have more and more oscillations. An example is given in Figure 6 for the $\ell = 4$ waveforms. The result of this is that the spectra become more and more peaked for higher order ℓ values and the maximum frequency increases slightly for each increment in ℓ. The slope of each peak as $\omega \to 0$ increases with ℓ. The slope of each spectrum as $\omega \to \infty$ is -2 for all ℓ. Figure 7 shows the individual P1 spectra for $\ell = 3$, 4, 5 and 6. The magnitude of these peaks will vary with angle as the corresponding vector spherical harmonic. It will therefore vary more rapidly with angle than pure shear.

These results shed some light on the old argument about low frequency spectral peaks in relaxation problems. Archambeau (1968) solved the problem for the radiation from a spherical cavity in pure shear, but he made an approximation for a more localized stress field by truncating the volume integral (similar to equation 3.2) at a radius R_s. This always leads to a low frequency spectral peak in the far field. Minster (1973) discussed this problem in some detail. Snoke (1976) showed that this approximation leads to acausal results in the time domain and concluded that the approximation was incorrect and that the spectral peaks were therefore spurious. Our results are somewhat different from those of Archambeau's R_s spectral peak. That approximation removed energy from the low frequency part of the

spectrum at wavelengths greater than R_s. Our results show that a spectral peak can in fact exist, but the effect is to add in additional energy at frequencies slightly above the "corner frequency" defined by the pure shear spectrum. Also, the magnitude of the spectral peak will vary with angle. If the prestress is predominantly pure shear, then a spectral peak will be observed only near the quadrupole nodes. If the stress were more inhomogeneous then the peak can be observed at all angles of observation. Examples of this are given in the next section. There have been a number of observations of spectral peaks from earthquakes and explosions (e.g., Linde and Sacks, 1971) and an inhomogeneous prestress is a likely reason for this.

Also shown in figures 4, 5 and 6 are the waveforms and spectra for the relaxation/stress pulse term (eq. 5.11) alone. Physically, the stress pulse term corresponds to a sudden stress equal in magnitude to minus the initial prestress on a spherical surface in an infinite medium. Thus scattering diffraction by the cavity are neglected and the stress pulse is rapidly radiated away. The stress pulse term is a fairly good approximation to the exact solution, especially near the beginning of the pulse. The main differences are that the stress pulse term is smaller in amplitude and stops abruptly at $t = 2R/v$. The exact waveform looks like a stretched out version of the stress pulse term. The spectra contain many dips not present in the exact solution. These are due to the abrupt end to the waveform. These are the same features found by Burridge (1975) when he compared his exact solution for a growing spherical cavity in a pure shear field against Archambeau's "transparent source approximation" to the same problem. Use of the stress pulse term alone is similar to the transparent source approximation, but has some advantages. The transparent source required the solution of the static problem before the dynamic problem could be done. Minster (1973) attempted to

use the transparent source approximation for an ellipsoidal rupture, but found the static problem extremely difficult. Also, Archambeau's use of potentials have some singular properties which lead to difficulties in other problems than the case of pure shear he considered. In particular, for the case of a pure compressive stress field, the method gives no radiation. The stress pulse term, on the other hand, is easily evaluated for any geometry. It simply requires doing the surface integral (eq. (3.3)) on an ellipsoidal surface or other surface of interest. It is singular in the limiting case of the dislocation (a flat surface), but can be performed for any surface enclosing a finite volume.

6. Preexisting localized stress fields

In this section we want to examine two physically plausible prestress fields. The first is due to a point source of compression, the second due to a point dislocation. An interesting fact is that both of these stress concentrations look like uniform static shear field when far away from the cavity, but have some anomalous features when nearby.

The simplest inhomogeneous prestress field is due to a point source of compression. Consider a spherical region in the earth which has expanded or contracted. The displacement about the center of the sphere is spherically symmetric and is given outside the spherical region by:

$$\underset{\sim}{u} = -\frac{c}{r^2}\hat{e}_r = c\,\underset{\sim}{\nabla}\frac{1}{r} \tag{6.1}$$

where c is a constant depending on the magnitude of the contraction.

We now consider the seismic radiation when a spherical cavity forms somewhere outside the center of compression. The coordinates are shown in figure 8. To translate the displacement field from the center of compression to the center of the sphere we use the well known expansion of 1/r in spherical harmonics.

$$\frac{1}{r} = \sum_{\ell=0}^{\infty} \frac{R^{\ell}}{L^{\ell+1}} P_{\ell}(\cos\theta) \qquad R < L \tag{6.2}$$

Taking the gradient of this expression, rewriting in terms of vector spherical harmonics and using equation (5.8) to compute the normal tractions, we find

$$\underset{\approx}{T}(\underset{\sim}{u})\cdot\hat{e}_r = 2\mu c \sum_{\ell=2}^{\infty} \frac{R^{\ell-2}}{L^{\ell+1}} \left[\ell(\ell-1)\, P_{\ell 0}(\theta) + (\ell-1)\sqrt{\ell(\ell+1)}\, B_{\ell 0}(\theta) \right] \qquad (6.3)$$

Note that for L >> R

$$\underset{\approx}{T}(\underset{\sim}{u})\cdot\hat{e}_r = \frac{4\mu c}{L^3}\left[\underset{\sim}{P}_{20}(\theta) + \frac{\sqrt{6}}{2}\underset{\sim}{B}_{20}(\theta) \right] \qquad (6.4)$$

which was shown in section 4 to be a pure shear stress field, as noted earlier.

It only remains to compute the coefficients of $\underset{\sim}{u}^*$. The actual static displacement field cannot be expanded as in the last section, but the difference field $\underset{\sim}{u}^*$ can. We can determine the coefficients $a_{\ell m}$, $c_{\ell m}$ by comparison of equation (6.3) with equation (5.9)

For L >> R, the spectra and waveforms are identical to figures 2 and 3. Some interesting features appear when the cavity is closer to the stress concentration. Figure 9 shows the spectra and waveforms near the quadrupole nodes when L = 2R. Instead of vanishing at these angles, the amplitude is reduced by about a factor of 3. The spectra of both the P and S waves are sharply peaked. At angles away from the nodes, the spectra are flat. As the source is moved still closer to the cavity, the spectra change dramatically. Figure 10 show the spectra near the quadrupole maxima when the stress concentration is .1 radius from the cavity surface. The corner frequency is increased by an order of magnitude. The slope above the corner frequency is also changed. The corner frequency is no longer a measure of the size of a cavity. Instead, it is a measure of the area of high stress on the cavity surface. An important and interesting fact is that from observations of first motions only, the radiation pattern appears to be very nearly that of a quadrupole source although the waveforms and spectra vary greatly with angle (see Figure 12).

As a second example we consider a prestress due to a point dislocation located at r = L. The coordinate system is the same as that shown in Figure 8. The initial stress field and the spectra and waveforms are considerably more complicated than for the point source of compression, but the main effects are the same.

The displacement field due to a dislocation is given by the Volterra relation (e.g. Steketee, 1958)

$$\underset{\sim}{u}(\underset{\sim}{x}) = \int_S \underset{\sim}{u}(\underset{\sim}{x}_o) \cdot \underset{\approx}{T}(\underset{\approx}{G}(\underset{\sim}{x},\underset{\sim}{x}_o)) \cdot \hat{n}\, dA_o \tag{6.5}$$

where the integral is over the surface of the dislocation and G is the static elastic Green's tensor. Since we consider only a point Green's tensor, the integral becomes:

$$\underset{\sim}{u}(\underset{\sim}{x}) = \underset{\sim}{S} \cdot \underset{\approx}{T}(\underset{\approx}{G}) \cdot \hat{n} \tag{6.6}$$

where $\underset{\sim}{S}$ is the slip vector $\underset{\sim}{S} = \Delta\underset{\sim}{u}\Delta A$. The dot products with $\hat{n}$ and $\underset{\sim}{S}$ are interchangeable. The static Green's tensor is given by Ben-Menahem and Singh (1968) and can be written for $|\underset{\sim}{x}| < |\underset{\sim}{x}_o|$:

$$\underset{\approx}{G}(\underset{\sim}{x},\underset{\sim}{x}_o) = \frac{1}{4\pi\mu} \sum_{\ell=1,1,0}^{\infty} \sum_{m=-\ell}^{\ell} \frac{(\ell-m)!}{(\ell+m)!} \left[\frac{\underset{\sim}{M}^{+}_{\ell m}(\underset{\sim}{x})\, \underset{\sim}{M}^{*-}_{\ell m}(\underset{\sim}{x}_o)}{\ell(\ell+1)} + \frac{\underset{\sim}{N}^{+}_{\ell m}(\underset{\sim}{x})\, \underset{\sim}{F}^{*-}_{\ell m}(\underset{\sim}{x}_o)}{\ell(2\ell-1)} + \frac{\underset{\sim}{F}^{+}_{\ell m}(\underset{\sim}{x})\, \underset{\sim}{N}^{*-}_{\ell m}(\underset{\sim}{x}_o)}{(\ell+1)\ (2\ell+3)} \right] \tag{6.7}$$

The vectors indexed with a minus are the same as those in equation (5.1). The remaining eigenvectors are:

$$\begin{aligned}
\underset{\sim}{N}^{+}_{\ell m} &= r^{\ell-1}\left[\sqrt{\ell(\ell+1)}\ \underset{\sim}{B}_{\ell m} + \ell\ \underset{\sim}{P}_{\ell m}\right] \\
\underset{\sim}{F}^{+}_{\ell m} &= r^{\ell+1}\,\frac{1}{\gamma}\left[(\ell+1+\gamma)\ \sqrt{\ell(\ell+1)}\ \underset{\sim}{B}_{\ell m} - (\gamma-\ell-2)\ (\ell+1)\ \underset{\sim}{P}_{\ell m}\right] \qquad (6.8) \\
\underset{\sim}{M}^{+}_{\ell m} &= r^{\ell}\ \sqrt{\ell(\ell+1)}\ \underset{\sim}{C}_{\ell m}
\end{aligned}$$

If we restrict the problem so that either the slip vector $\underset{\sim}{S}$ or the normal $\hat{n}$ is in the direction of the radial vector $\hat{e}_r$, we can use equations (5.8) for the stress derivatives. We take the slip direction to be radial, take $S \equiv |\underset{\sim}{S}|$, and for convenience take the normal vector to be $\hat{e}_\theta$. Then

$$\underset{\sim}{u}(\underset{\sim}{x}) = S(\underset{\approx}{T}(\underset{\approx}{G})\cdot\hat{e}_r)\cdot\hat{e}_\theta \qquad (6.9)$$

Most of the terms vanish when the point dislocation is located at $\theta,\phi = 0$. Ben-Menahem and Singh show that in this limit

$$\begin{aligned}
\underset{\sim}{P}_{\ell m} &= \delta_{om}\,\hat{e}_r \\
\sqrt{\ell(\ell+1)}\ \underset{\sim}{B}_{\ell m} &= \frac{1}{2}\left\{\ell(\ell+1)\ \delta_{1m} - \delta_{-1m}\right\}\hat{e}_\theta \\
&\quad + \frac{i}{2}\left\{\ell(\ell+1)\ \delta_{1m} + \delta_{-1m}\right\}\hat{e}_\phi \qquad (6.10) \\
\sqrt{\ell(\ell+1)}\ \underset{\sim}{C}_{\ell m} &= \frac{i}{2}\left\{\ell(\ell+1)\ \delta_{1m} + \delta_{-1m}\right\}\hat{e}_\theta \\
&\quad - \frac{1}{2}\left\{\ell(\ell+1)\ \delta_{1m} - \delta_{-1m}\right\}\hat{e}_\phi
\end{aligned}$$

After some tedious but straightforward calculations, we find that the stress field at the surface of the cavity is:

$$\underset{\approx}{T}(\underset{\sim}{u}^*)\cdot\hat{e}_r\Big|_{r=R} = \frac{S}{4\pi}\left[\sum_{\ell=2}^{\infty}\frac{i\mu(\ell-1)(\ell+2)}{2L^3}\left(\frac{R}{L}\right)^{\ell-1}\left(\frac{\underset{\sim}{C}_{\ell 1}}{\sqrt{\ell(\ell+1)}}+\underset{\sim}{C}_{\ell-1}\sqrt{\ell(\ell+1)}\right)\right.$$

$$+\sum_{\ell=2}^{\infty}\frac{\mu(2\ell^2-\gamma)(\ell-1)}{\gamma\ell(2\ell-1)\,L^3}\left(\frac{R}{L}\right)^{\ell-2}\left(\ell\,\underset{\sim}{P}_{\ell 1}+\sqrt{\ell(\ell+1)}\,\underset{\sim}{B}_{\ell 1}\right.$$

$$\left.-\ell(\ell+1)\left[\ell\,\underset{\sim}{P}_{\ell-1}+\sqrt{\ell(\ell+1)}\,\underset{\sim}{B}_{\ell-1}\right]\right) \qquad (6.11)$$

$$+\sum_{\ell=0}^{\infty}\frac{-(\ell+2)}{\gamma(\ell+1)(2\ell+3)\,L^3}\left(\frac{R}{L}\right)^{\ell}\left(s_1\,\underset{\sim}{P}_{\ell 1}+s_2\sqrt{\ell(\ell+1)}\,\underset{\sim}{B}_{\ell 1}\right.$$

$$\left.\left.-\ell(\ell+1)\left[s_1\underset{\sim}{P}_{\ell-1}+s_2\sqrt{\ell(\ell+1)}\,\underset{\sim}{B}_{\ell-1}\right]\right)\right]$$

where

$$s_1 = \lambda(\ell+1)(2-\gamma)(2\ell+3) + 2\mu\,(\ell+2-\gamma)(\ell+1)^2$$

$$s_2 = \mu(2(\ell+1)^2-\gamma)$$

For L >>R the only remaining term is

$$\underset{\approx}{T}(\underset{\sim}{u}^*)\cdot\hat{e}_r = \frac{A}{L^3}\left[\left(\underset{\sim}{P}_{\ell 1}+\frac{\sqrt{6}}{2}\,\underset{\sim}{B}_{\ell 1}\right)-6\left(\underset{\sim}{P}_{\ell-1}+\frac{\sqrt{6}}{2}\,\underset{\sim}{B}_{\ell-1}\right)\right] \qquad (6.12)$$

which is pure shear field as shown in section 4.

Comparing equation (6.11) with equation (5.9), we can solve for the unknown coefficients $a_{\ell m}$, $c_{\ell m}$, $f_{\ell m}$. We then use equation (5.11) for the initial value field and use the technique for section 3 to find the exact radiation field.

The results are shown in figure 11 for a dislocation located at L = 1.5R, one half radius from the cavity surface. Both the P and S spectra are peaked at all angles. There is a large variation in the slope above the "corner frequency". The pulse is very sharp on the side of the sphere closest to the stress concentration. It is very broad on the other side. The dislocation causes a region of high, nonuniform stress on the closest part of the cavity. This acts as the source of the radiation. The pulses are widest where diffraction is most obvious, on the far side of the cavity. The relaxation/stress pulse term alone matches the exact waveform very well (except for the diffracted arrival) for angles less than 90°, but rather poorly at larger angles. This is to be expected since the surface term which is neglected in that approximation includes the effects of diffraction. An interesting feature of the waveforms is the second arrival seen at low angles. This is a diffracted wave which has travelled around the cavity and back again. An analysis of the first motions shows a relatively simple angular distribution. The distribution is nearly quadrupole for L > 2R. For smaller distances, the angular distribution is more complex (see figure 12). Note that the first motion for angles greater than 90° has actually reversed direction. The distribution is still relatively simple and could easily be misinterpreted as a quadrupole distribution with a finite number of observation points.

Conclusion

We have developed a general method for computing the radiation due to the instantaneous creation of a spherical cavity in an arbitrarily prestressed medium. Vector spherical harmonics were found to be convenient for solving the Green's tensor integral equation in the frequency domain. Transforming the initial value problem to a boundary value (stress pulse) problem proves to be a great simplification and provides an approximate solution as well as an exact solution. The approximate solution is valid when diffraction by the source is not too important. For the case of pure shear, the results of this technique agree with previous solutions.

We have examined the case of inhomogeneous prestress in both a general manner and for the specific cases of a nearby point source of compression and a dislocation. Localized stress concentrations result in:

1. The appearance of energy above the usual corner frequency. This can increase the corner frequency substantially.
2. Far field spectra peaks. These exist near the quadrupole nodes for a slightly inhomogeneous prestress and at all angles for a very localized stress concentration.
3. Non-zero amplitude at the quadrupole nodes.
4. The creation of a diffracted wave which travels around the cavity.
5. A radiation pattern which may or may not appear to be quadrupole in nature but is generally less complex than the change in waveforms and spectra.
6. A sharp wave on the side of the cavity nearest the stress concentration and a broad, more complex wave on the other side.

The results given here may be useful in observational studies since it has implications for both earthquakes and explosion induced tectonic release. In particular, the corner frequency is often used as a measure of the size of the source $R \approx v/\omega_c$ where R is the cavity radius or fault length depending on the type of source being studied and v is the wave velocity. For localized stress concentrations, the corner frequency seems to give an estimate of the size of the stress concentration which may be much smaller than the source dimension. Further, the existence of spectral peaks could lead to errors in estimates of seismic moments. The seismic moment is defined by $M = \mu \bar{u} A$ where μ is the shear modulus, $\bar{u}$ is the mean displacement and A is the surface area of the fault. It is also proportional to the zero frequency far field spectral amplitude (e.g., Kostrov (1974)). If observations are made of spectra only close to the corner frequency, the apparent low frequency amplitude could be much higher than the actual zero frequency amplitude leading to overestimates of seismic moment. This could lead to misinterpretation involving not only fault length, but stress drops as well. In addition to these problems, great care must be taken to remove the effects of the source when doing studies of earth structure since the variation of pulse shape with ("take-off") angle could cause confusion between the effect of earth structure and the effect of localized stress fields.

On the other hand, these results should make it possible to study the local stress variations in the earth. The techniques used in section 5 can be used to invert for the stress (difference) field after an explosion. If a large earthquake is to occur in some region, it means that a large stress concentration has developed which is not relieved by small earthquakes nearby. Observations of a change in the waveforms and spectra of small earthquakes in

an area could indicate a developing stress concentration. Such an observation was made recently by Zoll (1979), who reported a change in the high frequency slope of the spectra of small earthquakes in Missouri from ω^{-1} before a large earthquake to ω^{-2} after the earthquake. He also reported a variation of the slope with azimuth. This is the sort of behavior that is to be expected if a local stress concentration is relieved by the large earthquake. In addition to this, observations of the features described in this paper in the variation of spectra and waveforms with angle could be used to identify the location of developing stress concentrations.

Acknowledgements

I wish to thank C.B. Archambeau for a number of helpful discussions. This work was sponsored by the Advanced Research Project Agency (DOD), ARPA Order No. 3291, Grant No. AFOSR-75-2775 and NSF Grant No. DES 75-20137.

References.

Archambeau, C.B., 1968. General theory of elastodynamic source fields, Rev. Geophys., 16, 241-288.

Archambeau, C.B., 1972. The theory of stress wave radiation from explosions in prestressed media, Geophys. J.R. astr. Soc., 29, 329-366.

Archambeau, C.B., and Minster, J.B., 1978. Dynamics in prestressed media with moving phase boundaries: A continuum theory of failure in solids, Geophys. J. R. astr. Soc., 52, 65-96.

Bache, T.C., and Barker, T.G., 1978. The San Fernando Earthquake, Systems, Science and Software Final Technical Report SSS-R-78-3552.

Ben-Menahem, A., and Singh, J., 1968. Eigenvector expansions of Green's Dyads with applications to geophysical theory, Geophys. J. R. astr. Soc., 16, 417-452.

Burridge, R., 1975. The pulse shapes and spectra of elastic waves generated when a cavity expands in an initial shear field, J. Geophys. Res., 80, 2606-2607.

Burridge, R., and Alterman, Z., 1972. The elastic radiation from an expanding spherical cavity, Geophys. J. R. astr. Soc., 30, 451-477.

Hirasawa, T., and Sato, R., 1963. Propagation of elastic waves from a spherical origin: Part 1 and 2 (in Japanese) Zisin, 16, 52-77.

Kostrov, V.V., 1974. Seismic Moment and Energy of Earthquakes and Seismic Flow of Rock, Izvestia, Earth Physics, 1, 23-40.

Koyama, J., Hāriuchi, S.E., and Hirasawa, T., 1973. Elastic waves generated from sudden vanishing of rigidity in a spherical region, J. Phys. Earth, 21, 213-226.

Landau, L.D., and Lifshitz, E.M., 1970. Theory of Elasticity, Pergamon Press, New York.

Linde, A.T., and Sacks, I.S., 1971. Errors in the spectral analysis of long-period seismic body waves, J. Geophys. Res., 76, 3326-3336.

Madariaga, R., 1976. Dynamics of an expanding circular fault, Bull. Seism. Soc. Am., 66, 639.

Minster, J.B., and Suteau, A., 1977. Far-field waveforms from an arbitrarily expanding transparent spherical cavity in a prestressed medium, Geophys. J. R. astr. Soc., 50, 215-233.

Minster, J.B., 1973. Elastodynamics of failure in a continuum, Ph.D. Thesis, California Institute of Technology, Pasadena, California.

Morse, P.M., and Feshbach, H., 1953. Methods of Theoretical Physics, McGraw-Hill, New York.

Randall, M.J., 1964a. On the mechanism of earthquakes, Bull. Seism. Soc. Am., 54, 1283-1289.

Randall, M.J., 1964b. Seismic energy generated by a sudden volume change, Bull. Seism. Soc. Am., 54, 1291-1298.

Randall, M.J., 1966. Seismic radiation from a sudden phase transition, J. Geophys. Res., 71, 5297-5302.

Snoke, J.A., 1976. Archambeau's elastodynamical source-model solution and low-frequency spectral peaks in the far-field displacement amplitude, Geophys. J.R. astr. Soc., 44, 27-44.

Steketee, I.A., 1958. Some geophysical applications of the elasticity theory of dislocations, Can. J. Phys., 36, 1168.

Zollweg, J.E., 1979. Spectral characteristics of some earthquakes near Centerville, Missouri, Abstract, 74th Annual Meeting of the Seismological Society of America, Earthquake Notes, 49, 42.

Figure Captions.

Fig. 1. The problem considered here. A cavity suddenly forms in a prestressed medium. The radiation due to the relaxation of the stressed material can be computed using a Green's tensor integral equation with the aid of vector harmonics appropriate for the cavity geometry.

Fig. 2. Far field P and S wave spectra for a uniform shear field. The first figures show the spectra for the stress pulse term alone. The second are the exact solutions. The dips in the spectra are removed. The frequency is in units of $\omega R/V$. All examples in this paper use α = 8 km/sec, β = 5 km/sec.

Fig. 3. Far fieldpulse due to the creation of a stress free sphere in a uniform shear field. The exact solutions agree with the solutions of Hirasawa and Sato.

Fig. 4. The most general $\ell = 2$ mode radiation consists of three independent waves-two coupled P and S waves labeled P1, SV1 and P2, SV2 and an uncoupled S wave labeled SH. The spectra for the $\ell = 2$ modes are shown here. Two modes are flat and three are peaked. All higher modes ($\ell > 2$) have peaked spectra.

Fig. 5. Waveforms for general $\ell = 2$ case. A particular linear combination of these produces the pure shear waveforms shown in Figure 3. The second column shows waveforms using the stress pulse term alone. The exact solution is a stretched out version of the approximate solution.

Fig. 6. Waveform for $\ell = 4$. All higher ℓ modes are oscillatory. The number of oscillations increases with ℓ.

Fig. 7. The effect of an inhomogeneous prestress is to add in energy at frequencies higher than the usual corner frequency corresponding to uniform shear. Shown here are the spectra of the far-field first P-wave for $\ell = 3$ to $\ell = 6$ and the pure shear spectrum for comparison. A sufficiently inhomogeneous prestress can result in a low frequency spectral peak which varies in magnitude with angle.

Fig. 8. Coordinate system used when a cavity is created near a preexisting center of compression.

Fig. 9. Far field radiation near the quadrupole nodes. When the center of compression is located one radins away from the cavity, the radiation field is much like a pure shear field. Near the quadrupole nodes however, there is a substantial difference. The displacement does not vanish. It is reduced from the maximum by about a factor of 3. The pulse is oscillatory and the spectrum is peaked.

Fig. 10. Far field spectra near quadrupole maxima. The spectrum is strongly affected by the location of the stress concentration. Note the increase in corner frequency and the change in slope near the corner.

Fig. 11. Radiation field from spherical cavity created one-half radius from a point dislocation. Shown here are the far field spectra and waveforms as a function of angle around the cavity. The spectra are all strongly peaked. The waveforms are narrow on the side of the sphere near the stress concentration, broad on the other side. The second arrival seen on the first three shear waves is a diffracted phase which has travelled around the cavity.

Fig. 12. First motions for localized prestress fields. For $L \geq 2R$, the first motions are very nearly quadrupole in nature. At closer distances, the patterns shift. For the center of compression, there is simply a change in the "nodal" angles. For the dislocation a pulse directed opposite to the quadrupole pulse gradually becomes prominent at large angles. The angular distribution of first motions is less complex than the angular variation of spectra and waveforms.

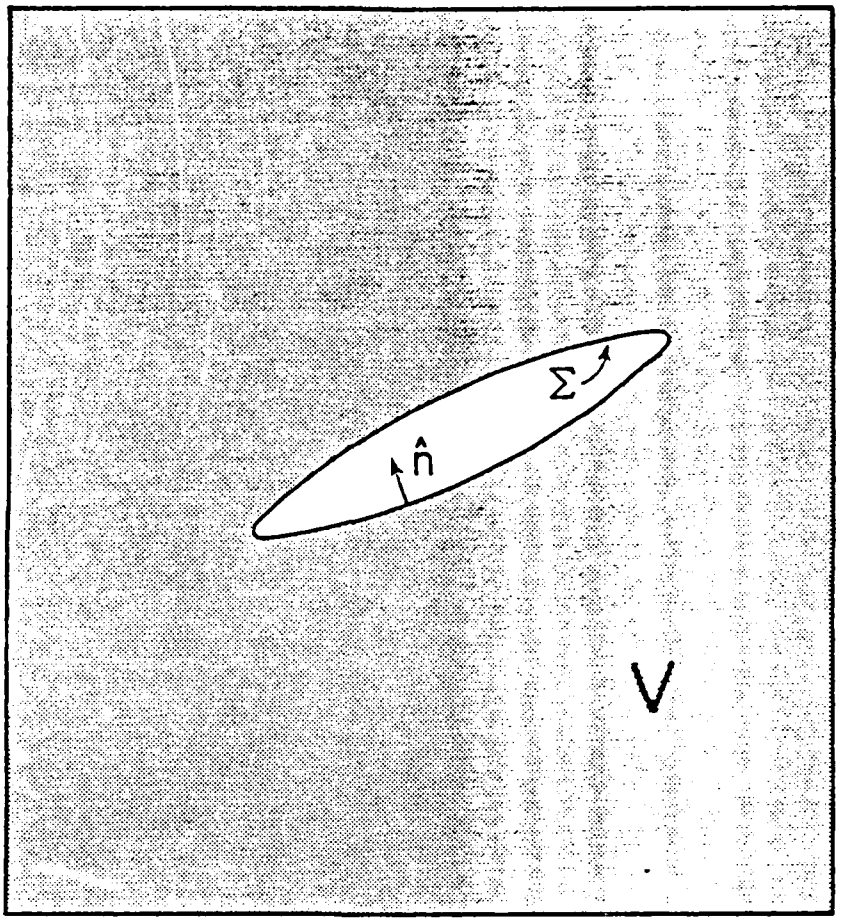
Σ
n̂
V

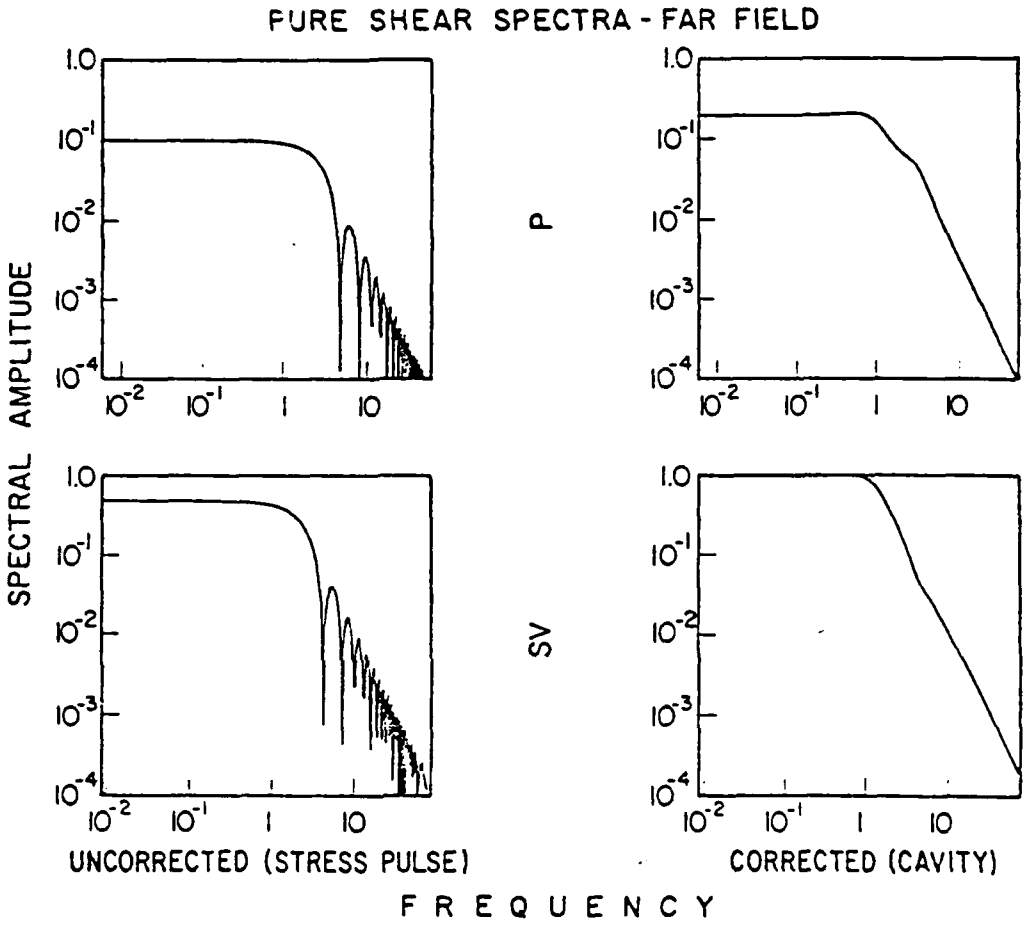
PURE SHEAR SPECTRA - FAR FIELD
SPECTRAL AMPLITUDE
1.0
10^{-1}
10^{-2}
10^{-3}
10^{-4}
10^{-2}
10^{-1}
1
10
P
SV
UNCORRECTED (STRESS PULSE)
CORRECTED (CAVITY)
FREQUENCY

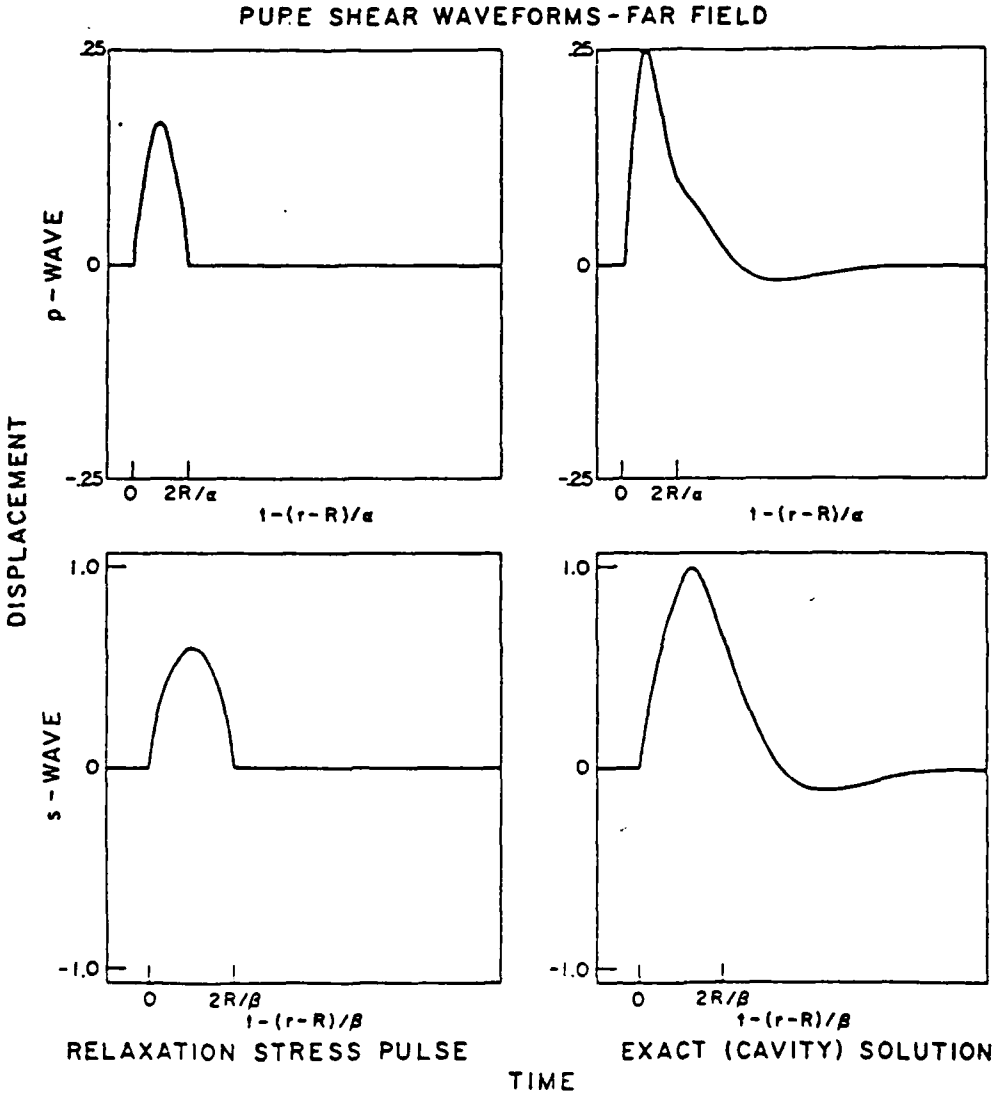
PUPE SHEAR WAVEFORMS - FAR FIELD
DISPLACEMENT
p - WAVE
s - WAVE
.25
0
-.25
1.0
-1.0
0
2R/α
2R/β
1-(r-R)/α
1-(r-R)/β
RELAXATION STRESS PULSE
EXACT (CAVITY) SOLUTION
TIME

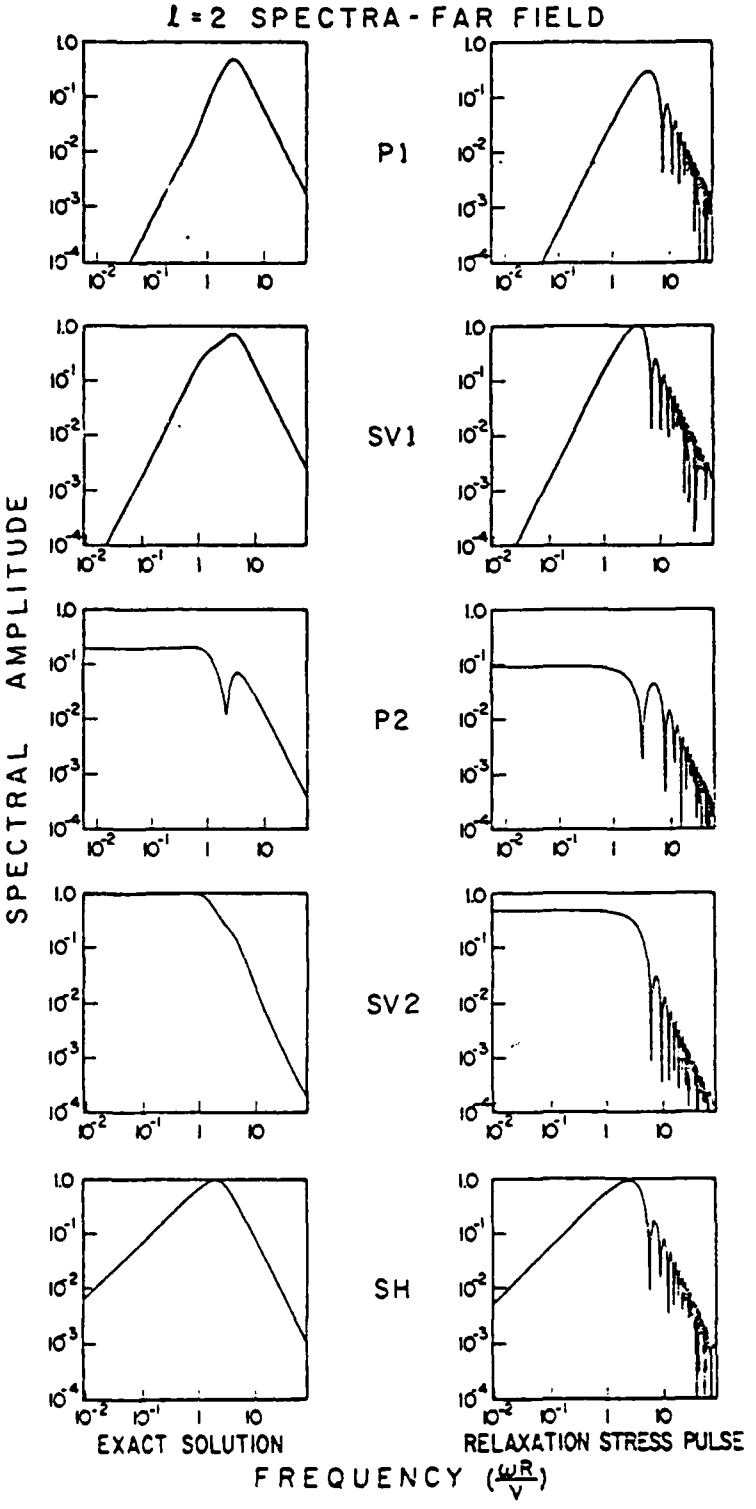
ℓ = 2 SPECTRA - FAR FIELD
P1
SV1
P2
SV2
SH
SPECTRAL AMPLITUDE
EXACT SOLUTION
RELAXATION STRESS PULSE
FREQUENCY (ωR/V)

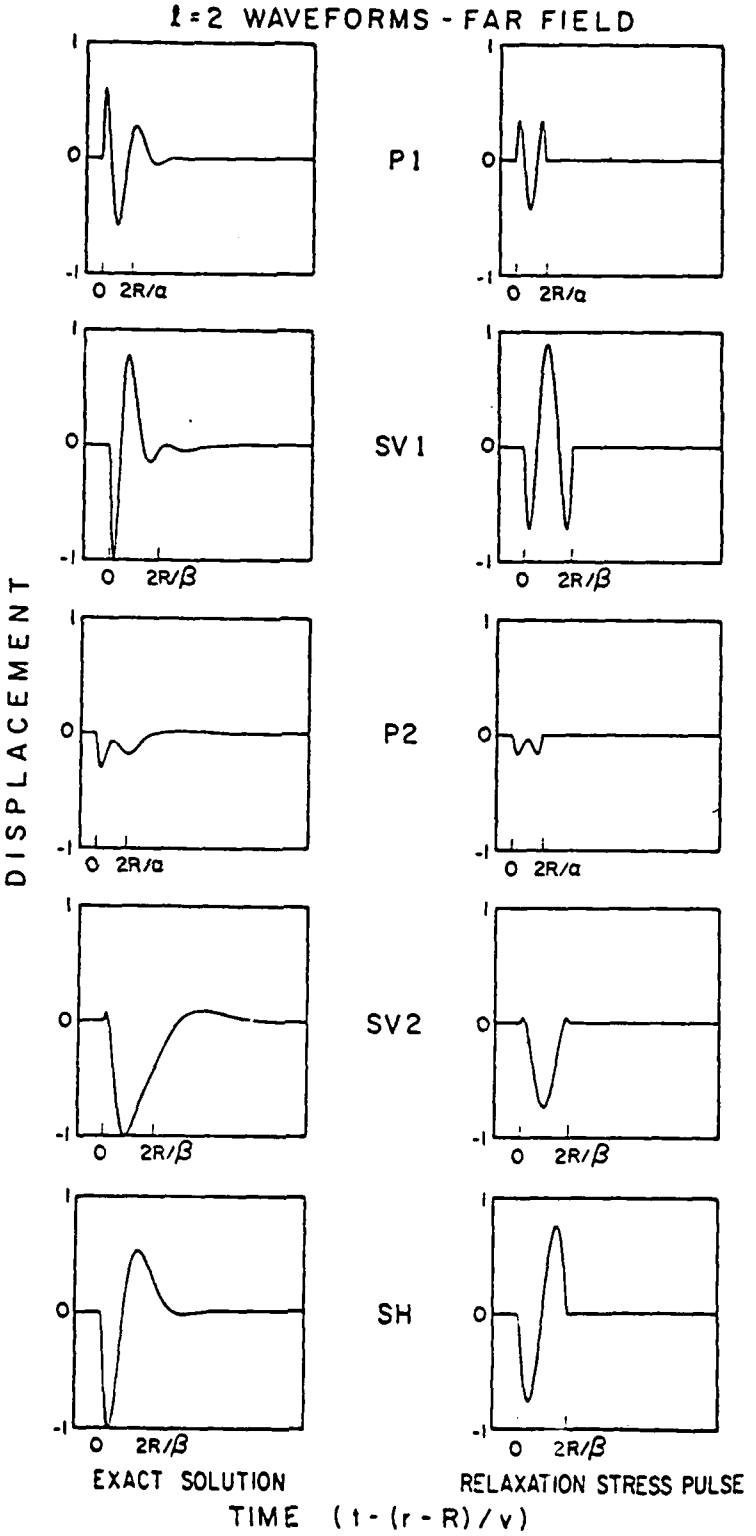
ℓ=2 WAVEFORMS - FAR FIELD
P1
SV1
P2
SV2
SH
DISPLACEMENT
0 2R/α
0 2R/β
EXACT SOLUTION
RELAXATION STRESS PULSE
TIME (t-(r-R)/v)

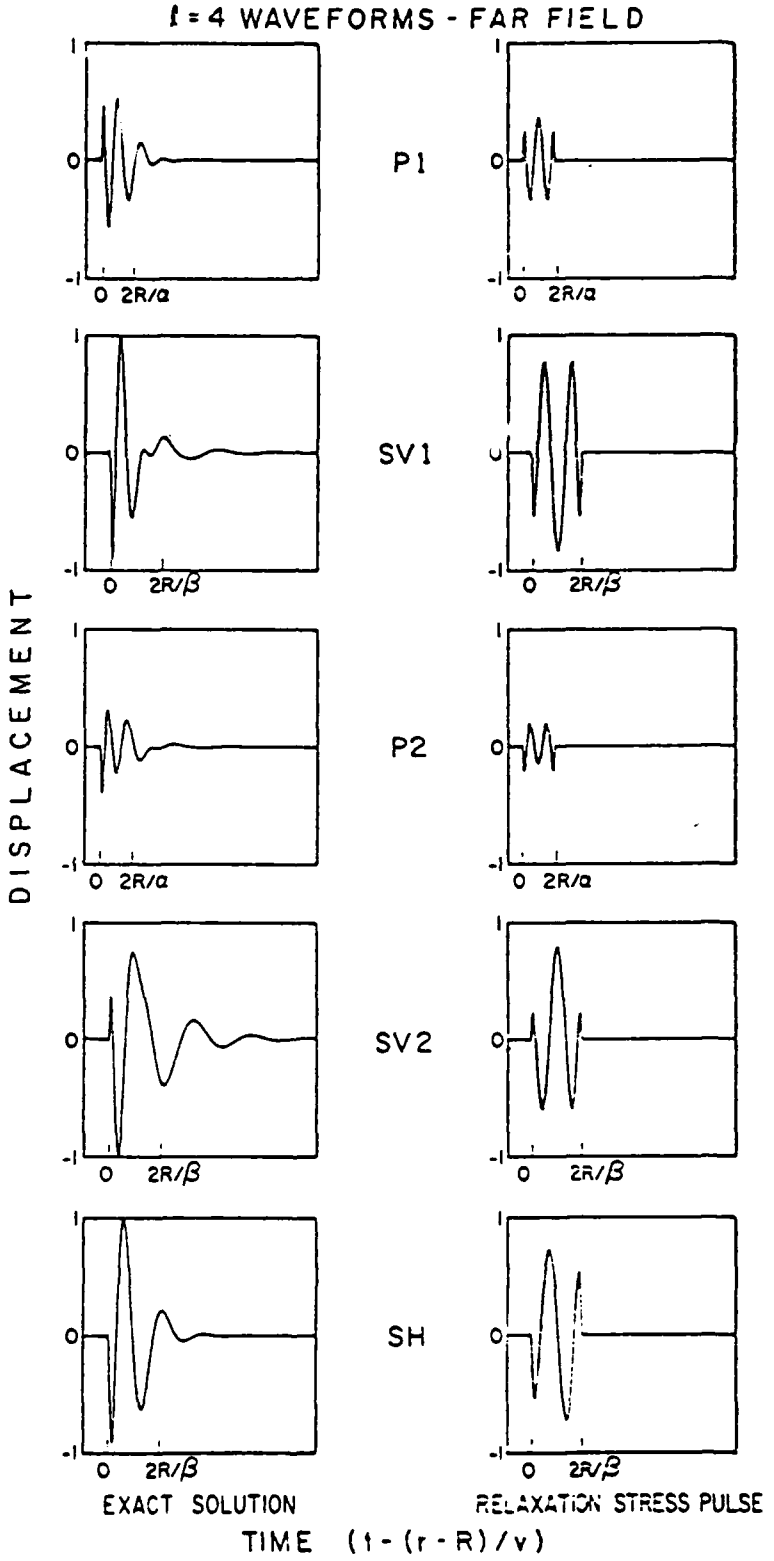
ℓ = 4 WAVEFORMS - FAR FIELD
P1
SV1
P2
SV2
SH
DISPLACEMENT
0 2R/α
0 2R/β
EXACT SOLUTION
RELAXATION STRESS PULSE
TIME (t - (r - R)/v)

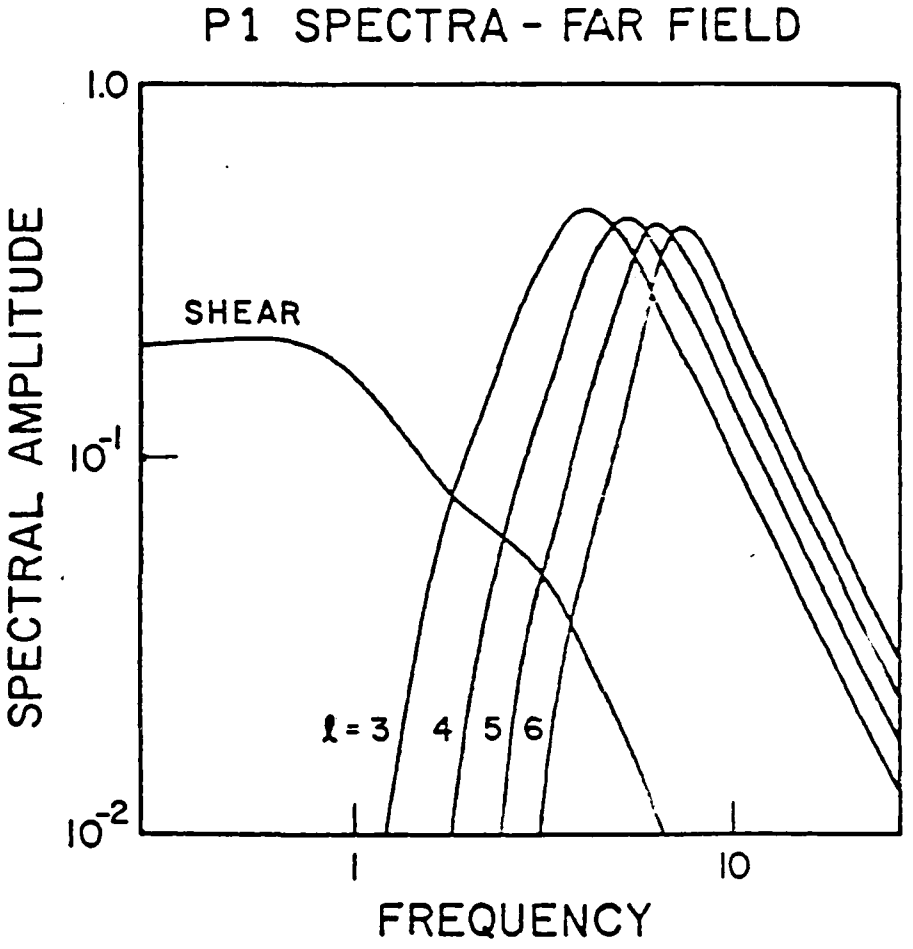
P1 SPECTRA - FAR FIELD
1.0
10^{-1}
10^{-2}
SPECTRAL AMPLITUDE
SHEAR
ℓ = 3
4
5
6
1
10
FREQUENCY

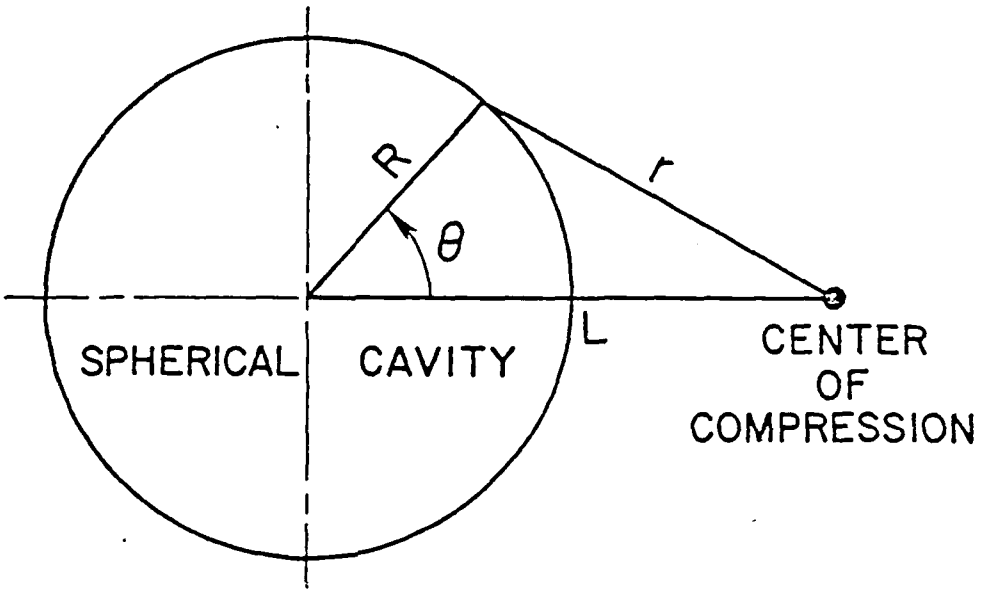
R
θ
r
L
SPHERICAL
CAVITY
CENTER
OF
COMPRESSION

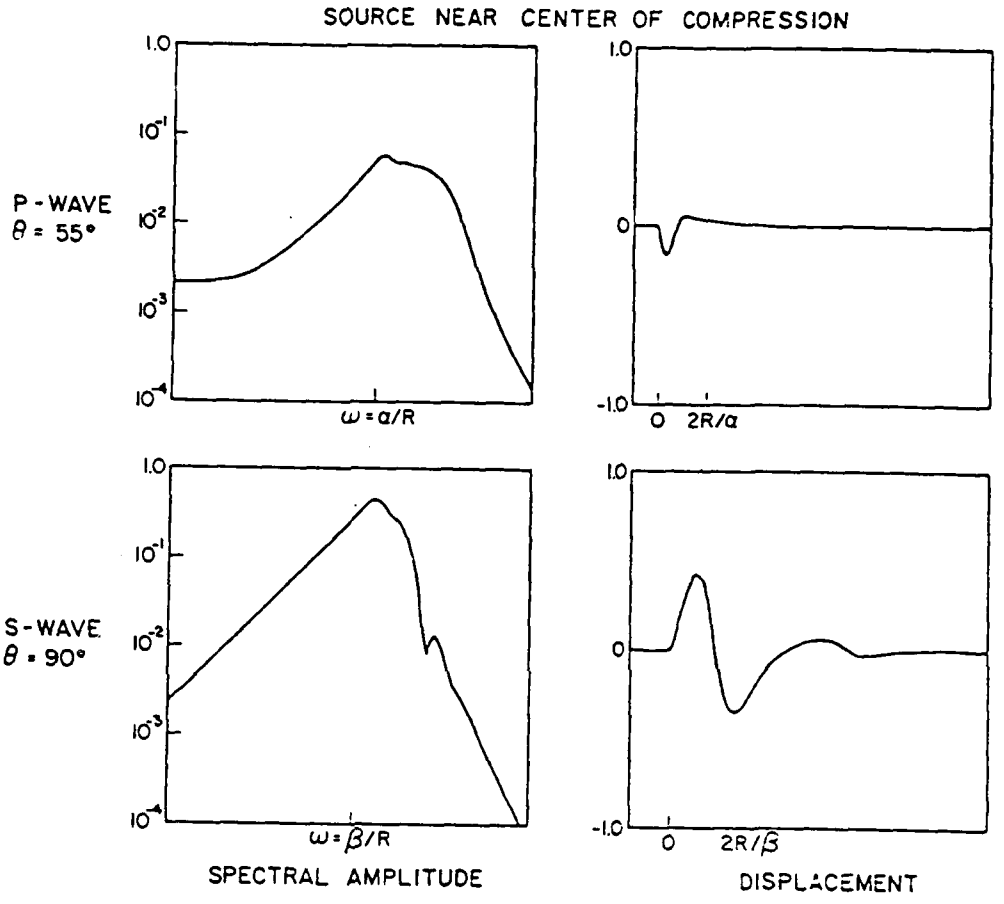
SOURCE NEAR CENTER OF COMPRESSION
P - WAVE
θ = 55°
S - WAVE
θ = 90°
1.0
10⁻¹
10⁻²
10⁻³
10⁻⁴
ω = α/R
ω = β/R
1.0
0
-1.0
0 2R/α
0 2R/β
SPECTRAL AMPLITUDE
DISPLACEMENT

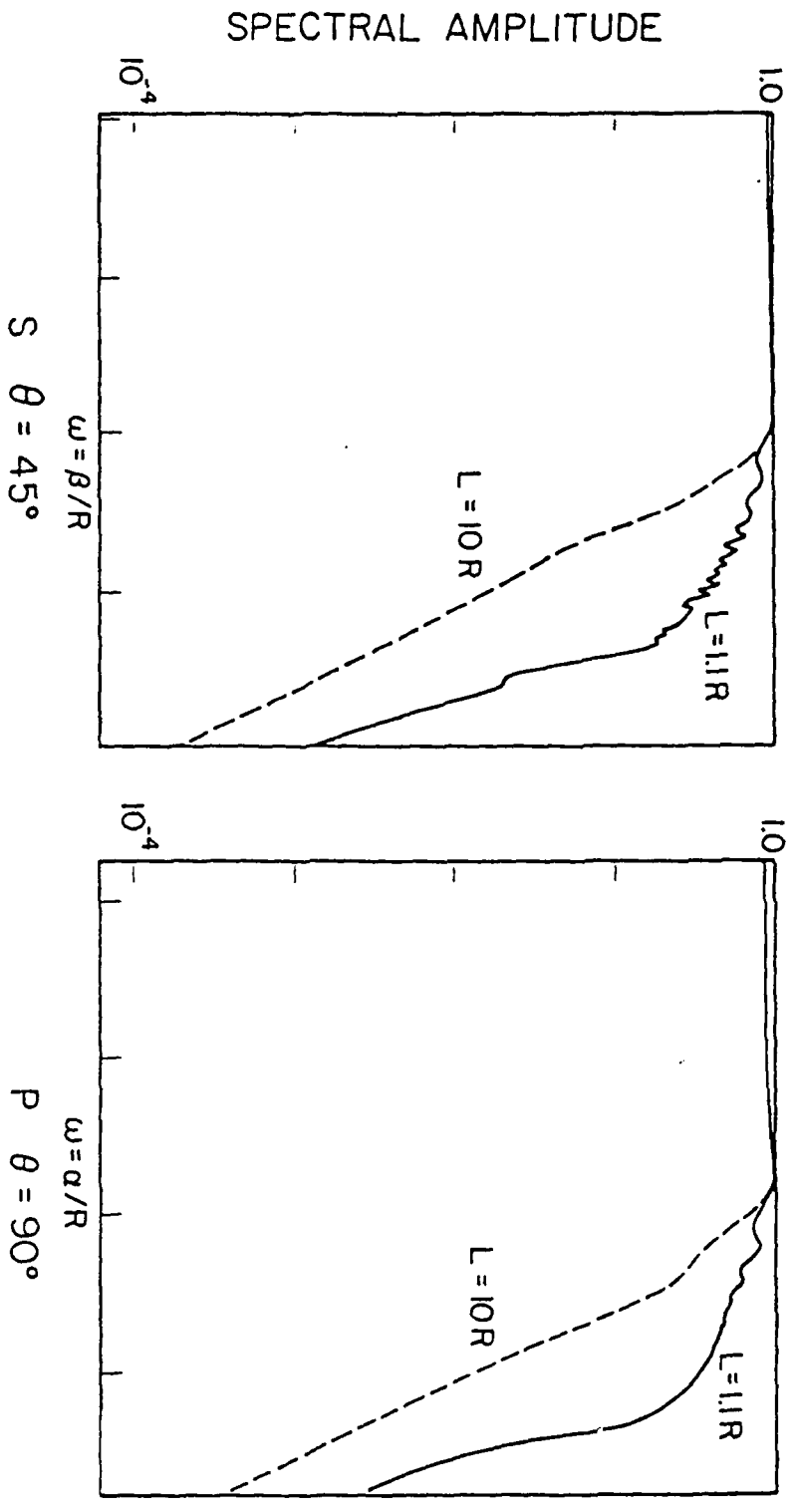
SPECTRAL AMPLITUDE
10^{-4}
1.0
S $\theta = 45°$
$\omega = \beta/R$
L = 10 R
L = 1.1 R
10^{-4}
1.0
P $\theta = 90°$
$\omega = \alpha/R$
L = 10R
L = 1.1R

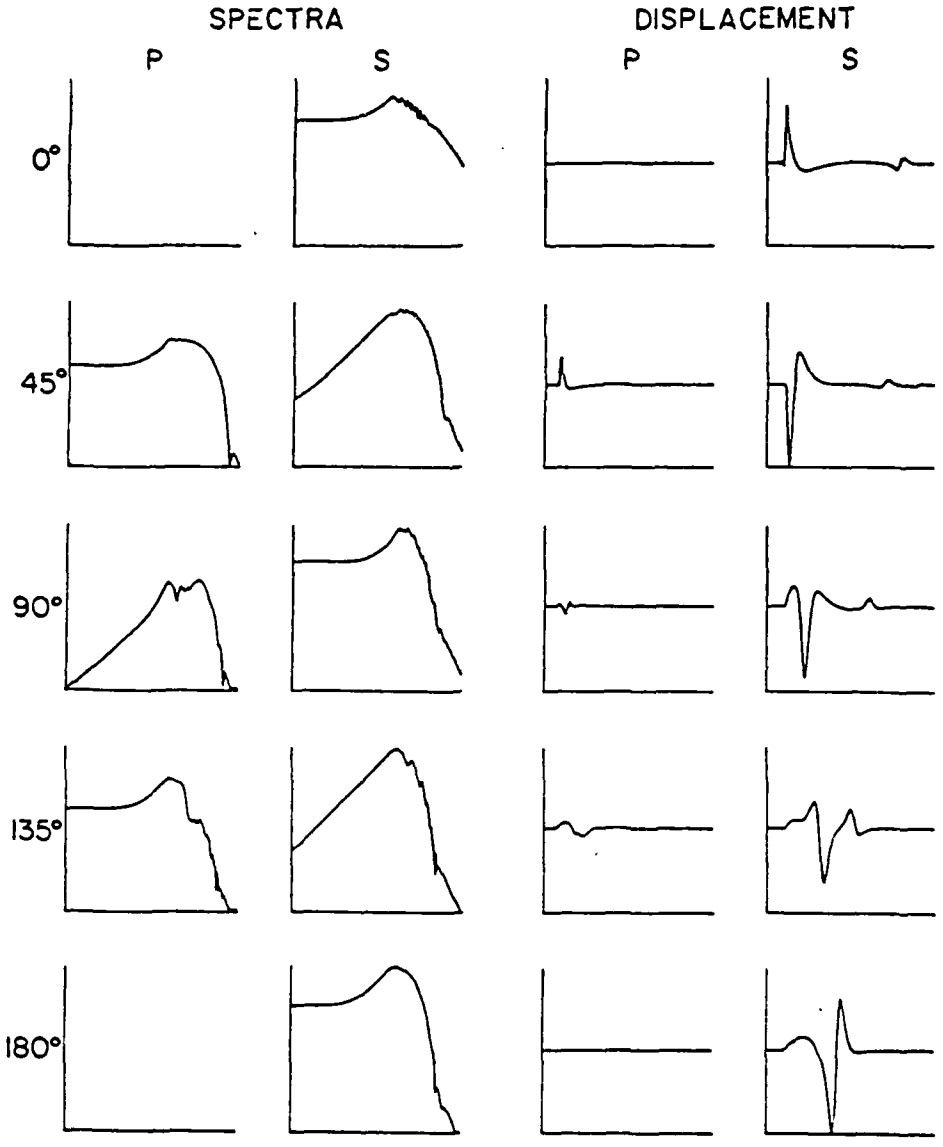

STATIC DISLOCATION AT L=1.5 R

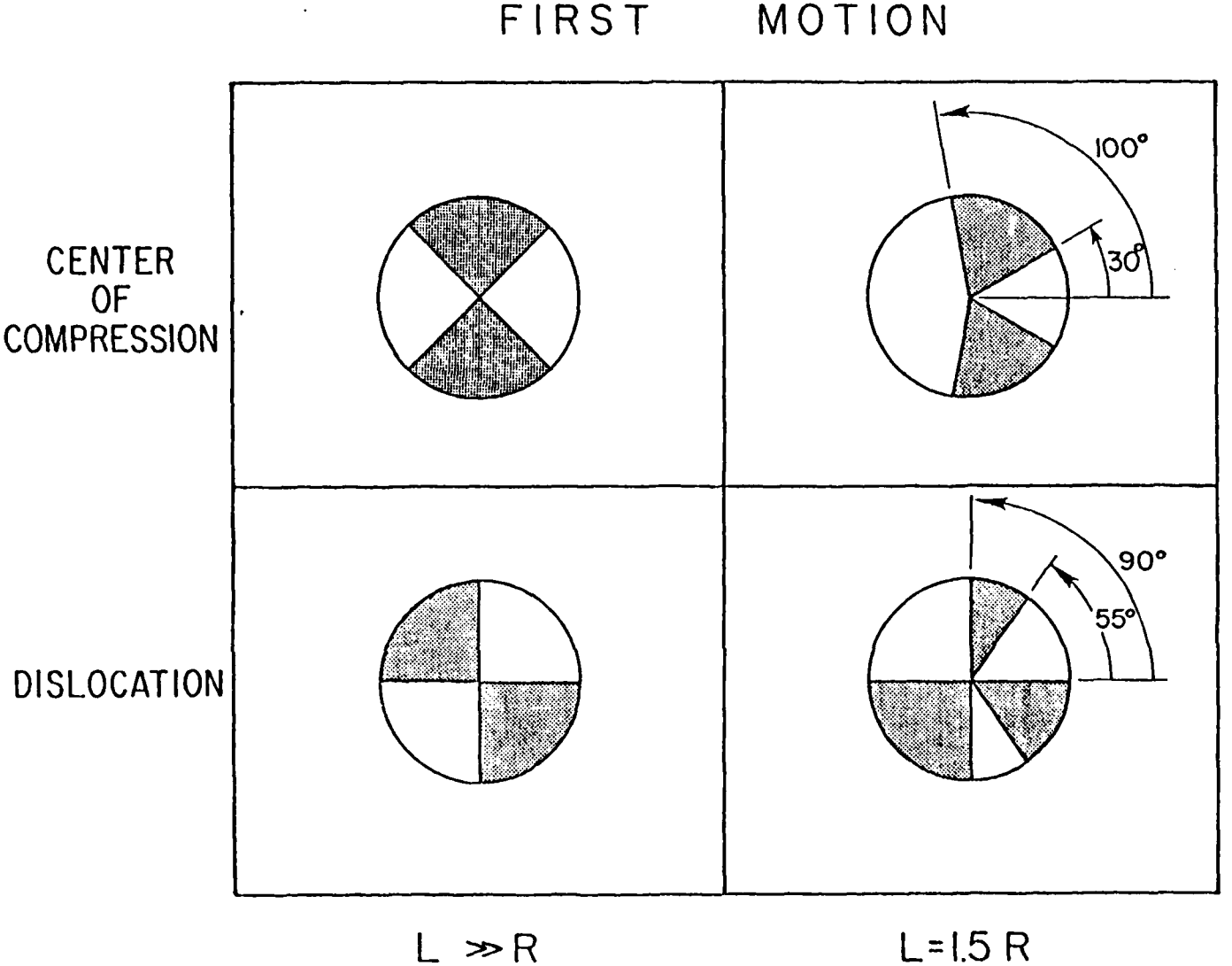
FIRST MOTION
CENTER OF COMPRESSION
DISLOCATION
100°
30°
90°
55°
L ≫ R
L=1.5 R

Appendix B

The Synthesis of Complete Seismograms In an Earth Model Specified by Radially Inhomogeneous Layers

Vernon F. Cormier

ABSTRACT

Traditional methods of synthesizing seismograms in the near or regional distance range (0 to 500 km.) describe the earth model with planar homogeneous layers. In the high frequency band (.2 - 10 Hz.), in which the seismic ground motion is primarily observed, uniformly asymptotic solutions to the depth eigenfunctions can instead allow a radially symmetric earth model to be described by inhomogeneous spherical layers. Ground displacement u is calculated in the frequency domain by

$$u(\omega,\phi,\Delta) = \int_\Gamma M(\omega,p,\phi,\Delta) f(\omega,p) dp \ ,$$

where Γ is a contour in the complex ray parameter (p) plane, and $M(\omega,p,\phi,\Delta)$ a point representation of the earthquake or explosion source including the effect of horizontal propagation to Δ. The response of the earth model $f(\omega,p)$, calculated from the propagator matrix equation for a source in a radially inhomogeneous sphere, includes all possible body and surface waves. Airy functions are chosen to define the inhomogeneous layer matrices. Numerical difficulties usually encountered in the calculation of $f(\omega,p)$ in layered media are avoided by the calculation of subdeterminants of the fundamental matrix solution and by the decomposition of the propagator matrix in a layer into a sum of matrices of differing numerical order whenever the Airy functions behave exponentially. The contour integral can be evaluated by the residue theorem or by numerical integration, the time domain response obtained by fast Fourier transform. Most applications require an earth model to be described by no more than four to five inhomogeneous layers.

INTRODUCTION

At teleseismic distances in the frequency band (0.2 - 10 Hz.), surface and direct body waves are sufficiently separated in time that either may independently be used to extract source and structural properties. In the distance range 0 to 500 km., however, a complete or much larger set of seismic waves must be employed to properly predict ground motion in even a small time window. Although complicating the problem of waveform synthesis, the shorter signal duration offers an opportunity with high frequency recordings for resolving finer structural details and near field source properties impossible with longer period teleseismic recordings.

At sufficiently high frequencies asymptotic solutions for the radial or depth eigenfunctions accurately approximate the exact solutions for radially inhomogeneous layers even with relatively severe velocity gradients. Formalisms developed by Langer (1932, 1949), Olver (1954), and Wasow (1965) can be employed to obtain asymptotic solutions (in frequency) to either the radial component of seismic potentials (Richards, 1976) or to the radial vector-matrix equations of seismic motion (Chapman, 1975; Woodhouse, 1978). Such solutions allow a much simpler description of complicated earth models by a small number of radially inhomogeneous layers. By their validity at high frequency these solutions are particularly suited to applications in the frequency band in which near and regional seismic ground motion is primarily observed and interpreted. Compared to a model specified by planar homogeneous layers, a model specified by radially inhomogeneous layers will usually require many fewer mathematical operations to construct its frequency-ray parameter response. This objective is met in the following sections by detailing a procedure for synthesizing complete seismograms in such an earth model. The procedure combines (1) the zeroth order (in frequency) asymptotic solutions to the propagator and fundamental matrix, (2) the

notation of generalized vertical slownesses or cosines developed by Richards (1976), and (3) the vector-matrix methods of Abo-Zena (1979) for avoiding the numerical difficulties in calculating the response of a layered medium. The THEORY section of the paper develops notation and the generalized solution for displacement. The reader primarily interested in developing practical numerical codes may proceed directly to the section titled EXAMPLE USES OF GENERAL SOLUTION FORM, referring as needed to the sections EVALUATION OF PROPAGATOR PRODUCTS, THEORY, and Appendices A and B.

THEORY

General Solution Form

By applying the vector representation theorem for a sphere, the seismic displacement vector $\underline{u} = u_r\underline{r} + u_\theta\underline{\theta} = u_\phi\underline{\phi}$ may be written as

$$\underline{u}(r,\theta,\phi,t) = \int_{-\infty}^{\infty} d\omega e^{-i\omega t} \sum_{n=0}^{\infty} \sum_{m=-n}^{n} (U\underline{P}_n^m + V\underline{B}_n^m + W\underline{C}_n^m) \qquad (1)$$

where $\underline{P}_n^m$, $\underline{B}_n^m$, and $\underline{C}_n^m$ are vector spherical harmonics defined by

$$\begin{aligned} \underline{P}_n^m &= \underline{r}Y_n^m(\theta,\phi) \\ \underline{B}_n^m &= \underline{\nabla}_1 Y_n^m(\theta,\phi)/[n(n+1)]^{\frac{1}{2}} \\ \underline{C}_n^m &= -r\underline{x}\underline{\nabla}_1 Y_n^m(\theta,\phi)/[n(n+1)]^{\frac{1}{2}} \end{aligned} \qquad (2a)$$

$$(\underline{\nabla}_1 = \underline{\theta}\frac{\partial}{\partial\theta} + \operatorname{cosec}\theta\,\underline{\phi}\frac{\partial}{\partial\phi}).$$

Here the $\underline{P}_n^m$, $\underline{B}_n^m$, and $\underline{C}_n^m$ are fully normalized:

$$Y_n^m(\theta,\phi) = (-)^m \left[\frac{2n+1}{4\pi}\frac{(n-m)!}{(n-m)!}\right]^{\frac{1}{2}} P_n^m(\cos\theta)e^{im\phi} \qquad (2b)$$

$$\int_0^{2\pi}\int_0^{\pi} \underline{P}_n^m \cdot \underline{P}_{n'}^{m'} \sin\theta d\theta d\phi = \int_0^{2\pi}\int_0^{\pi} \underline{B}_n^m \cdot \underline{B}_{n'}^{m'} \sin\theta d\theta d\phi =$$
$$\int_0^{2\pi}\int_0^{\pi} \underline{C}_n^m \cdot \underline{C}_{n'}^{m'} \sin\theta d\theta d\phi = \delta mm'\delta nn'. \qquad (3)$$

$\underline{r}$, $\underline{\theta}$, and $\underline{\phi}$ are unit vectors in the spherical coordinate directions r,θ,ϕ. $P_n^m(\cos\theta)$ is an associated Legendre function. The radial eigenfunctions, U, V, and W satisfy vector-matrix equations of the form

$$\frac{\partial}{\partial r}\underline{v}^T = \omega(\underline{\underline{A}}_0 + \omega^{-1}\underline{\underline{A}}_1{}^T + \omega^{-2}\underline{\underline{A}}_2{}^T)\underline{v}^T \qquad (4)$$

for SH type body waves and toroidal free oscillations, and

$$\frac{\partial}{\partial r}\underline{v}^S = \omega(\underline{\underline{A}}_0{}^S + \omega^{-1}\underline{\underline{A}}_1{}^S + \omega^{-2}\underline{\underline{A}}_2{}^S)\underline{v}^S \qquad (5)$$

for P-SV type body waves and spheroidal free oscillations (e.g., Chapman, 1973). When gravitational effects can be ignored, the displacement-stress vectors $\underline{v}^T$, $\underline{v}^S$ are defined

$$\underline{v}^T = \begin{bmatrix} W \\ T \end{bmatrix}, \quad \underline{v}^S = \begin{bmatrix} U \\ V \\ R \\ S \end{bmatrix}, \qquad (6)$$

where the radial stress functions, T, R, and S are defined in terms of U, V, and W by Alterman et al. (1959). Here and later, quantities written vertically within brackets denote a column vector and quantities written horizontally and separated by commas denote a row vector.

A matrix $\underline{\underline{F}}$ satisfying either (4) or (5) in the column vectors $\underline{v}^T$, $\underline{v}^S$ is defined as a fundamental matrix (Gilbert and Backus, 1966) or matricant (Gantmacher, 1959). As shown by Gilbert and Backus (1966), the fundamental matrices of these

equations allow a convenient and notationally compact method of satisfying the boundary conditions at layers of an earth model having discontinuities in elastic moduli and/or density. The stress displacement vector $\underline{v}$ at a radius "a" is related to that at a radius r_n through a product of propagator matrices $\underline{\underline{K}}_i$ constructed from the fundamental matrices $\underline{\underline{F}}_i$ for each i-th layer:

$$\underline{v}(a) = \underline{\underline{K}}(a,r_n)v(r_n) = \underline{\underline{K}}_1 \ldots \underline{\underline{K}}_n\underline{v}(r_n), \tag{7}$$

$$\text{where} \quad \underline{\underline{K}}_i(r_{i-1}, r_i) = \underline{\underline{F}}_i(r_{i-1})\underline{\underline{F}}_i^{-1}(r_i) \tag{8}$$

with r_{i-1} and r_i denoting the radii bounding the top and bottom boundaries of the i-th layer respectively. Figure 1 illustrates the layering scheme and conventions used for indices.

The general solution to (4) or (5) for the displacement-stress vector $\underline{v}$, including the effects of a source vector term $\underline{\gamma}$, can be written as

$$\underline{v}(a) = \underline{\underline{K}}(a,r_0)\underline{v}(r_0) + \int_{r_0}^{a} \underline{\underline{K}}(a,\xi)\underline{\gamma}(\xi)d\xi \tag{9}$$

where r_0 is some reference radius at which a starting solution $v(r_0)$ is defined (Wasow, 1965). The complete displacement solution can then be obtained by substituting the results for U,V, and W determined from (9) into the displacement representation given by (1).

Fundamental Matrices of Radially Inhomogeneous Layers

The basic form of solution for the displacement-stress vector given by (9) is independent of any representation of the earth model, e.g., planar homogeneous layers, spherical inhomogeneous layers, etc. Assume now that the earth model is specified by radially inhomogeneous layers and apply the zeroth order uniformly asymptotic solutions to the fundamental matrix and propagator of such layers. Adopting the notation and solutions

given by Aki and Richards (1980), omitting source normalization, and rearranging rows and columns to agree with the stress-displacement vector used by Woodhouse (1978) gives

$$\underline{\underline{F}}(r) = r^{-1}\sqrt{\frac{i}{\rho}}\begin{bmatrix} \acute{\xi}g^{(1)} & -\check{\xi}g^{(3)} & r^{-1}ph^{(1)} & r^{-1}ph^{(3)} \\ -ir^{-1}pg^{(1)} & -ir^{-1}g^{(3)} & i\acute{\eta}h^{(1)} & -i\check{\eta}h^{(3)} \\ -iAg^{(1)} & -iAg^{(3)} & iB\acute{\eta}h^{(1)} & -iB\check{\eta}h^{(3)} \\ B\acute{\xi}g^{(1)} & -B\check{\xi}g^{(3)} & Ah^{(1)} & Ah^{(3)} \end{bmatrix} \tag{10a}$$

$$\underline{\underline{F}}(r)^{-1} = r\sqrt{\frac{i}{\rho}}\begin{bmatrix} iAg^{(3)} & B\check{\xi}g^{(3)} & -\check{\xi}g^{(3)} & -ir^{-1}pg^{(3)} \\ -iAg^{(1)} & B\acute{\xi}g^{(1)} & -\acute{\xi}g^{(1)} & ir^{-1}pg^{(3)} \\ -iB\check{\eta}h^{(3)} & Ah^{(3)} & -r^{-1}ph^{(3)} & i\check{\eta}h^{(3)} \\ -iB\acute{\eta}h^{(1)} & -Ah^{(1)} & r^{-1}ph^{(1)} & i\acute{\eta}h^{(1)} \end{bmatrix} \tag{10b}$$

for P-SV waves where $A=2r^{-2}p^2\mu-\rho$, $B=2r^{-1}p$, $i=\sqrt{-1}$, μ is the shear modulus profile $\mu(r)$ and ρ the density profile $\rho(r)$; and

$$\underline{\underline{F}}'(r) = r^{-1}\sqrt{r}\begin{bmatrix} \mu^{-\frac{1}{2}}h^{(1)} & \mu^{-\frac{1}{2}}h^{(3)} \\ i\mu^{\frac{1}{2}}\acute{\eta}h^{(1)} & -i\mu^{\frac{1}{2}}\check{\eta}h^{(3)} \end{bmatrix} \tag{11a}$$

$$\underline{\underline{F}}'^{-1}(r) = r\sqrt{r}\begin{bmatrix} -i\mu^{\frac{1}{2}}\check{\eta}h^{(3)} & -\mu^{-\frac{1}{2}}h^{(3)} \\ -i\mu^{\frac{1}{2}}\acute{\eta}h^{(1)} & \mu^{-\frac{1}{2}}h^{(1)} \end{bmatrix} \tag{11b}$$

for SH waves. $g^{(1)}$, $g^{(3)}$, $h^{(1)}$, $h^{(3)}$ are generalized radial eigenfunctions defined in terms of Airy functions (see Appendix). $\acute{\xi}$, $\check{\xi}$, $\acute{\eta}$, $\check{\eta}$ are generalized vertical slownesses defined with the generalized radial eigenfunctions by

$$\acute{\xi} = \frac{g'^{(1)}}{\omega i g^{(1)}} \quad , \qquad \check{\xi} = \frac{-g'^{(3)}}{\omega i g^{(3)}} \quad , \tag{12}$$

$$\acute{\eta} = \frac{h'^{(1)}}{\omega i h^{(1)}} \quad , \qquad \check{\eta} = \frac{-h'^{(3)}}{\omega i h^{(3)}} \quad .$$

The ray parameter p in the fundamental matrices can be associated with the degree n of the vector spherical harmonics in equation (1) by

$$p = (n + \tfrac{1}{2})/\omega. \qquad (13)$$

Functions analytic in radius specify the seismic velocity behavior in all layers. Appendix A outlines and references methods of fast evaluation of the radial eigenfunctions and generalized vertical slownesses in such profiles.

The fundamental matrices may be defined using any one of several different pairs of linearly independent Airy functions. The pair Ai(-z) and Bi(-z) chosen by Woodhouse (1978) represent standing waves that exponentially decay or grow with increasing depth below a ray turning point. The pair $Ai(-ze^{i2\pi/3})$ and $Ai(-z^{-i2\pi/3})$ chosen by Richards (1976) represent up- or down-going travelling waves. The intermediate choice of $Ai(-ze^{i2\pi/3})$ and Ai(-z) still allows identification of travelling waves within a single layer, but, as will be shown in a later section, avoids a numerical problem in the computation of the response of a layered model. The superscript $^{(1)}$ in equations (10a-12) refers to the use of Airy function appropriate for upgoing travelling waves, $Ai(-z^{i2\pi/3})$. The individual layer propagator $\underline{\underline{K}}_i$ defined using the set $Ai(-ze^{i2\pi/3})$, $Ai(-ze^{-i2\pi/3})$ equals that defined using the set $Ai(-ze^{i2\pi/3})$, Ai(-z). Thus, provided the propagator within a layer is formed by (8), the superscript $^{(3)}$ can refer to either the use of $Ai(-ze^{-i2\pi/3})$ or the use of Ai(-z) when convenient.

Boundary Conditions

The propagator formalism satisfies boundary conditions on stress and displacement components at each layer interface. The only remaining boundary conditions are the vanishing of stress at the free surface and a radiation condition in the lowermost layer. For a sphere of radius "a" the free surface condition

requires that R(a)=S(a)=T(a)=0. Two possible boundary conditions may be invoked in the last layer. (1) The last layer possesses only standing waves that exponentially decay with increasing depth below their turning points. (2) If it is desired to exclude any waves from propagating in the last layer from the solution at the free surface, the last layer must possess only downward propagating waves. Henceforth the term "decay" will refer to boundary condition (1) and "reflectivity" to boundary condition (2). With these boundary conditions and when the superscript (3) refers to the Airy function Ai(-z), the stress-displacement vector for P-SV waves has the form

$$\underline{v}(r_0) = \underline{\underline{F}}(r_0) \begin{bmatrix} 0 \\ b_1 \\ 0 \\ b_2 \end{bmatrix} \qquad \text{for decay}$$

$$\text{or} \quad = \underline{\underline{F}}(r_0) \begin{bmatrix} -b_1 \\ b_1 \\ -b_2 \\ b_2 \end{bmatrix} \qquad \text{for reflectivity.}$$

For SH waves the form becomes

$$\underline{v}(r_0) = \underline{\underline{F}}'(r_0) \begin{bmatrix} 0 \\ b_3 \end{bmatrix} \qquad \text{for decay}$$

$$\text{or} \quad = \underline{\underline{F}}'(r_0) \begin{bmatrix} -b_3 \\ b_3 \end{bmatrix} \qquad \text{for reflectivity.}$$

The quantities b_1, b_2, and b_3 are constants.

The analytic velocity profiles in the last inhomogeneous layer specify the velocity up to the center of the earth. They need only accurately model the P and S velocities, however, up to the maximum depth that rays bottom in the ray parameter (p) domain needed for the solution of a particular problem. The velocity profiles may have multiple turning points but only one turning point may exist in this p domain. Because radial

inhomogeneity and sphericity allow rays to have turning points, the last layer automatically radiates seismic energy back towards the surface with the decay boundary condition. With the reflectivity condition applied to the last layer, only waves reflecting from or bottoming above the last layer reach the surface.

The reference radius r_0 can be imagined to be far below the lowest level for which rays turn in the p domain of interest. A particular r_0 need not be specified because the functions evaluated in r_0 cancel in the subsequent solution procedure.

Including the free surface and decay boundary conditions in the general solution form of (9) gives

$$\begin{bmatrix} U(a) \\ V(a) \\ 0 \\ 0 \end{bmatrix} = \underline{\underline{K}}(a,r_n)\underline{\underline{F}}_n(r_{n-1}) \begin{bmatrix} 0 \\ b_1 \\ 0 \\ b_2 \end{bmatrix} + \int_{r_0}^{a} \underline{\underline{K}}(a,\xi)\underline{\gamma}(\xi)\,d\xi \qquad (14)$$

for P-SV waves, and

$$\begin{bmatrix} W(a) \\ 0 \end{bmatrix} = \underline{\underline{K}}'(a,r_n)\underline{\underline{F}}'_n(r_{n-1}) \begin{bmatrix} 0 \\ b_3 \end{bmatrix} + \int_{r_0}^{a} \underline{\underline{K}}'(a,\xi)\underline{\gamma}'(\xi)\,d\xi \qquad (15)$$

for SH waves. The unprimed and primed fundamental matrices, propagators, and source vectors correspond to the P-SV and SH cases respectively.

Solution in a Layered Sphere

Multiplying (14) by $\underline{\underline{F}}_n^{-1}(r_{n-1})\underline{\underline{K}}(r_n,a)$ and (15) by $\underline{\underline{F}}'^{-1}_n(r_{n-1})\underline{\underline{K}}'(r_n,a)$ and rearranging terms gives

$$\begin{bmatrix} 0 \\ b_1 \\ 0 \\ b_2 \end{bmatrix} = \underline{\underline{R}}^{-1} \begin{bmatrix} U(a) \\ V(a) \\ 0 \\ 0 \end{bmatrix} + \begin{bmatrix} G_1 \\ G_2 \\ G_3 \\ G_4 \end{bmatrix} \qquad (16)$$

for P-SV waves, and

$$\begin{bmatrix} 0 \\ b_3 \end{bmatrix} = \underline{\underline{R}}'^{-1} \begin{bmatrix} W(a) \\ 0 \end{bmatrix} + \begin{bmatrix} G_1' \\ G_2' \end{bmatrix} \tag{17}$$

for SH waves, where

$$\begin{bmatrix} G_1 \\ G_2 \\ G_3 \\ G_4 \end{bmatrix} = \underline{\underline{S}}^{-1} \int_{\bar{r}_s}^{r_{s-1}} \underline{\underline{F}}_s^{-1}(\xi)\underline{\gamma}(\xi)d\xi \quad , \tag{18}$$

$$\begin{bmatrix} G_1' \\ G_2' \end{bmatrix} = \underline{\underline{S}}'^{-1} \int_{\bar{r}_s}^{r_{s-1}} \underline{\underline{F}}_s'^{-1}(\xi)\underline{\gamma}'(\xi)d\xi \quad ,$$

$$\begin{aligned} \underline{\underline{R}}^{-1} &= \underline{\underline{F}}_n^{-1}(r_{n-1})\underline{\underline{K}}(r_{n-1},a) \quad , \\ \underline{\underline{S}}^{-1} &= \underline{\underline{F}}_n^{-1}(r_{n-1})\tilde{\underline{\underline{K}}}(r_{n-1},\bar{r}_s) \quad , \end{aligned} \tag{19}$$

and

$$\begin{aligned} \underline{\underline{K}}(r_{n-1},a) &= \underline{\underline{K}}_{n-1}(r_{n-1},r_{n-2})\cdots\underline{\underline{K}}_1(r_1,a) \quad , \\ \tilde{\underline{\underline{K}}}(r_{n-1},\bar{r}_s) &= \underline{\underline{K}}_{n-1}(r_{n-1},r_{n-2})\cdots\underline{\underline{K}}_{s+1}(r_{s+1},\bar{r}_s)\underline{\underline{F}}_{s+1}(\bar{r}_s) \end{aligned} \tag{20}$$

$\underline{\underline{R}}'^{-1}$, $\underline{\underline{S}}'^{-1}$ are defined analogously from the primed fundamental matrices and propagators. The sbuscript s refers to the layer index of the source layer, $\bar{r}_s$ denoting the radius at its lower boundary (see Figure 1).

Solutions of equations (16-17) for the radial functions U(a), V(a) and W(a) are

$$U(a) = \frac{G_1 R_{32}^{-1} - G_3 R_{12}^{-1}}{R_{11}^{-1}R_{32}^{-1} - R_{31}^{-1}R_{12}^{-1}} \tag{21}$$

$$V(a) = \frac{G_1 R_{31}^{-1} - G_3 R_{11}^{-1}}{R_{11}^{-1} R_{32}^{-1} - R_{31}^{-1} R_{12}^{-1}} \tag{22}$$

$$W(a) = \frac{G_1'}{R_{11}'^{-1}} \tag{23}$$

where R_{ij}^{-1} denotes the ij-th element of $\underline{\underline{R}}^{-1}$.

EVALUATION OF PROPAGATOR PRODUCTS

Care must be taken in the evaluation of the propagator products of equation (20) not to lose precision from the subtraction of large quantities of nearly equal value. Knopoff (1964), Dunkin (1965), and recently Abo-Zena (1979) have shown how to avoid this difficulty in models having planar homogeneous layers. All of these methods propagate a matrix of minors of the inverse fundamental matrix. The methods used by Abo-Zena, however, free the layered model from any constraints on its total thickness. Because the precision problem also exists for models composed of radially inhomogeneous layers, the matrix methods developed by these authors can similarly be applied.

The R_{ij}^{-1} Elements

The elements R_{ij}^{-1} and $R_{ij}^{-1\prime}$ in (21-23) may be written as

$$R_{11}^{-1} = \underline{E}_p \underline{\underline{K}} \begin{bmatrix} 1 \\ 0 \\ 0 \\ 0 \end{bmatrix},$$

$$R_{12}^{-1} = \underline{E}_p \underline{\underline{K}} \begin{bmatrix} 0 \\ 1 \\ 0 \\ 0 \end{bmatrix}, \tag{24}$$

$$\begin{bmatrix} 1 \\ 0 \end{bmatrix}.$$

$$R^{-1}_{32} = \underline{E}_{SV} \underline{\underline{K}} \begin{bmatrix} 0 \\ 1 \\ 0 \\ 0 \end{bmatrix} , \qquad (24)$$

$$R^{-1}_{11} = \underline{E}_{SH} \underline{\underline{K}}' \begin{bmatrix} 1 \\ 0 \end{bmatrix} ,$$

where the row vectors $\underline{E}_P$, $\underline{E}_{SV}$, $\underline{E}_{SH}$ are determined by

$$\underline{E}_P = \left[1,0,0,0\right] \underline{\underline{F}}_n^{-1}(r_{n-1}) = r_{n-1}\sqrt{\frac{i}{\rho_{n-1}}} \left[\ldots (3), B\check{\xi}g^{(3)}, -\check{\xi}g^{(3)}, \right.$$

$$\left. , -ir^{-1}pg^{(3)} \right] \Big|_{r_{n-1}}$$

$$\underline{E}_{SV} = [0,0,1,0]\, \underline{\underline{F}}_n^{-1}(r_{n-1}) = \qquad (25)$$

$$r_{n-1}\sqrt{\frac{i}{\rho_{n-1}}} \left[-iB\eta\check{h}^{(3)}, -Ah^{(3)}, -r^{-1}ph^{(3)}, i\check{\eta}h^{(3)} \right] \Big|_{r_{n-1}}$$

$$\underline{E}_{SH} = [1,0]\, \underline{\underline{F}}_n^{-1\prime}(r_{n-1}) =$$

$$r_{n-1}\sqrt{i} \left[-i\mu^{1/2}\check{\eta}h^{(3)}, -\mu^{1/2}h^{(3)} \right] \Big|_{r_{n-1}}$$

Because the elements R^{-1}_{ij} do not depend on the order number m of the spherical harmonics, they may be moved outside of the m summation when (21-23) are substituted in equation (1). It is then convenient to perform the summation over m of the products $G_1\underline{P}^m_n$, $G_3\underline{P}^m_n$, $G_1\underline{B}^m_n$, $G_3\underline{B}^m_n$, and $G'_1\underline{C}^m_n$. These quantities may be written as:

$$\sum_{m=-n}^{n} [G_1 \underline{P}_n^m + G_1 \underline{B}_n^m] = [1,0,0,0]\underline{\underline{S}}^{-1}(\underline{s}_r\underline{r} + \underline{s}_\theta\underline{\theta} - \underline{s}_\phi\underline{\phi}) = \underline{\underline{E}}_P\underline{\underline{\tilde{K}}}\underline{t}$$

$$\sum_{m=-n}^{n} [G_3 \underline{P}_n^m + G_3 \underline{B}_n^m] = [0,0,1,0]\underline{\underline{S}}^{-1}(\underline{s}_r\underline{r} + \underline{s}_\theta\underline{\theta} - \underline{s}_\phi\underline{\phi}) = \underline{\underline{E}}_{SV}\underline{\underline{\tilde{K}}}\underline{t} \qquad (26)$$

$$\sum_{m=-n}^{n} G'_1 \underline{C}_n^m = [1,0,0,0]S'^{-1}(\underline{s}'_\theta\underline{\theta} + \underline{s}'_\phi\underline{\phi}) = \underline{\underline{E}}_{SH}\underline{\underline{\tilde{F}}}'\underline{t}'.$$

Appendix B defines the column vectors $\underline{s}_r$, $\underline{s}_\theta$, $\underline{s}_\phi$, $\underline{s}'_\theta$ and $\underline{s}'_\phi$ for generalized earthquake and explosion point sources. $\underline{t}$ and $\underline{t}'$ are the sums of the column vectors defined in equation (B7) in the vector directions $\underline{r}$, $\underline{\theta}$, and $\underline{\phi}$:

$$\underline{t} = \underline{s}_r\underline{r} + \underline{s}_\theta\underline{\theta} + \underline{s}_\phi\underline{\phi}$$

$$\underline{t}' = \underline{s}'_\theta\underline{\theta} + \underline{s}'_\phi\underline{\phi} \qquad (27)$$

The Displacement Representation

The theorem for the transpose of the product of matrices $\underline{\underline{A}}\,\underline{\underline{B}}$,

$$(\underline{\underline{A}}\,\underline{\underline{B}})^T = \underline{\underline{B}}^T\underline{\underline{A}}^T \qquad (28)$$

and the fact that the transpose of a scalar leaves it unchanged, imply the identities

$$\underline{\underline{E}}_P\underline{\underline{\tilde{K}}}\underline{t} = \underline{t}^T\underline{\underline{\tilde{K}}}^T\underline{\underline{E}}_P^T \quad ,$$

$$\underline{\underline{E}}_{SV}\underline{\underline{\tilde{K}}}\underline{t} = \underline{t}^T\underline{\underline{\tilde{K}}}^T\underline{\underline{E}}_{SV}^T \quad , \qquad (29)$$

$$\underline{\underline{E}}_P\underline{\underline{K}}\begin{bmatrix}1\\0\\0\\0\end{bmatrix} = [1,0,0,0]\underline{\underline{K}}^T\underline{\underline{E}}_P^T \quad ,$$

$$\underline{\underline{E}}_{SV}\underline{\underline{K}}\begin{bmatrix}1\\0\\0\\0\end{bmatrix} = [1,0,0,0]\underline{\underline{K}}^T\underline{\underline{E}}_{SV}^T \quad .$$

The transposes of $\underline{t}$ and $\underline{t}'$ are taken as

$$\begin{aligned} \underline{t}^T &= \underline{s}_r^T \underline{r} + \underline{s}_\theta^T \underline{\theta} + \underline{s}_\phi^T \underline{\phi} \\ \underline{t}'^T &= \underline{s}_\theta'^T \underline{\theta} + \underline{s}_\phi'^T \underline{\phi} . \end{aligned} \tag{30}$$

$\underline{s}_r^T$ etc. are now row vectors. Using equations (1), (21-24) and (29), it then follows that for a generalized point source and for a model described by radially inhomogeneous layers, the displacement $\underline{u}$ can be written as

$$\underline{u}(r,\theta,\phi,t) = \int_{-\infty}^{\infty} e^{-i\omega t} \int_0^{\infty} \left\{ \frac{\underline{t}^T \tilde{\underline{K}}^T [\underline{E}_P^T \underline{E}_{SV} - \underline{E}_{SV}^T \underline{E}_P] \underline{K} \begin{bmatrix} 0 \\ 1 \\ 0 \\ 0 \end{bmatrix}}{[1,0,0,0] \underline{K}^T [\underline{E}_P^T \underline{E}_{SV} - \underline{E}_{SV}^T \underline{E}_P] \underline{K} \begin{bmatrix} 0 \\ 1 \\ 0 \\ 0 \end{bmatrix}} + \frac{\underline{E}_{SH} \tilde{\underline{K}}' \underline{t}'}{\underline{E}_{SH} \underline{K}' \begin{bmatrix} 1 \\ 0 \end{bmatrix}} \right\} \omega dp d\omega \tag{31}$$

The n summation has been converted to an integral over p by taking the first term in a Poisson transform (e.g., Nussenzweig, 1965).

Matrix Multiplication Scheme

The matrix $[\underline{E}_P^T \underline{E}_{SV} - \underline{E}_{SV}^T \underline{E}_P]$ is an anti-symmetric matrix of minors of $\underline{F}_n^{-1}$ of the form

$$[\underline{E}_P^T \underline{E}_{SV} - \underline{E}_{SV}^T \underline{E}_P] = \underline{Y}_n = \quad \text{(cont'd)} \tag{32}$$

$$= \frac{r_{n-1}^2}{\rho_{n-1}} \begin{bmatrix} 0 & d_1 & d_2 & d_3 \\ -d_1 & 0 & d_4 & -d_2 \\ -d_2 & -d_4 & 0 & d_5 \\ -d_3 & d_2 & -d_5 & 0 \end{bmatrix} g^{(3)} h^{(3)} \qquad (32)$$

(cont'd)

where

$$\begin{aligned} d_1 &= -(A^2 + B^2 \check{\xi}\check{\eta}) \\ d_2 &= (r^{-1} pA + B\check{\eta}\check{\xi}) \\ d_3 &= i\rho\check{\eta} \\ d_4 &= i\rho\check{\xi} \\ d_5 &= (\check{\eta}\check{\xi} + r^{-2}p^2) \end{aligned} \qquad (33)$$

If the reflectivity instead of the decay boundary condition had been used in the last layer, the Airy function $Ai(-ze^{-i2\pi/3})$ would replace $Ai(-z)$ in the definitions of the vertical slownesses appearing in the quantities d_i.

All elements of $\underline{\underline{Y}}_n$ are evaluated at the boundary of the last layer and in the analytic velocity profiles of the last layer. Evaluation of the P-SV terms in the brackets of (31) involves a successive redefinition of a $\underline{\underline{Y}}_i$ matrix at each i-th higher layer boundary starting at the lowest layer boundary:

$$\begin{aligned} \underline{\underline{Y}}_{n-1} &= \underline{\underline{K}}_{n-1}^T \underline{\underline{Y}}_n \underline{\underline{K}}_{n-1} \\ \underline{\underline{Y}}_{n-2} &= \underline{\underline{K}}_{n-2}^T \underline{\underline{Y}}_{n-1} \underline{\underline{K}}_{n-2} \\ &\vdots \\ \underline{\underline{Y}}_1 &= \underline{\underline{K}}_1^T \quad \underline{\underline{Y}}_2 \underline{\underline{K}}_1 \end{aligned}$$

Each newly defined $\underline{\underline{Y}}_i$ matrix remains an antisymmetric matrix. Only five independent terms are needed to specify each new $\underline{\underline{Y}}_i$ (Menke, personal communication).

The denominator for the P-SV term is given by the intersection of the first row and the second column of the result for $\underline{\underline{Y}}_i$. The numerator is calculated by first evaluating the product

$$\underline{\underline{Y}}_{s-1} = \underline{\underline{\tilde{K}}}\underline{\underline{Y}}_n\underline{\underline{\tilde{K}}} \quad ; \tag{35}$$

right multiplying $\underline{\underline{Y}}_{s-1}$ by $\underline{\underline{K}}_s(\bar{r}_s, r_{s-1})\ldots\underline{\underline{K}}_1(r_1, a)$, and left multiplying the second column of this result by the row vectors of $\underline{t}^T$.

The methods of Abo-Zena (1979) can be applied to evaluate the products of equation (31) for the P-SV term and the products $\underline{\underline{E}}_{SH}\underline{\underline{K}}'$, $\underline{\underline{E}}_{SH}\underline{\underline{\tilde{K}}}'$ for the SH term. These methods decompose the propagator matrix of a layer into a sum of matrices of differing numerical order whenever the depth eigenfunctions are exponentially small or large. In an inhomogeneous layer this happens at ray parameters for which a P or S wave bottoms far above the layer. At such ray parameters only tunneled energy can reside in the layer. Because tunneling is a frequency dependent phenomenon, a particular exponential decay value depends on frequency. When this situation occurs in the i-th layer, define the positive integers m_j (j=1-4) and the complex numbers $\hat{a}_j$ (j=1-4) with magnitude of order 1 from the products

$$\begin{aligned} g^{(1)}(r_i)g^{(3)}(r_{i-1}) &= \hat{a}_1 e^{m_1}, \\ g^{(3)}(r_i)g^{(1)}(r_{i-1}) &= \hat{a}_2 e^{-m_2}, \\ h^{(1)}(r_i)h^{(3)}(r_{i-1}) &= \hat{a}_3 e^{m_3}, \\ h^{(3)}(r_i)h^{(1)}(r_{i-1}) &= \hat{a}_4 e^{-m_4}. \end{aligned} \tag{36}$$

The $\hat{a}_j$ and m_j values can be calculated and returned by an Airy function subroutine based on the exact and asymptotic formulae given in Abramowitz and Stegun (1964). (More detailed references are given in Appendix A.) Next define the matrices $\underline{v}_j\underline{h}_j$ from the product of column vectors $\underline{v}_j$ and row vectors $\underline{h}_j$. After the

exponential scale factors of the fundamental matrices are removed, $\underline{v}_j$ is given by the jth column of the $\underline{\underline{F}}_i(r_i)$ matrix and $\underline{h}_j$ by the jth row of the $\underline{\underline{F}}_i(r_{i-1})$ matrix. The propagator $\underline{\underline{K}}_i$ can then be written as

$$\underline{\underline{K}}_i = \underline{v}_1\underline{h}_1 e^{m_1} + \underline{v}_2\underline{h}_2 e^{-m_2} + \underline{v}_3\underline{h}_3 e^{m_3} + \underline{v}_4\underline{h}_4 e^{-m_4} . \qquad (37)$$

In Abo-Zena (1979) such a decomposition of $\underline{\underline{K}}_i$ is invoked to varying degrees depending on which of three diferent relations exist between phase velocity and layer velocities. For inhomogeneous layers these cases are restated in terms of the exponential behavior of the Airy functions used in the definition of the fundamental matrices:

I. $m_1 = m_2 = m_3 = m_4 = 0$

All radial eigenfunctions behave either as sinusoidal or phasor type functions having a magnitude of order 1. Compute $\underline{\underline{K}}_i$ directly and determine $\underline{\underline{Y}}_i$ from

$$\underline{\underline{Y}}_i = \underline{\underline{K}}_i^T \underline{\underline{Y}}_{i+1} \underline{\underline{K}}_i \qquad (38)$$

II. m_3 and $m_4 = 0$, m_1 and/or $m_2 \neq 0$

A matrix $\underline{og}$ may be defined as

$$\underline{og} = \underline{v}_3\underline{h}_3 + \underline{v}_4\underline{h}_4$$

Compute $\underline{\underline{Y}}_i$ from

$$\begin{aligned}\underline{\underline{Y}}_i = {} & (\underline{og})^T \underline{\underline{Y}}_{i+1} \underline{og} + (\underline{h}_1^T \underline{v}_1^T + \underline{h}_2^T \underline{v}_2^T)\underline{\underline{Y}}_{i-1}(\underline{v}_1\underline{h}_1 + \underline{v}_2\underline{h}_2) \\ & + e^{m_1}\left\{[\underline{h}_1^T \underline{v}_1^T + (\underline{og})^T]\underline{\underline{Y}}_{i+1}(\underline{v}_1\underline{h}_1 + \underline{og}) - (\underline{og})^T \underline{\underline{Y}}_{i+1}\underline{og}\right\} \qquad (39) \\ & + e^{-m_2}\left\{[\underline{h}_2^T \underline{v}_2^T + (\underline{og})^T]\underline{\underline{Y}}_{i+1}(\underline{v}_2\underline{h}_2 + \underline{og}) - (\underline{og})^T \underline{\underline{Y}}_{i+1}\underline{og}\right\}\end{aligned}$$

III. m_1 and/or $m_2 \neq 0$, m_3 and/or $m_4 \neq 0$

Compute $\underline{\underline{Y}}_i$ from

$$\begin{aligned}\underline{\underline{Y}}_i = {} & (\underline{h}_1^T\underline{v}_1^T + \underline{h}_2^T\underline{v}_2^T)\underline{\underline{Y}}_{i+1}(\underline{v}_2\underline{h}_2 + \underline{v}_1\underline{h}_1) + (\underline{h}_3^T\underline{v}_3^T + \underline{h}_4^T\underline{v}_4^T)\underline{\underline{Y}}_{i+1}(\underline{v}_4\underline{h}_4 + \underline{v}_3\underline{h}_3) \\ & + e^{(m_1+m_3)}(\underline{h}_1^T\underline{v}_1^T + \underline{h}_3^T\underline{v}_3^T)\underline{\underline{Y}}_{i+1}(\underline{v}_3\underline{h}_3 + \underline{v}_1\underline{h}_1) \\ & + e^{(m_1-m_3)}(\underline{h}_1^T\underline{v}_1^T + \underline{h}_4^T\underline{v}_4^T)\underline{\underline{Y}}_{i+1}(\underline{v}_4\underline{h}_4 + \underline{v}_1\underline{h}_1) \\ & + e^{(m_3-m_1)}(\underline{h}_2^T\underline{v}_2^T + \underline{h}_3^T\underline{v}_3^T)\underline{\underline{Y}}_{i+1}(\underline{v}_3\underline{h}_3 + \underline{v}_2\underline{h}_2) \\ & + e^{-(m_1+m_3)}(\underline{h}_2^T\underline{v}_2^T + \underline{h}_4^T\underline{v}_4^T)\underline{\underline{Y}}_{i+1}(\underline{v}_4\underline{h}_4 + \underline{v}_2\underline{h}_2)\end{aligned} \tag{40}$$

All of the symmetries noted by Abo-Zena can be exploited in the evaluation of the matrix products of algorithms I-III.

The propagator products in the SH calculation can be evaluated using simpler analogous algorithms for the decomposition of the SH propagator. New row vectors $\underline{E}_{SH}$ are given by right multiplying by the propagators.

At large m_i the product having the largest exponential factor in algorithms II and III dominates the final result for $\underline{\underline{Y}}_i$ and the other terms may be ignored. The exponential behavior assumed here is based on the travelling-standing choice for the Airy functions used in defining the fundamental matrices, $Ai(-ze^{i2\pi/3})$ and $Ai(-z)$. The displacement representation given by (31) equals that given by substituting $Ai(-ze^{-i2\pi/3})$ for $Ai(-z)$ in (31) in all but the last layer. Thus the response calculation may alternate between either choice of independent Airy functions when convenient. If the travelling wave choice, $Ai(-ze^{\pm i2\pi/3})$, had been used, the propagator in algorithms II and III would be dominated by exponentially large terms of nearly equal magnitude and opposite sign whenever the parameter N defined in the Appendix A equaled ±1. In this case the travelling-standing choice avoids the numerical difficulties of the travelling choice.

Algorithm I always involves fewer mathematical operations than II and III if all of the terms in II and III are calculated. Branching between the algorithms can be allowed at

non-zero values of m_j, maximizing the use of algorithm I. Care must be taken, however, that the branching value of m_j is small enough that precision is not lost in algorithm I.

The exponential scale factor accumulated from each redefinition of $\underline{\underline{Y}}_i$ cancels in the numerator and denominator of the integrand until the boundary below the source layer is reached. The scale factor for propagation below the source boundary can thus be discarded. The scale factors separately accumulated by the numerator and denominator for propagation through and above the source layer can be saved and used to scale the final result for the integrand.

Only tunneled energy can reside in a layer at ray parameters corresponding to rays bottoming far above the layer. These p points occur whenever the parameter N in the Appendix equals ±1. The parameters $|\omega\tau_\alpha|$ and $|\omega\tau_\beta|$ defined in Appendix A then serve to quantify the tunneling phenomenon. When the tunneled energy in a layer is sufficiently small for both P and SV waves ($|\omega\tau_\alpha|>10$ and $|\omega\tau_\beta|>10$), the propagator for the layer can be ignored and the $\underline{\underline{Y}}_i$ matrix redefinitions begun in the next higher layer.

EXAMPLE USES OF GENERAL SOLUTION FORM

I. Inhomogeneous Unlayered Sphere

As an example of the generality of (31), consider an explosive point source at radius r_s in an unlayered inhomogeneous sphere with radius r_0. For the radial displacement component calculate

$$\sum_{m=-n}^{n} U(r_s)\underline{P}_n^m\cdot\underline{r} = \sum_{m=-n}^{n} \frac{G_1 R_{32}^{-1}\underline{P}_n^m\cdot\underline{r}}{R_{11}^{-1}R_{32}^{-1}-R_{31}^{-1}R_{12}^{-1}} \quad , \tag{41}$$

where for an unlayered sphere

$$\sum_{m=-n}^{n} G_1\underline{P}_n^m\cdot\underline{r} = [1,0,0,0]\underline{s}_r \text{ and } R_{ij}^{-1} = F_{ij}^{-1}(r_0). \tag{42}$$

Next evaluate the source vector $\underline{s}_r$ from the radiation factors defined in Appendix B. For an explosive point source the moment tensor is isotropic, giving in equation (B10)

$$L_P^1 = L_P^2 = L_{SV}^1 = L_{SV}^2 = L_{SH}^1 = L_{SH}^2 = 0$$
$$L_P^3 = L_{PS}^4 = M_0 \quad . \tag{43}$$

In the far field, the non-zero radiation factors then become, from equation (B9)

$$F_{\ell p}^{\check{}} = F_{\ell p}^{\hat{}} = \frac{M_0}{\alpha_s^2} P_n(\cos\Delta) \tag{44}$$

Substituting $\underline{s}_r$ using equations (B9) and $\underline{\underline{F}}_{ij}^{-1}(r_0)$ using the definition of the inverse fundamental matrix in equation (10b) gives

$$\tilde{u}_r(\Delta,\omega) = \int_0^\infty \left\{ \frac{-i\omega p(\frac{1}{\beta_0})^2 [\frac{1}{\beta_0^2} - \frac{2r_0^2}{p^2}] g^{(3)}(r_s) P_n(\cos\Delta)}{\pi\alpha_s^2 r_s r_0 \sqrt{\rho_s \rho_0} [(\frac{1}{\beta_0^2} - \frac{2r_0^2}{p^2})^2 + \frac{4p^2 \check{\nu}\check{\nu}}{r^2} \xi\eta] g^{(3)}(r_0)} \right\} dp \tag{45}$$

for the radial component of the Fourier time transform of displacement. $(n = \omega p - 1/2)\xi$, and η are evaluated at r_0. The denominator factor,

$$[(\frac{1}{\beta_0^2} - \frac{2r_0^2}{p^2})^2 + \frac{4p^2}{r^2} \check{\nu}\check{\nu}],$$

can be recognized as a form of Rayleigh's dispersion function with generalized vertical slownesses substituting for the more familiar plane wave cosines.

This solution must possess a ray-mode duality equivalent to that of the layered half space described by Pekeris (1948). To demonstrate this duality, reduce (45) to either (1) a sum of modes of free oscillation of the sphere or (2) to a sum of individual displacements due to all possible seismic rays interacting with the free surface.

A modal representation can be derived by omitting the Poisson transform of the n summation and evaluating the inverse Fourier transform by contour integration, giving a double summation over radial order number n and poles $_i\omega_n$ of Rayleigh's function in complex frequency (e.g., Sato et al., 1963). An alternate mode representation can be derived by the spectral method, which evaluates the p integral in (45) at the discrete frequency points needed for the application of a fast Fourier transform. The p integral is then evaluated by contour integration, which together with the inverse FFT results in a double summation over frequency ω_n and poles $_ip_n$ in the complex p plane.

The validity of ray theory improves with increasing frequency. A ray representation can thus be most simply illustrated by incorporating a high frequency approximation of the radial eigenfunctions in (45). At sufficiently high frequency and small ray parameter, the first term in an asymptotic representation of the Airy functions can be used to approximate the radial eigenfunctions. This approximation, which is equivalent to the WKBJ approximation, can be used to expand the integrand of (45) into a sum of phasor terms that can be identified with seismic rays. The displacement generated by each ray can then be determined by either the spectral method combined with saddle point integration (Richards, 1973), or by Chapman's (1978a) technique of WKBJ seismograms.

II. Inhomogeneous Layered Sphere

Again consider a buried explosive point source but now evaluate the matrix products of equation (31). As a specific example take the layered earth model shown in Figure 2, and an explosion source at 1 km. depth. Radial displacement is calculated by the spectral method using a real fast Fourier transform:

$$u_r(t,\phi,\Delta) = \mathrm{Re}\int_0^\infty e^{-i\omega t}\int_\Gamma \frac{N_{P\text{-}SV}}{D_{P\text{-}SV}}\, dp d\omega \qquad (46)$$

$$\frac{N_{P\text{-}SV}}{D_{P\text{-}SV}} = \frac{ip\sqrt{\frac{i\omega}{r_s}}}{8\pi r_s \alpha_s^2} M_0 P_n(\cos\Delta) \cdot \frac{\left\{[-g^{(3)}(r_s), g^{(1)}(r_s), 0, 0]\underline{\underline{K}}^T[\underline{E}_P^T\underline{E}_{SV}^T - \underline{E}_{SV}^T\underline{E}_P]\cdot\underline{\underline{K}}\begin{bmatrix}0\\1\\0\\0\end{bmatrix}\right\}}{\left\{[1,0,0,0]\underline{\underline{K}}^T[\underline{E}_P^T\underline{E}_{SV} - \underline{E}_{SV}^T\underline{E}_P]\underline{\underline{K}}\begin{bmatrix}0\\1\\0\\0\end{bmatrix}\right\}}$$

where Γ is a contour in the complex p plane.

The matrix products in (46) are evaluated at points in the complex ray parameter plane, applying the methods of Abo-Zena (1979) as previously described in the section EVALUATION OF PROPAGATOR PRODUCTS. The approximations to the radial eigenfunctions at each layer are constructed to be continuous functions in the complex ray parameter plane (see Appendix A), allowing the integration path to be deformed off the real p axis. Deformation of the p contour below the real p axis reduces the large oscillations of the integrand associated with poles on and near the real p axis. Numerical integration thus becomes a computationally efficient procedure without invoking an unreasonably attenuating earth model to move the p poles off the real axis.

Residues at poles in the first quadrant of the p plane (Figure 3) describe seismic radiation at the free surface. Application of the reflectivity boundary condition to the lowermost layer boundary produces poles in the fourth quadrant whose residues describe transmitted radiation into the last layer. The integration contour in the p plane must therefore be deformed such that these fourth quadrant poles are excluded from the response at the free surface. Application of the decay boundary condition in the lowermost layer eliminates the fourth quadrant poles at the expense of packing poles more densely along the real ray parameter axis at small ray para-

meter values. The reflectivity boundary condition is thus preferred for the deformation of the left end of the contour across the real ray parameter axis.

Provided that the Legendre function $P_n(\cos\Delta)$ is not decomposed into horizontal travelling waves as in equation (B11), the integrand vanishes as p goes to zero and the p contour may end at the origin as in the antipode problem described by Rial and Cormier (1979). In the distance range for which sample seismograms were synthesized (75-150 km.),near vertically incident body waves, however, were not important in the complete response. Rays having take-off angles more vertical and bottoming at depths deeper than the direct P wave reach the receiver only by suffering partial reflections from layer boundaries. Such arrivals are consequently much smaller in amplitude and delayed in time relative to the earlier portion of the waveform. These arrivals can be excluded by deforming the left end of the contour across the real p axis into the left portion of the first quadrant where the integrand decays. The p point at which the contour may be so deformed can be estimated from the lowest bottoming depth of the direct P waves in the distance range of calculation. The range of distances, frequencies, and ray parameters needed for the synthetics shown in Figures 4-5 required the inclusion of only the $Q^{(2)}$ travelling wave in the decomposition of the Legendre function, and the left end of the integration contour was deformed across the real p axis.

Decay of the integrand of equation (46) also occurs along the real p axis at large values of p (e.g., Frazer, 1977). The integrand decays more rapidly, however, by deforming the right end of the contour upward into the upper right portion of the first quadrant around the last ray parameter pole (Figure 3). The residue at this pole accounts for the fundamental Rayleigh wave. For the earth model chosen here the position of the fundamental Rayleigh pole is well separated in the complex p plane from all other poles. It is thus convenient to evaluate the displacement response in two

stages (Figure 4), separately calculating the response due to the fundamental Rayleigh pole with one contour and the response of all other modes with another contour.

Figures 4-5 show unfiltered traces of synthetic displacements. The contour deformations shown in Figure 3 do not introduce truncation pulses common to methods that apply a phase velocity filter to the contour integration. The earliest disturbance in the wave-forms represents the direct P wave. Some numerical noise occurs at the Nyquist frequency (2 Hz.).

The real axis contour can be alternately deformed to completely enclose p poles in the first quadrant. The steps in the contour deformation would be identical to those described by Ugincius and Überall (1968) for the problem of the elastic cylinder. The spectral response could then be evaluated by applying Cauchy's residue theorem to the p poles. The mode sum obtained would be analogous to that obtained by Harvey (1979) for planar homogeneous layers.

In either the numerical integration method or the mode sum method most of the layer calculations can be saved and catalogued for use at different distances with different sources at different depths. To achieve this economy in the numerical integration method, catalogue the d_2 element of $\underline{\underline{Y}}_1$ matrix and all elements of the $\underline{\underline{Y}}_{s-1}$ matrix at the frequency and ray parameter points needed for the FFT and p integration.

MODEL SPECIFICATION

A spherical earth model need not be first flattened before the inhomogeneous layers are specified. The zero order asymptotic solutions account for the curvature of layer boundaries as well as inhomogeneity in the layers. Formulae for a flattened model are redundant. The expressions for τ and Q needed for the calculation of Airy functions in Appendix A are equivalent to those for a spherical model; $P_n^m(\cos\Delta)$ is approximately replaced by $(kx)^m J_m(kx)$ with the use of Szegos (1934) asymptotic expression for P_n^m. (See for example Chapman, 1973, or Müller, 1977.)

The asymptotic solution used in this paper restricts the

velocity profiles to having only one turning point. The presence of a low velocity zone would thus preclude an earth model having only one layer (a simple inhomogeneous sphere).

How accurately do the zero order asymptotics model the radial eigenfunctions of an inhomogeneous layer? The accuracy depends on both frequency and the magnitude of boundary curvature and first and higher order radial derivatives of density and elastic moduli. Higher frequency allows larger magnitudes for curvature and radial derivatives. For a given velocity profile the error can be estimated from either the higher order terms in the radial component of the potential equations (Richards, 1976), or from the first higher order solution term for the fundamental matrix obtained by Woodhouse (1978). With the use of smooth relatively linear velocity gradients, the zeroth order asymptotics can be used in the frequency band (0.2 - 10 Hz.) with a relative error in a radial eigenfunction bounded by 0.1% at 0.2 Hz. for a velocity gradient of 0.1 sec $^{-1}$.

Asymptotic series type solutions, however, fail to properly account for narrow angle reflections from regions having rapid velocity variations over short distances (Chapman, 1978b). Layer boundaries should thus be introduced at points best described by a first order discontinuity such as the moho. If the errors in the zeroth order solution become unacceptably large in a given frequency band, then the layer should be broken up into thinner layers of weaker velocity and density gradient. Inflections and kinks in the velocity profile, expressed by a large value of second and higher order radial derivatives, should be avoided. In many practical applications at 500 km. or less distance, no more than four to five inhomogeneous layers should be necessary to describe the velocity variation from crustal layers, high velocity mantle, and low velocity zone.

CONCLUSIONS

The preceding has demonstrated the practicality of including an inhomogeneously layered model in a calculation of the complete

displacement response at short distances. The isolation of the fundamental surface wave pole in the complex p plane allows the synthesis, if desired, of only the fundamental surface wave mode by numerical integration.

When only a small subset of body waves at large distances is desired, the inhomogeneous layer matrices and response function calculation can be modified for a reflectivity type calculation analogous to that of Fuchs and Müller (1971) for planar homogeneous layers. For such subsets of body waves it would not be difficult to extend the decomposition and multiplication scheme used for the evaluation of the layer matrix $\underline{\underline{K}}_i$ to the boundary matrix $\underline{\underline{Q}}_i$ used in the reflection matrix method described by Kennet (1974), where

$$\underline{\underline{Q}}_i = \tilde{\underline{\underline{F}}}_{i-1}^{-1}(r_{i-1})\tilde{\underline{\underline{F}}}_i(r_{i-1})$$

In this method the fundamental matrices $\tilde{\underline{\underline{F}}}_{i-1}^{-1}$ and $\tilde{\underline{\underline{F}}}_i$ must be defined such that they can be partitioned into four 2 X 2 matrices each of which can be associated solely with up- or down-going waves.

In any of these applications the layer inhomogeneity minimizes the number of layers needed to describe the response function and thereby the computation time required to synthesize displacement. The zero order asymptotics adequately model the behavior of the radial eigenfunctions of an inhomogeneous layer in the frequency band (0.2 - 10 Hz.) for the velocity gradients common to wide regions of the crust and upper mantle.

ACKNOWLEDGEMENTS

This research was originally inspired from discussions with C.B. Archambeau and D. Harvey at the Co-operative Institute for Research in the Environmental Sciences, University of Colorado/NOAA, Boulder, Colorado 80309. The author is indebted to P.G. Richards for his revised LANGER subroutine that made the contour deformations

in the p plane possible. The research was initiated at CIRES with support provided by the Air Force Office of Scientific Research under grant AFSOR-75-2775 and completed at Harvard University with support provided by the National Science Foundation under grant EAR 79-04167.

REFERENCES

Abo-Zena, A.M. (1979). Dispersion function computations for unlimited frequency values, Geophys. J.R. astr. Soc. 58, 91-105.

Abramowitz, M. and I.A. Stegun (1964). Handbook of Mathematical Functions, Dover Publications, New York.

Aki, K. and P.G. Richards (1980). Quantitative Seismology Theory and Methods, W.A. Freeman and Co., San Francisco, in press.

Alterman, Z., H. Jarosch, and C.L. Pekeris (1959). Oscillations of the Earth, Proc. Roy. Soc. London A. 252, 80-95.

Archambeau, C.B. (1968). General theory of elastodynamic source fields, Rev. Geophys. 6, 241-288.

Archambeau, C.G., E.H. Flinn, and D.G. Lambert (1969). Fine structure of the upper mantle, J. Geophys. Res. 75, 2825-2865.

Červený, V., I.A. Molotkov, and I. Pšenčik (1977). Ray Method in in Seismology, Univerzita Karlova, Praha.

Chapman, C.H. (1973). The earth flattening transformation in body wave theory, Geophys. J.R. Astr. Soc. 35, 55-70.

Chapman, C.H. (1974). The turning point of elastodynamic waves, Geophys. J.R. Astr. Soc. 39, 613-622.

Chapman, C.H. (1978a). A new method for computing synthetic seismograms, Geophys. J.R. Astr. Soc. 54, 481-518.

Chapman, C.H. (1978b). Long period corrections to WKBJ seismograms (Abstract), Trans. Am. Geophys. Union 12, 1129.

Choy, G.L. (1977). Theoretical seismograms of core phases calculated by frequency-dependent full wave theory, and their interpretation, Geophy. S.R. Astr. Soc. 51, 275-312.

Cormier, V.F. (1976). PH.D. Thesis, Columbia University, New York.

Cormier, V.F. and P.G. Richards (1976). Comments on 'The damping of core waves' by Anthony Qamar and Alfredo Eisenberg, J. Geophys. Res. 81, 3066-3068.

Cormier, V.F. and P.G. Richards (1977). Full wave theory applied to a discontinuous velocity increase: the inner core boundary, J. Geophy. 43, 3-31.

Dunkin. J.W. (1965). Computations of modal solutions in layered elastic media at high frequencies, Bull. Seism. Soc. Am. 55, 335-358.

Frazer, L.N. (1977). Synthesis of shear-coupled PL, PH.D. Thesis, Princeton University, Princeton, New Jersey.

Fuchs, K. and G. Muller (1971). Computation of synthetic seismograms with the reflectivity method and comparison with observations, Geophys. J.R. Astr. Soc. 23, 417-433.

Futterman, W.I. (1962). Dispersive body waves, J. Geophys. Res. 67, 5279-5291.

Gantmacher, F.R. (1959). The theory of matrices, 2 volumes, Chelsea, New York (translated from the Russian by K.A. Hirsch).

Garmany, J. and J.A. Orcutt (1979). Travel time inversion: a geometrical approach, J. Geophys. Res. 84, 3615-3622.

Gilbert, F. and G.E. Backus (1966). Propagator matrices in elastic wave and vibration problems, Geophys. J.R. Astr. Soc. 31, 326-332.

Gilbert, F. (1971). The excitation of the normal modes of the earth by earthquake sources, Geophys. J.R. Astr. Soc. 22, 223-226.

Harvey, D. (1979). Seismogram synthesis using normal mode superposition: the locked mode approximation method, submitted to Geophys. J.R. Astr. Soc.

Hudson, J.A. (1969). A quantitative evaluation of seismic signals at teleseismic distances: I. Radiation from point sources, Geophys. J.R. Astr. Soc. 18, 233-249.

Kanamori, K. and D. Hadley (1975). Crustal structure and temporal velocity change in southern California, Pageoph 113, 280-285.

Kennett, B.L.N. (1974). Reflections, rays and reverberations, Bull. Seism. Soc. Am. 64, 1685-1696.

Knopoff, L. (1964). A matrix method for elastic wave problems, Bull. Seism. Soc. Am. 54, 431-438.

Langer, R.E. (1932). On the asymptotic solutions of differential equations, with an application to the Bessel functions of large complex order, Trans. Am. Math. Soc. 34, 447-480.

Langer, R.E. (1949). The asymptotic solutions of ordinary linear differential equations of the second order, with special reference to a turning point, Trans. Am. Math. Soc. 67, 461-490.

Mondt, J.C. (1977). SH-waves: theory and observations for epicentral distances greater than 90 degress, Phys. Earth Planet. Inst. 15, 46-59.

Müller, G. (1977). Earth flattening transformation for body waves derived from geometric ray theory - improvements, corrections, and range of applicability, J. Geophys. 42, 429-436.

Nussenzweig, H.M. (1965). High frequency scattering by an impenetrable sphere, An. Phys. 34, 23-95.

Olver, F.W.J. (1954). The asymptotic solution of linear differential equations of the second order for large values of a parameter, Philos. Trans. Roy. Soc. London. Ser. A. 247, 307-327.

Pekeris, C.L. (1948). Theory of propagation of explosive sound in shallow water, in Propagation of Sound in the Ocean, Geol. Soc. Am. Memoir 27.

Rial, J.A. and V.F. Cormier (1979). Seismic waves at the epicenters antipode, in press, J. Geophys. Res.

Richards, P.G. (1973). Calculations of body waves for caustics and tunneling in core phases, Geophys. J.R. Astr. Soc. 35, 243-264.

Richards, P.G. (1976). On the adequacy of plane wave reflection/transmission coefficients in the analysis of seismic body waves, Bull. Seism. Soc. Am. 66, 701-717.

Richards, P.G. (1978). A basis for quantifying seismic sources from body wave data (Abstract), Trans. Am. Geophys. Union 12, 1139.

Saito, M. (1967). Excitation of free oscillations and surface waves by a point source in a vertically heterogeneous earth, J. Geophys. Res. 72, 3689.

Sato, Y., T. Usami, M. Landisman, and M. Ewing (1963). Basic study on the oscillation of a sphere. Part I: Propagation of torsional disturbances on a radially heterogeneous sphere. Case of the homogeneous mantle with a liquid core, Geophys. J.R. Astr. Soc. 8, 44-63.

Singh, J.S. and A. Ben-Menahem (1969). Eigenvibrations of the earth excited by finite dislocations - I: toroidal oscillations, Geophys. J.R. Astr. Soc. 17, 151-177.

Szego, von G. (1934). Über einege asymptotische enwicklungen der Legendreschen funktionen, Proc. Land. Math. Soc., Ser.2, 36, 427-470.

Uginčius, P., and H. Überall (1968). Creeping-wave analysis of acoustic scattering by elastic cylindrical shells, J. Acoust. Soc. Am. 43, 1025-1035.

Ward, S.N. (1979). Body wave calculations using moment tensor sources in spherically symmetric, inhomogeneous media, Geophys. J.R. astr. Soc. (in press).

Wasow, W. (1965). Asymptotic expansions for ordinary differential equations, Wiley-Interscience, New York.

Woodhouse, J.H. (1974). Aspects of high frequency seismic wave propagation, PH.D. Thesis, Cambridge University.

Woodhouse, J.H. (1978). Asymptotic results for elastodynamic propagator matrices in palne stratified and spherically stratified earth models, Geophys. J.R. Astr. Soc. 54, 263-281.

FIGURE CAPTIONS

Figure 1 Layering index scheme.

Figure 2 Earth model based on the southern California crustal model of Kanamori and Hadley (1975) and model CIT 109 of the upper mantle (Archambeau et al., 1969).

Figure 3 Paths in the complex ray parameter plane for the evaluation of displacement in a spherical earth model having a single discontinuity at which the P and S velocity increase discontinuously. Position of poles in the P-SV response are shown schematically by x's. Rayleigh poles lie near the real axis. Franz poles emanate upward and downward from the real p axis at approximately ±60 degree angles. The poles of the P-SV response of the earth model shown in Figure 2 differ from this form only in having additional Franz poles in the first quadrant associated with higher layer boundaries.

Figure 4 Displacement calculated from the spectral response (0 - 2 Hz.) given by the numerical integration along the contours shown in Figure 3. Polarity is reversed. Source was an explosion at 1 km. depth. Time domain records were obtained by inverse FFT using 128 frequencies.

Figure 5 Synthetic displacement at 75 to 150 km.

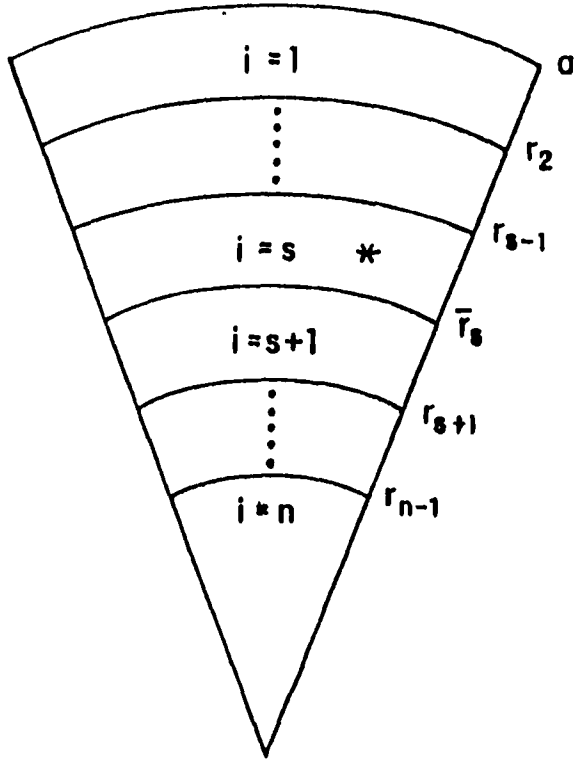

Figure 1

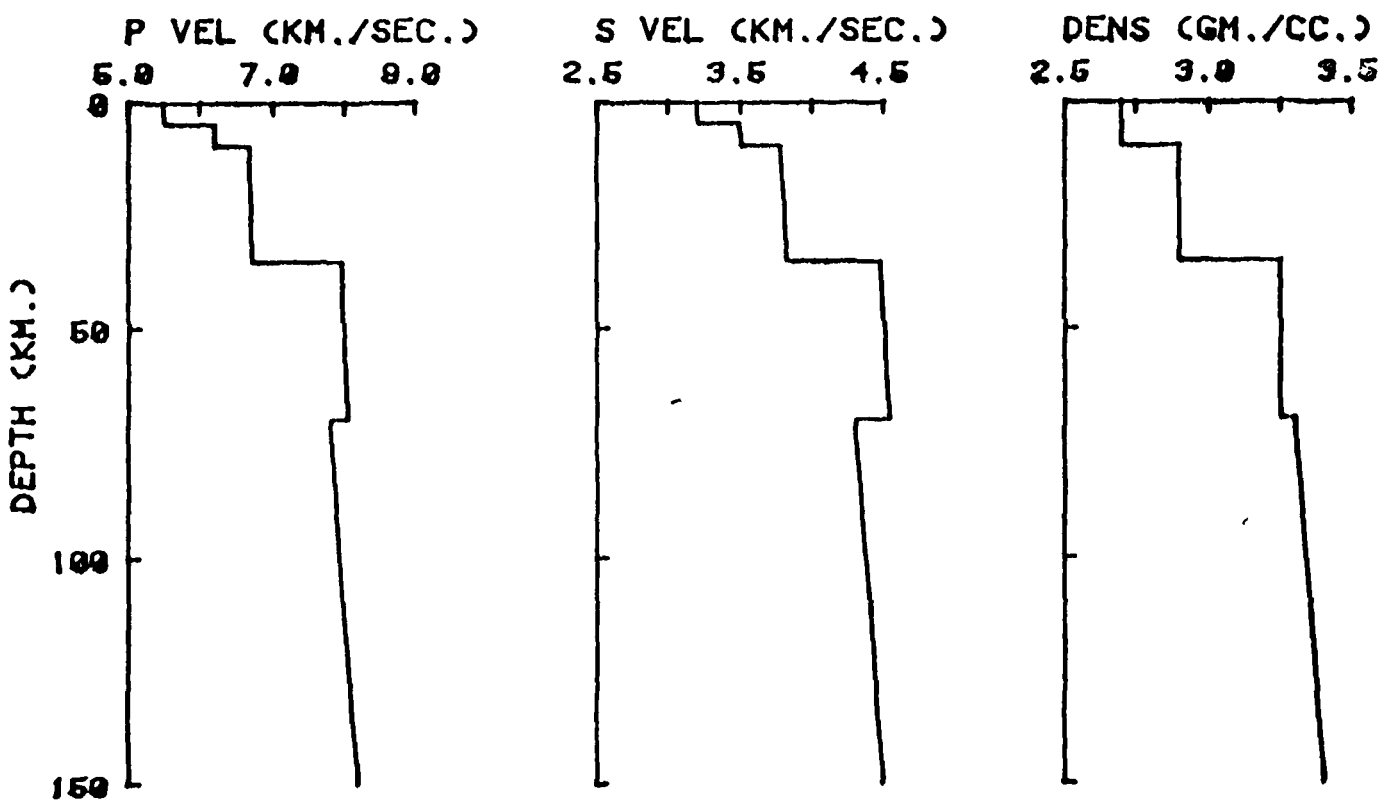
P VEL (KM./SEC.)
5.0
7.0
9.0
S VEL (KM./SEC.)
2.5
3.5
4.5
DENS (GM./CC.)
2.5
3.0
3.5
DEPTH (KM.)
0
50
100
150

Figure 2

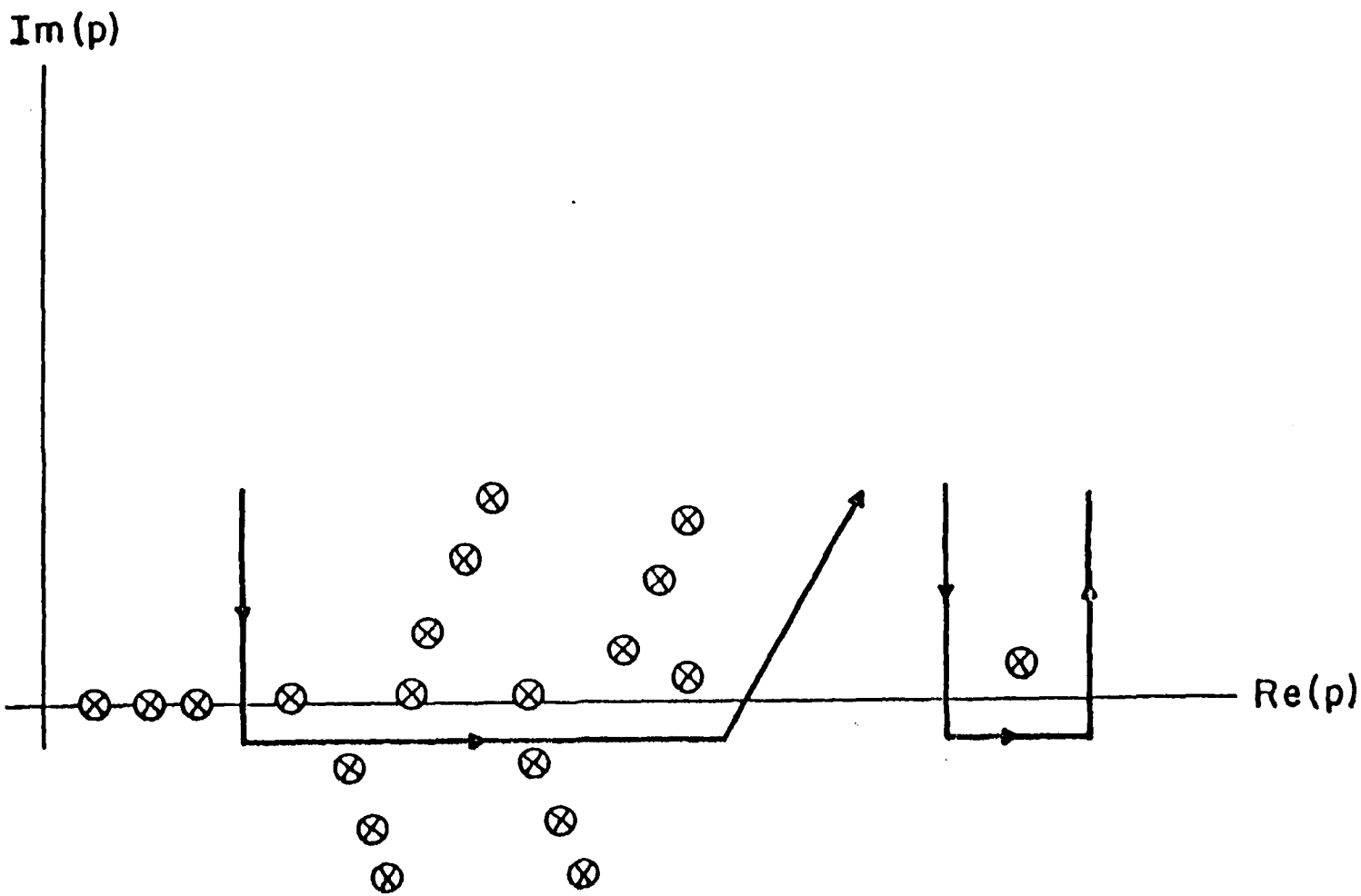

Figure 3

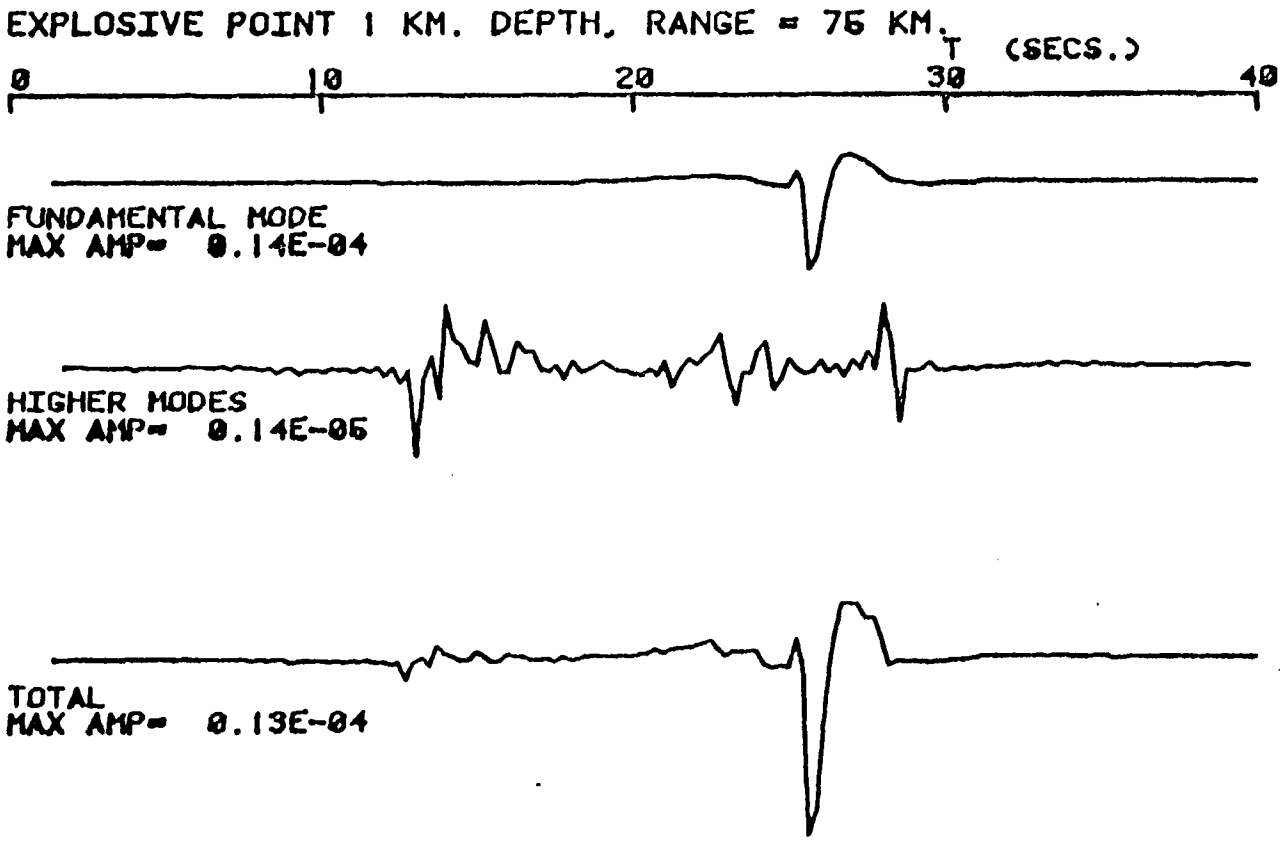
EXPLOSIVE POINT 1 KM. DEPTH, RANGE = 75 KM.
T (SECS.)
0
10
20
30
40
FUNDAMENTAL MODE
MAX AMP= 0.14E-04
HIGHER MODES
MAX AMP= 0.14E-05
TOTAL
MAX AMP= 0.13E-04

Figure 4

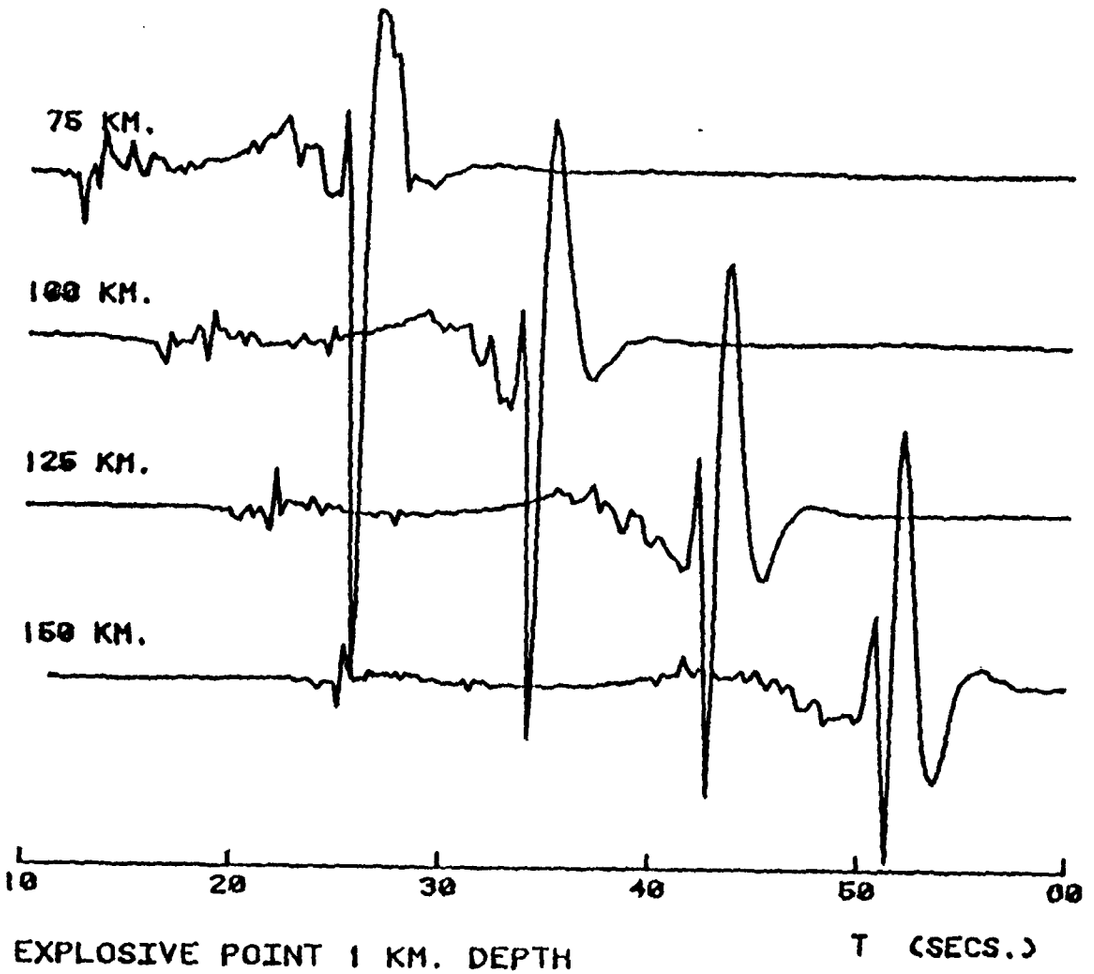
75 KM.
100 KM.
125 KM.
150 KM.
10
20
30
40
50
00
EXPLOSIVE POINT 1 KM. DEPTH
T (SECS.)

Figure 5

APPENDIX A: RADIAL EIGENFUNCTIONS

Practical Evaluation of Airy Functions

The radial eigenfunctions are defined in terms of the Airy function Ai:

$$
\begin{aligned}
g^{(1)}(r) &= \sqrt{\frac{\pi}{2}}\,\omega^{1/6}\,\frac{\tau_\alpha^{1/4}}{Q_\alpha^{1/2}}\,\mathrm{Ai}(-z_\alpha e^{i2\pi/3}), \\
g^{(3)}(r) &= \sqrt{\frac{\pi}{2}}\,\omega^{1/6}\,\frac{\tau_\alpha^{1/4}}{Q_\alpha^{1/2}}\,\mathrm{Ai}(-z_\alpha), \\
&\text{or} \\
&= \sqrt{\frac{\pi}{2}}\,\omega^{1/6}\,\frac{\tau_\alpha^{1/4}}{Q_\alpha^{1/2}}\,\mathrm{Ai}(-z_\alpha e^{-i2\pi/3}), \\
h^{(1)}(r) &= \sqrt{\frac{\pi}{2}}\,\omega^{1/6}\,\frac{\tau_\beta^{1/4}}{Q_\beta^{1/2}}\,\mathrm{Ai}(-z_\beta e^{i2\pi/3}), \\
h^{(3)}(r) &= \sqrt{\frac{\pi}{2}}\,\omega^{1/6}\,\frac{\tau_\beta^{1/4}}{Q_\beta^{1/2}}\,\mathrm{Ai}(-z_\beta), \\
&\text{or} \\
&= \sqrt{\frac{\pi}{2}}\,\omega^{1/6}\,\frac{\tau_\beta^{1/4}}{Q_\beta^{1/2}}\,\mathrm{Ai}(-z_\beta e^{-i2\pi/3}),
\end{aligned}
\qquad \text{(A1)}
$$

$$
\begin{aligned}
z_\alpha &= (3/2\omega\tau_\alpha)^{2/3}, \\
z_\beta &= (3/2\omega\tau_\beta)^{2/3},
\end{aligned}
$$

$$
\tau_\alpha = \int_{r_p}^{r} Q_\alpha dr \quad , \qquad \tau_\beta = \int_{r_p}^{r} Q_\beta dr \quad ,
$$

$$
Q_\alpha = \left(\frac{1}{\alpha^2} - \frac{p^2}{r^2}\right)^{1/2} \quad , \qquad Q_\beta = \left(\frac{1}{\beta^2} - \frac{p^2}{r^2}\right)^{1/2} .
$$

The exact radial eigenfunctions of an inhomogeneous layer are analytic functions in the complex p plane. The fractional powers used in defining the arguments of the Airy functions, however, place branch cuts in the complex p plane of the asymptotic approximations of the radial eigenfunctions. These branch cuts

may be removed by multiplying $\omega\tau$ by $e^{i2\pi N}$, where N=0, ±1 depending on the phase of the complex τ and ray parameters p. Cormier (1976a) discusses how N may be determined in a complex velocity profile when subroutine packages for Hankel functions or order 1/3 calculate the Airy functions. The Airy functions, however, can be most efficiently calculated with the exact and asymptotic formulae given in Abramowitz and Stegun (1964). P.G. Richards (personal communication) has used this approach, patching the exact and approximate formulae together when $|\omega\tau| = 3.5$. The subroutine LANGER written and tested by Richards together with an improved algorithm for calculating N (a portion of his subroutine ROMTAU) have been used in the calculations of this paper. The integers m_j needed in propagator multiplication scheme of equations (39-40) can be constructed from normal LANGER output.

Practical Evaluation of the Delay Time τ

The integral defining τ may be (1) analytically evaluated using the velocity profile $v = ar^b$ in each layer (Richards, 1973, 1976; Choy, 1977; Frazer, 1977; Mondt, 1977); (2) numerically integrated in an analytic velocity profile given by a polynomial in radius (Cormier and Richards, 1977); or (3) analytically integrated by parameterizing the logarithm of radius in the Bullen parameter ($\ln = r/v(r)$) (Woodhouse, 1974).

Method (3) is equivalent to the parameterization described by Cerveny et al. (1977) and used by Garmany, et al. (1979) for flat inhomogeneous layers. It is usually the most computationally efficient. For the calculation of the seismograms in Figures 4-5, each layer of the velocity model in Figure 2 was parameterized using method (3) with

$$\ln(r/r_0) = a + b(\eta/\eta_0)^2 \qquad \text{(A2)}$$

where r_0 and η_0 are the values of r and η at the top of the layer. The constants a and b were determined from the values of radius and velocity at the boundaries of the layer. The delay time

was then given by

$$\tau(p) = 2\eta_0 [1 - (p/\eta_0)^2]^{3/2} \; b/3 \qquad \text{(A3)}$$

Incorporation of Attenuation

Incorporation of attenuation in any of the above methods for computing τ can be accomplished by a complex velocity profile (e.g., Cormier and Richards, 1976). When a complex velocity profile can be specified by the form

$$\hat{v}(r) = v_0(r) \cdot (1 + \hat{\varepsilon}) \qquad \text{(A4)}$$

method (3) reduces to the form

$$\tau_A(p) = (1 + \hat{\varepsilon})^{-1} \tau_U(p \cdot (1 + \hat{\varepsilon})) \qquad \text{(A5)}$$

where $\hat{\varepsilon}$ is a small complex number constant in radius, $v_0(r)$ a real velocity, τ_A the delay time in the attenuating layer, and τ_U the delay time in the layer having the real velocity profile evaluated at the ray parameter $p=p\cdot(1+\hat{\varepsilon})$. To include the dispersive effect of linear attenuation mechanisms $\hat{\varepsilon}$ must have non-zero real and imaginary parts, each of which is frequency dependent (Futterman, 1962). If dispersion can be ignored in the frequency band of interest, then $\hat{\varepsilon}$ may be taken to be pure imaginary and frequency independent.

APPENDIX B: SOURCE RADIATION

Simplification of Source Radiation Properties

In the computation of the complete response function it is convenient to compute the summation over order number m of products of the source factors G_i and vector spherical harmonics. Three such combinations can be rewritten as follows:

$$\sum_{m=-n}^{n} [G_1 \underline{P}_n^m + G_1 \underline{B}_n^m] = [1,0,0,0]\underline{\underline{S}}^{-1}(\underline{s}_r \underline{r} + \underline{s}_\theta \underline{\theta} + \underline{s}_\phi \underline{\phi})$$

$$\sum_{m=-n}^{n} [G_3 \underline{P}_n^m + G_3 \underline{B}_n^m] = [0,0,1,0]\underline{\underline{S}}^{-1}(\underline{s}_r \underline{r} + \underline{s}_\theta \underline{\theta} + \underline{s}_\phi \underline{\phi}) \qquad \text{(B1)}$$

$$\sum_{m=-n}^{n} G'_1 \underline{C}_n^m = [1,0,0,0]\underline{\underline{S}}'^{-1}(\underline{s}'_\theta \underline{\theta} + \underline{s}'_\phi \underline{\phi})$$

Equation (19) defines the matrix $\underline{\underline{S}}^{-1}$ as the product of propagators. The column vectors $\underline{s}_r$, $\underline{s}_\theta$, $\underline{s}_\phi$, $\underline{s}'_\theta$, and $\underline{s}'_\phi$ now emphasize the major properties of the source radiation pattern and are defined by

$$\underline{s}_r = \sum_{m=-n}^{n} \int_a^{r_0} \underline{\underline{F}}_S^{-1}(\xi)\underline{\gamma}(\xi)\, d\xi\, Y_n^m$$

$$\underline{s}_\phi = \sum_{m=-n}^{n} \int_a^{r_0} \underline{\underline{F}}_S^{-1}(\xi)\underline{\gamma}(\xi)\, d\xi \frac{1}{\sin\theta} \frac{\partial Y_n^m}{\partial \phi} \Big/ [n(n+1)]^{1/2} \qquad \text{(B2)}$$

$$\underline{s}_\theta = \sum_{m=-n}^{n} \int_a^{r_0} \underline{\underline{F}}_S^{-1}(\xi)\underline{\gamma}(\xi)\, d\xi \frac{\partial Y_n^m}{\partial \theta} \Big/ [n(n+1)]^{1/2}$$

$$\underline{s}'_\theta = \sum_{m=-n}^{n} \int_a^{r_0} \underline{\underline{F}}'^{-1}_S(\xi)\underline{\gamma}'(\xi)\, d\xi \frac{1}{\sin\theta} \frac{\partial Y_n^m}{\partial \phi} \Big/ [n(n+1)]^{1/2}$$

$$\underline{s}'_{\phi} = \sum_{m=-n}^{n} \int_{a}^{r_0} \underline{F}_S^{-1}(\xi)\underline{s}'(\xi)\,d\xi \left.\frac{\partial Y_n^m}{\partial\theta}\right/ [n(n+1)]^{1/2} \qquad \text{(B2) (cont'd)}$$

Specification of a Seismic Point Source

The expressions in equations (B2) can be simplified by specifying the seismic source vectors $\underline{\gamma}$ and $\underline{\gamma}'$. Consider a seismic source specified by the Fourier time transform $\tilde{\underline{f}}$ of a vector $\underline{f}$ of body force density acting at a point. As in Saito (1967), $\underline{\gamma}$ and $\underline{\gamma}'$ are determined from an expansion of $\tilde{\underline{f}}$ in vector spherical harmonics:

$$\underline{\gamma}(\xi) = \begin{bmatrix} 0 \\ 0 \\ \frac{f_1^S}{\omega^2} \\ \frac{f_2^S}{\omega^2} \end{bmatrix}, \qquad \underline{\gamma}'(\xi) = \begin{bmatrix} 0 \\ \frac{f_3^T}{\omega^2} \end{bmatrix} \qquad \text{(B3)}$$

with f_1^S, f_2^S and f_4^T determined from

$$\tilde{\underline{f}}(\xi,\theta,\phi) = \sum_{n=0}^{\infty} \sum_{m=-n}^{n} [f_1^S \underline{P}_n^m + f_2^S \underline{B}_n^m + f_3^T \underline{C}_n^m] ,$$

$$f_1^S = \int_0^{2\pi} \int_0^{\pi} \tilde{\underline{f}}\cdot\underline{P}^{*m}_n \sin\theta\,d\theta\,d\phi , \qquad \text{(B4)}$$

$$f_2^S = \int_0^{2\pi} \int_0^{\pi} \tilde{\underline{f}}\cdot\underline{B}^{*m}_n \sin\theta\,d\theta\,d\phi , \quad \int_0^{2\pi}\int_0^{\pi} \tilde{\underline{f}}\cdot\underline{C}^{*m}_n \sin\theta\,d\theta\,d\phi,$$

*denoting the compex conjugate.

$\tilde{\underline{f}}$ can then be described with the zeroth order (in frequency) moment rate tensor $\underline{M}$ by

$$\tilde{\underline{f}} = -\underline{M}\cdot\nabla\delta(\underline{r} - \underline{r}_S) \qquad \text{(B5)}$$

Gilbert (1971), where $\delta(\underline{r} - \underline{r}_s)$ is a three dimensional delta function given at a point with radius vector $\underline{r}_s$. In spherical polar coordinates,

$$\delta(\underline{r} - \underline{r}_s) = \frac{\delta(r-r_s)\delta(\theta-\theta_0)\delta(\phi-\phi_0)}{r^2 \sin\theta} \qquad (B6)$$

A distributed source can be represented by a point source with the device of multipolar expansions (Archambeau, 1968). A sufficiently accurate approximation of the radiation pattern of a distributed source a high frequency, however, can require the inclusion of many terms in such an expansion. The equivalent definition with a moment tensor requires many higher order moment tensors (Gilbert, 1971) together with higher order spatial derivatives of the delta function (Hudson, 1969). The radiation factors given here consider only the first term in such an expansion, a source representation always valid at sufficiently low frequency. The same solution procedure may be used when higher order moment tensors are included.

The properties of $\underline{\underline{M}}$ have been discussed by Gilbert (1971). By conservation of angular momentum, $\underline{\underline{M}}$ must be a symmetric matrix ($M_{r\theta} = M_{\theta r}$, $M_{r\phi} = M_{\phi r}$, $M_{\theta\phi} = M_{\phi\theta}$). For a point double couple, quadrapole source $\underline{\underline{M}}$ must have zero trace ($M_{rr} + M_{\theta\theta} + M_{\phi\phi} = 0$). For a pure explosive point source, $\underline{\underline{M}}$ must be isotropic, i.e., all off diagonal elements are equal ($M_{r\theta} = M_{r\phi} = M_{\theta\phi} = 0$), and all diagonal elements are equal ($M_{rr} = M_{\theta\theta} = M_{\phi\phi} = M_0$). An exposion having some tectonic stress release may be represented by an $\underline{\underline{M}}$ in which the off diagonal elements are non-zero. The elements of $\underline{\underline{M}}$ have been defined by Gilbert (1971) and Aki and Richards (1980) in terms of earthquake fault plane parameters.

Results for the Source Radiation Vectors $\underline{s}_r$, etc.

Simplified expressions for $\underline{s}_r$ etc. may now be found from

substituting equations (10b),(B3),(B4),(B5), and (B6) into equations (B2) and applying the addition theorem for vector spherical harmonics. For examples of the simplification procedure see Singh and Ben-Menahem (1969) and Ward (1979). In the results that follow, Δ is the epicentral distance. The azimuthal angles C and B are defined by Singh and Ben-Menahem for a generalized co-ordinate system at the source and by Richards (1978) and Ward (1979) for a north-east-down (NED) co-ordinate system.

$$\underline{s}_r = \frac{\omega^{-1/2} ip\sqrt{i}}{8\pi r_s \sqrt{\rho_s}} \begin{bmatrix} -g^{(3)}\check{\ell}_P \\ g^{(1)}\check{\ell}_P \\ -h^{(3)}\check{\ell}_{SV} \\ h^{(1)}\check{\ell}_{SV} \end{bmatrix}$$

$$\underline{s}_\theta = \frac{\cos C\omega^{-1/2} ip\sqrt{i}}{8\pi r_s \sqrt{\rho_s}} \begin{bmatrix} -g^{(3)}\check{\ell}_P \\ g^{(1)}\check{\ell}_P \\ -h^{(3)}\check{\ell}_{SV} \\ h^{(1)}\check{\ell}_{SV} \end{bmatrix} \qquad \text{(B7)}$$

$$\underline{s}_\phi = \frac{\sin C\omega^{-1/2} ip\sqrt{i}}{8\pi r_s \sqrt{\rho_s}} \begin{bmatrix} -g^{(3)}\check{\ell}_P \\ g^{(1)}\check{\ell}_P \\ -h^{(3)}\check{\ell}_{SV} \\ h^{(1)}\check{\ell}_{SV} \end{bmatrix}$$

$$\underline{s}'_\theta = \frac{\sin C\omega^{-1/2} ip\sqrt{i}}{8\pi r_s \sqrt{\rho_s}\ \beta_s} \begin{bmatrix} -g^{(3)}\check{\ell}_{SH} \\ g^{(1)}\check{\ell}_{SH} \end{bmatrix}$$

$$\underline{s}'_\phi = \frac{\cos C\omega^{-1/2} ip\sqrt{i}}{8\pi r_s \sqrt{\rho_s}\ \beta_s} \begin{bmatrix} -h^{(3)}\check{\ell}_{SH} \\ h^{(1)}\check{\ell}_{SH} \end{bmatrix}$$

$g^{(3)}$, $g^{(1)}$, $h^{(3)}$, and $h^{(1)}$ are evaluated at the source radius

r_S in the analytic velocity profiles of the source layer.

The radiation factors consist of far field terms ($^F\ell_P$, $^F\ell_{SV}$, $^F\ell_{SH}$) and near field terms ($^N\ell_P$, $^N\ell_{SV}$, $^N\ell_{SH}$):

$$
\begin{aligned}
\check{\ell}_P &= {}^F\check{\ell}_P + {}^N\check{\ell}_P \\
\acute{\ell}_P &= {}^F\acute{\ell}_P + {}^N\acute{\ell}_P \\
\check{\ell}_{SV} &= {}^F\check{\ell}_{SV} + {}^N\check{\ell}_{SV} \\
\acute{\ell}_{SV} &= {}^F\acute{\ell}_{SV} + {}^N\acute{\ell}_{SV} \\
\check{\ell}_{SH} &= {}^F\check{\ell}_{SH} + {}^N\check{\ell}_{SH} \\
\acute{\ell}_{SH} &= {}^F\acute{\ell}_{SH} + {}^N\acute{\ell}_{SH}
\end{aligned}
\tag{B8}
$$

with

$$
\begin{aligned}
{}^F\check{\ell}_P &= [p^2/r^2 L_1^P + 1/\alpha_S^2 L_3^P] P_n(\cos\Delta) - 2\check{\xi}p/r\ L_2^P\ P_n^1\ (\cos\Delta)/(i\omega p) \\
{}^F\acute{\ell}_P &= [p^2/r^2\ L_1^P + 1/\alpha_S^2\ L_3^P] P_n(\cos\Delta) + 2\acute{\xi}p/r\ L_2^P P_n^1(\cos\Delta)/(i\omega p) \\
{}^F\check{\ell}_{SV} &= (Q_\beta^2 - p^2/r^2) L_1^{SV} P_n^1(\cos\Delta)/(i\omega p) - \check{\eta}p/r\ L_2^{SV} P_n(\cos\Delta) \\
{}^F\acute{\ell}_{SV} &= (Q_\beta^2 - p^2/r^2) L_1^{SV} P_n^1(\cos\Delta)/(i\omega p) + \acute{\eta}p/r\ L_2^{SV} P_n(\cos\Delta) \\
{}^F\check{\ell}_{SH} &= \check{\eta} L_{SH}^1 P_n(\cos\Delta) - p/r\ L_{SH}^2 P_n^1(\cos\Delta)/(i\omega p) \\
{}^F\acute{\ell}_{SH} &= -\acute{\eta} L_{SH}^1 P_n(\cos\Delta) - p/r\ L_{SH}^2 P_n^1(\cos\Delta)/(i\omega p) \\
{}^N\check{\ell}_P &= {}^N\acute{\ell}_P = p^2/r^2\ L_{PS}^4 \cot\Delta\ P_n^1\ (\cos\Delta)/(\omega^2 p^2)
\end{aligned}
\tag{B9}
$$

$$
\begin{aligned}
{}^{N}\check{\ell}_{SV} &= -\eta p/r\, L^{4}_{PS}\, \cot\Delta P^{1}_{n}(\cos\Delta)/(\omega^{2}p^{2}) \\
{}^{N}\acute{\ell}_{SV} &= \eta p/r L^{4}_{PS}\cot\Delta P^{1}_{n}(\cos\Delta)/(\omega^{2}p^{2}) \\
{}^{N}\check{\ell}_{SH} &= -2\eta L^{1}_{SH}\cot\Delta P^{1}_{n}(\cos\Delta)/(\omega^{2}p^{2}) - p/r\, L^{2}_{SH}[2\cot\Delta P_{n}(\cos\Delta)/(i\omega p) + \\
&\quad (2\csc^{2}\Delta - 4\cot^{2}\Delta)P^{1}_{n}(\cos\Delta)/(i\omega^{3}p^{3})] \\
{}^{N}\acute{\ell}_{SH} &= 2\eta L^{1}_{SH}\cot\Delta P^{1}_{n}(\cos\Delta)/(\omega^{2}p^{2}) - p/r\, L^{2}_{SH}[2\cot\Delta P_{n}(\cos\Delta)/(i\omega p) + \\
&\quad (2\csc^{2}\Delta - 4\cot^{2}\Delta)P^{1}_{n}(\cos\Delta)/(i\omega^{3}p^{3})
\end{aligned}
\qquad \text{(B9) (cont'd)}
$$

where p independent factors are given by:

$$
\begin{aligned}
L^{1}_{P} &= M_{\theta\theta}\cos^{2}\beta + M_{\theta\phi}\sin 2\beta + M_{\phi\phi}\sin^{2}\beta - M_{rr} \\
L^{2}_{P} &= M_{r\theta}\cos\beta + M_{r\phi}\sin\beta \\
L^{3}_{P} &= M_{rr} \\
L^{1}_{SV} &= L^{2}_{P} \\
L^{2}_{SV} &= L^{1}_{P} \\
L^{1}_{SH} &= M_{r\phi}\cos\beta - M_{r\theta}\sin\beta \\
L^{2}_{SH} &= \sin\beta(M_{\phi\phi} - M_{\theta\theta})/2 + \cos 2\beta M_{\theta\phi} \\
L^{4}_{PS} &= \cos 2\beta M_{\theta\theta} + 2M_{\theta\phi}\sin 2\beta + 2M_{\phi\phi}\sin^{2}\beta
\end{aligned}
\qquad \text{(B10)}
$$

The radiation factors defined remain valid as Δ vanishes. For Δ not near 0, it is possible to divide $P_n(\cos\Delta)$ into travelling wave functions $Q_n^{(1)}(\cos\Delta)$ and $Q_n^{(2)}(\cos\Delta)$,

$$P_n(\cos\Delta) = Q_n^{(1)}(\cos\Delta) + Q_n^{(2)}(\cos\Delta) \qquad \text{(B11)}$$

For large ωp these behave asymptotically as

$$Q_n^{(1)(2)} \approx \sqrt{\frac{1}{2\omega p \pi \sin\Delta}}\ e^{\pm i[\omega p - \pi/4]} \qquad \text{(B12)}$$

Nussenzweig (1965). With $P_n^1 = \frac{\partial P_n}{\partial \Delta}$ and equations (B11-B12), it follows that

$$P_n^1(\cos\Delta) \approx i\omega p P_n(\cos\Delta). \qquad \text{(B13)}$$

Thus, for large $\omega p\Delta$ the far field terms behave like $P_n(\cos\Delta)$, and the near field terms like $P_n(\cos\Delta)/(\omega p\Delta)$ and $P_n(\cos\Delta)/(\omega p\Delta)^2$.

The radiation factors in equations (B10) are essentially the same as those given in Aki and Richards (1980) and Ward (1979). In the far field only three p independent factors are necessary to describe the radiation of P waves, and two p independent factors to describe the radiation of SV or SH waves. In order to fully account for the radiation pattern of the source in the near field, however, the L_{PS}^4 factor must be added to the results reported in Aki and Richards and the Legendre functions not divided into travelling wave functions near $\Delta=0$.